MARTIN KANNEL

Development of Broadband Aerosol
Optical Depth Models

TARTU ÜLIKOOL
UNIVERSITAS TARTUENSIS
1632

DISSERTATIONES GEOPHYSICALES UNIVERSITATIS TARTUENSIS

26

MARTIN KANNEL

Development of Broadband Aerosol Optical Depth Models

This study was carried out at the Institute of Physics, University of Tartu, Estonia.

The dissertation was admitted on April 5th, 2016 in partial fulfilment of the requirements for the degree of Doctor of Philosophy in physics (environmental physics), and was allowed for defence by the Council of the Institute of Physics, University of Tartu.

Supervisor: Assoc. Prof. Hanno Ohvril,
             Institute of Physics, University of Tartu, Estonia

Opponents: PhD Enn Kaup,
             Tallinn University of Technology, Estonia

             PhD Priit Tisler,
             Finnish Meteorological Institute, Finland

The public defense will take place on June 10th, 2016 in the University of Tartu, *Physicum*, W. Ostwald Str. 1.

European Union
Regional Development Fund   Investing in your future

CONTENTS

LIST OF ORIGINAL PUBLICATIONS

The dissertation is based on the following publications:

I.   Kannel, M., Ohvril, H., Teral, H., Russak, V., Kallis, A. 2007. A simple broadband parameterisation of columnar aerosol optical thickness. *Proceedings of the Estonian Academy of Sciences, Biology, Ecology*, **56** (1), 57–68.

II.   Ohvril, H., Teral, H., Neiman, L., Kannel, M., Uustare, M., Tee, M., Russak, V., Okulov, O., Jõeveer, A., Kallis, A., Ohvril, T., Terez, E. I., Terez, G. A., Gushchin, G. K., Abakumova, G. M., Gorbarenko, E. V., Tsvetkov, A. V., Laulainen, N. 2009. Global dimming and brightening versus atmospheric column transparency, Europe, 1906–2007. *Journal of Geophysical Research-Atmospheres*, **114**, 1–17.

III.   Kannel, M., Ohvril, H., Okulov, O. 2012. A shortcut from broadband to spectral aerosol optical depth. *Proceedings of the Estonian Academy of Sciences*, **61** (4), 266–278.

IV.   Kannel, M., Ohvril, H., Okulov, O., Kattai, K., Neiman, L. 2014. Spectral aerosol optical depth prediction by some broadband models. Validation with AERONET observations. *Proceedings of the Estonian Academy of Sciences*, **63** (4), 404–416.

Author's contribution

The publications that the dissertation is based on are a result of a collective effort with significant contribution from all of the authors.

The author's contribution to the articles I, III and IV is implementation of main ideas of the AOD parameterizations/models, preparation of initial data, elaboration of techniques and methods for further analysis, comparison of results obtained using different AOD models by different authors. The author's contribution includes submission and editing of the manuscripts.

The author's contribution to the article II is expressed by Section 11: "Transition from p_2 to AOD500", representing a practical application of column broadband transparency coefficient.

The author also contributed to a number of conference reports and papers in local collections listed below (V–XI).

Other publications of the dissertant

V.   Kannel, M., Ohvril, H., Okulov, O., Teral, H. 2006. A simple broadband parameterisation of spectral aerosol optical depth. Conference on Visibility, Aerosols, and Atmospheric Optics; Vienna, Austria; September 3–6, 2006, 36.

VI. Ohvril, H., Teral, H., Neiman, L., Kannel, M., Uustare, M., Tee, M., Russak, V., Okulov, O., Kallis, A., Ohvril, T., Terez, E., Terez, G., Gushchin, G., Abakumova, G., Gorbarenko, E., Tsvetkov, A., Laulainen, N. 2009. Global dimming/brightening versus atmospheric column transparency, Europe, 1906–2007. In: Atmospheric Studies by Optical Methods: 36 Annual European Meeting on Atmospheric Studies by Optical Methods. Kyiv, 15–15.

VII. Окулов, О., Охвриль, Х., Тераль, Х., Нейман, Л., Каннель, М., Уустаре, М., Тее, М., Руссак, В., Йыевеэр, А., Каллис, А., Охвриль, Т., Терез, Э. И., Терез, Г. А., Гущин, Г. К., Абакумова, Г. М., Горбаренко, Е. В., Цветков, А. В., Лаулайнен, Н. 2009. Всемирное потемнение/осветление и прозрачность толщи атмосферы, 1906–2007. В сборнике тезисов: Международрородный симпозиум стран СНГ «Атмосферная радиация и динамика» (МСАРД-2009). Санкт Петербург, 22–26 июня 2009, с. 105–106.

VIII. Kannel, M., Ohvril, H., Okulov, O. 2011. Otsetee aerosooli laiaribaliselt optiliselt paksuselt spektraalsele. Jaak Jaagus (Toim.). Publicationes Instituti Geographici Universitatis Tartuensis (195–216). Tartu Ülikooli Kirjastus.

IX. Kannel, M., Ohvril, H., Okulov, O. 2011. A shortcut from broadband to spectral aerosol optical depth. In: Sodankylä Geophysical Observatory Reports: 38th annual European Meeting on Atmospheric Studies by Optical Methods, Siuntio, Finland, 22.–26.08.2011. Enell, C.-F., (38th Annual European Meeting on Atmospheric Studies by Optical Methods Siuntio, Finland, 22–26 August 2011 Abstract book), 25.

X.   Ohvril, H., Kannel, M., Okulov, O., Kattai, K. 2013. Spectral Aerosol Optical Depth Prediction with Some Broadband Models. Validation with AERONET Observations. In: Proceedings: INTERNATIONAL SYMPOSIUM "ATMOSPHERIC RADIATION and DYNAMICS" (ISARD – 2013), Saint-Petersburg-Petrodvorets, 24–27 June 2013. Saint-Petersburg, 2013, 97–98.

XI. Ohvril, H., Neiman, L., Kannel, M., Kattai, K., Keernik, H., Tee, M., Russak, V., Okulov, O., Jõeveer, A., Kallis, A., Ohvril, T., Terez, E., Terez, G., Gushchin, G., Abakumova, G., Gorbarenko, E., Laulainen, N. 2015. European column transparency, 1906–2014. In: Program: Atmospheric radiation and dynamics (ISARD-2015), Saint-Petersburg-Petrodvorets, June 23–26, 2015. Saint-Petersburg, 49–50.

ACRONYMS

AERONET	Aerosol robotic network
ESR	European skynet radiation network
RIMA	Iberian network for aerosol measurements
MODIS	Moderate resolution imaging spectroradiometer
BSRN	Baseline surface radiation network
AITC	Atmospheric integral transparency coefficient
AOD	Aerosol optical depth
BAOD	Broadband aerosol optical depth
COD	Cloud optical depth
TOD	Total optical depth
TOA	Top of atmosphere
CDA	Clean and dry atmosphere
GPS	Global positioning system
TST	True solar time
SDI	Solar direct irradiance
FMF	Fine mode fraction
RMSD	Root mean square deviation
MARD	Mean absolute relative deviation
MBD	Mean bias deviation
FOV	Field of view

1. INTRODUCTION

Aerosol spectral optical depth, AODλ, is a central parameter for description of column aerosol content and column optical properties including rate of atmospheric turbidity. From the 1990s, after successful start of US NASA programs AERONET, TerraMODIS and AquaMODIS, this parameter became essentially more available to a wide scientific community (Holben *et al.*, 1998; Toledano *et al.*, 2007). However, continuous spectral measurements remain much sparser than the broadband pyrheliometric ones, even today. The main reason of that arises from the high initial cost of solar photometers and their expensive regular servicing (*e.g.* annual filter changing and recalibration, preferably at mountain locations with cloudless sky, high sun and very clear, stable atmosphere). As a result, not every observational site can be equipped with such instrumentation. Besides that, it is of great interest to utilize the available pyrheliometric measurements to derive AODλ for pre-1990 years when the photometric network was extremely sparse.

There are also two other practical reasons for AODλ proxy, mainly broadband estimations: (a) quality inspection of recently measured AODλ time series by an automated solar photometer – when the recorded values afterwards seem too large (overestimated for a certain period), a doubt always arises about an undesirable object (insect, spider's thread, trash, etc) dwelling on or inside the instrument's tube; (b) a quick AODλ estimation for correction of satellite remotely sensed data for regions or moments where/when spectral solar observations are not available but the broadband ones are.

Several AODλ broadband models can be found from an extensive literature survey. The high-performance models are laborious for processing large amounts of data or they require either special or very accurate input quantities. However, there are other models which, especially for physical climatology, allow easy programming with no need of ancillary meteorological input data. Continuing activity in development and modification of simple broadband models indicates that such approaches do correspond to practical needs.

The objective of this thesis is to present:
a) analysis of already existing AODλ calculation broadband-models and their enhancements;
b) creation of a new AODλ calculation model;
c) creation of an enhanced database of broadband-spectral and humidity measurements for testing AODλ calculation models;
d) performance testing of AODλ calculation models;
e) creation and implementation of a new algorithm for cloud screening of raw direct solar irradiance data;
f) an additional AERONET data verification for 2002–2011.

2. SOME TERMS AND DEFINITIONS

In this chapter the basic atmospheric optical terms, definitions and laws are introduced. Also an interpretation of atmospheric structure is given.

2.1. Aerosol optical depth and the Ångström wavelength exponent

In general, optical depth, or optical thickness, is a measure of turbidity (opacity) of an environment (medium). It expresses the part of light removed from a beam by scattering and absorption during its path through an environment.

If $I_{0\lambda}$ is the intensity (strictly speaking, the flux density) of radiation, at wavelength λ, before entering a medium, and I_λ is the intensity after leaving it, then the optical depth δ_λ is defined by the Bouguer-Lambert law:

$$I_\lambda = I_{0\lambda} e^{-\delta_\lambda} .$$
(2.1)

Optical depth is dimensionless, in a general approach it is a monotonically increasing function of path length, and reaches zero as the path length becomes zero.

In atmospheric optics, however, optical depth of the entire atmospheric layer corresponds to a unit relative airmass, $m = 1$, from Earth's surface to outer space. If $S_{0\lambda}$ is the intensity of solar radiation at the top of the atmosphere, and S_λ its counterpart in the bottom, at the underlying surface, then the optical depth δ_λ is given by

$$S_\lambda = S_{0\lambda} e^{-m\delta_\lambda} ,$$
(2.2)

here $m = 1$ refers to a vertical path, in case of slant path, $m > 1$.

The simplest initial approach to modeling atmospheric transparency and turbidity is to break the problem down into components that can be treated more or less as separate items. The optical depth of the atmosphere can be divided into several (usually to three) components: a clean and dry (*i.e.* ideal) atmosphere, water vapor and aerosol particles.

One of the first researchers of the atmospheric spectral aerosol optical depth was Swedish physicist Anders Knutsson Ångström (1888–1981) who also investigated solar activity problems and solar constant. Ångström defended his PhD in 1916 at the University of Uppsala. He was a member of International Radiation Committee since 1923, later a Docent at the University of Stockholm. His father Knut Johan Ångström (1857–1910) developed pyrheliometer and many other actinometric instruments. Anders Knutsson Ångström's grandfather

was Anders Jonas Ångström (1814–1874), known by a special unit of length, angstrom, $1Å = 10^{-10}$ m (Nordisk Familjebok, 1934).

Light scattering from different particles depends on particles size. Observations of aerosol size distributions have shown that they could be described with five modes by their diameter (Seinfeld and Pandis, 2006):
(a) nucleation mode, $d = 3 – 25$ nm,
(b) Aitken's mode, $d = 30 – 80$ nm,
(c) accumulation mode, $d = 0.1 – 1$ μm,
(d) coarse mode, $d > 1$ μm,
(e) giant particles mode, $d > 10$ μm.

Mostly, particles from accumulation mode dominate in the atmosphere. They grow from the nucleation and Aitken's mode, originating from biomass or fuel burning and often causing extensive degradation of both, horizontal and column transparency.

Concerning Eastern Europe, the last statement is impressively expressed during hazy dry summers, when the weather conditions favor large-scale forest and peat fires. During this kind of years (1972, 2002, 2010) hot, smoke-polluted air also arrives Estonia from southern and eastern directions (Chubarova *et al.*, 2011a, 2011b; Kattai, 2014; Toll *et al.*, 2014, 2015).

Anders Ångström (1929, 1930) is widely considered as a developer of the exponential law for presentation of spectral aerosol optical depth $\delta_{\lambda,aer}$ as a monotonously decreasing function of wavelength:

$$\delta_{\lambda,\,aer} = AOD\lambda = \beta\lambda^{-\alpha},$$ (2.3)

here, β is the turbidity coefficient and α the wavelength exponent.

However, a historical note is necessary. The matter is that strictly speaking, Anders Ångström himself (1929) cited Lindholm (Ångström, 1929, page 156) and Lundholm (page 159), who studied the absorption in thin layers of soot and in the particles of dust in the atmosphere (1912, in Uppsala?), and found that the absorption coefficient could be expressed in the form of (2.3). My supervisor (H. Ohvril) told that he wrote in 2004 to the Uppsala University Library with petition to find the publication (in Swedish) by Lindholm or Lundholm, but he got an answer that the citation by Ångström is not complete and this kind of publication was not found. Unfortunately the problem about priority for first using the power law formula for attenuation of spectral radiation was also raised by Schuster *et al*. (2006) who reported that they did find references to a F. Lindholm in Uppsala in Science Abstracts, but none of the abstracts mention the spectral dependence of particulate extinction. Subsequent references to Lindholm or Lundholm on this topic have not appeared in the atmospheric literature. For that, Anders Ångström, for use of Eq. (2.3) in his four classic papers, has deserved the honor to be named as the author of this relationship.

Evidently, aerosol optical depth is caused not only by absorption but also by scattering of radiation. Scattering is usually the main reason of attenuation of solar radiation.

The turbidity coefficient β can be interpreted as a non-dimensional scaling factor, proportional to column concentration of particles, and the wavelength exponent α as a shaping constant for a given column composition of particles. For sake of clarity, aerosol optical depth is often written as AODλ which also is, as noted above, a non-dimensional physical parameter. However, λ has a dimension of length, for that using different values for α, the Eq. (2.3) becomes physically incorrect. That discrepancy was resolved by Shifrin (1995) who added a base wavelength λ_0 into the source equation (2.3):

$$\mathbf{AOD\lambda = \beta \left(\frac{\lambda}{\lambda_0} \right)^{-\alpha}}, \qquad (2.4)$$

according to Ångström, $\lambda_0 = 1\ \mu m$.

Anders Knutsson Ångström (1888–1981) himself found that the average value of wavelength exponent is, α = 1.3. The limits of α variation he found to be between 1.0 and 1.5. According to later investigations (Qiu, 2001), the wavelength exponent can vary in a range of $-0.5 < \alpha < 2.5$.

Although below, in Sections 5.3, 6.2 and 6.3, I'll present some criticism in regard to the Ångström formula, it remains a useful tool for extrapolating AODλ through the shortwave spectral region, *i.e.* for transition from one λ to another (Schuster *et al*., 2006).

Using additional presumptions (like the Junge size distribution of particles), the Ångström wavelength exponent can be qualitatively related to particles size distribution. This is one of benefits of the Ångström wavelength exponent. The smaller particles, like molecules and clusters (radii < 0.5 μm), correspond to higher values of the wavelength exponent. The term "higher" has been evaluated as α > 2 (Schuster *et al*., 2006), however, according to current analysis of the Tõravere AERONET data, it is less, approximately, α > 1.5.

Scholar facts about the Ångström wavelength exponent:

a) a pure molecular (Rayleigh) scattering causes increase of wavelength exponent up to its maximal value, α = 4;

b) smaller values of Ångström wavelength exponent, α < 1, indicate size distributions dominated by coarse mode aerosol particles (radii > 0.5 μm) that are typically associated with old smoke, dust, sea salt, fog, cloud particles;

c) higher values of Ångström wavelength exponent, α > 1.5, indicate size distributions dominated by fine and accumulation mode particles (radii < 0.5 μm) that are usually associated with urban pollution and fresh biomass smoke;

d) for the Junge distribution, AODλ has also a smooth decreasing trend when wavelength λ increases.

On the other hand, studying observed values of AODλ as functions of wavelength λ, the Ångström's law is never exactly fulfilled. For that, experimental values of α depend on a spectral region used for calculations. Sometimes, especially for longer wavelengths, λ ≈ 1 μm, a course of AODλ is exceptionally increasing giving negative values for the wavelength exponent, as mentioned by Qiu (2001). Along this dissertation, four wavelengths, λ = 440, 500, 675, and 870 nm, are used for calculation of α and no negative values have been met.

It follows from (2.4) and the Ångström's assumption $\lambda_0 = 1$ μm, that $\beta =$ AOD1000. However, intensity of solar spectrum is weak in the region of 1000 nm, for that the wavelengths λ = 500 or λ = 550 nm are usually chosen. The AERONET team prefers 500 nm, this is also the main reason to tune models to this wavelength.

Figure 2.1 gives a visual review on evolution of AOD500 as measured by the AERONET Tõravere photometer during 2002–2004, *i.e.* during the first three years after its installation. Our first model for AOD500 calculations was derived according to these measurements.

Usually, AOD500 < 0.3 in Estonia. If larger values appear during the first half of year, they are usually caused by inflow of polluted air from southern and eastern directions. Later, during summer, local forest and bog fires can also raise turbidity in Estonia.
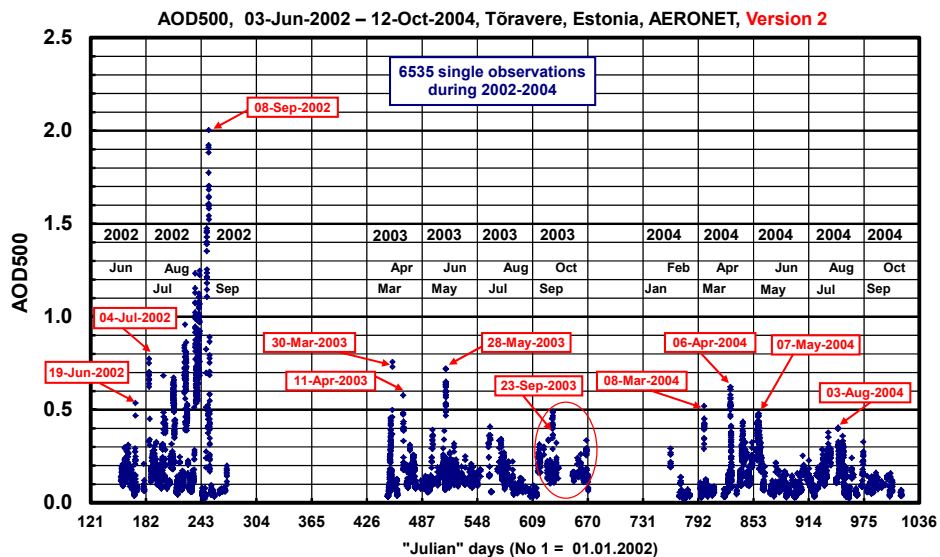
Fig. 2.1. Evolution of spectral aerosol optical depth, AOD500, at Tõravere, Estonia, as measured by the AERONET photometer during 2002–2004. The highest values, due to extended forest and bog fires, meet in late summer of 2002. The peak value, AOD500 = 2.0, occurred on 08-Sep-2002. During a period from 06-Sep-2003 to 30-Oct-2003 the values of AOD500 (exerted by ellipse) were ungroundedly high, apparently due to an artificial restriction in the field of view of the photometer.

Because both tubes of the AERONET photometer are open, insects can enter there and can restrict passage of solar radiation. These undesired events, in the absence of a parallel reference photometer, can be discovered only by calculation of a proxy AODλ time series, *e.g.* estimations on the basis of broadband direct irradiance. Series of such false turbidities occurred from 06-Sep-2003 to 30-Oct-2003, corresponding points in Fig. 2.1 are surrounded by an oval, in more details they will be discussed below, in Section 3.2.

Evolution of the Ångström wavelength exponent, for years 2002–2004, is given in Fig. 2.2.
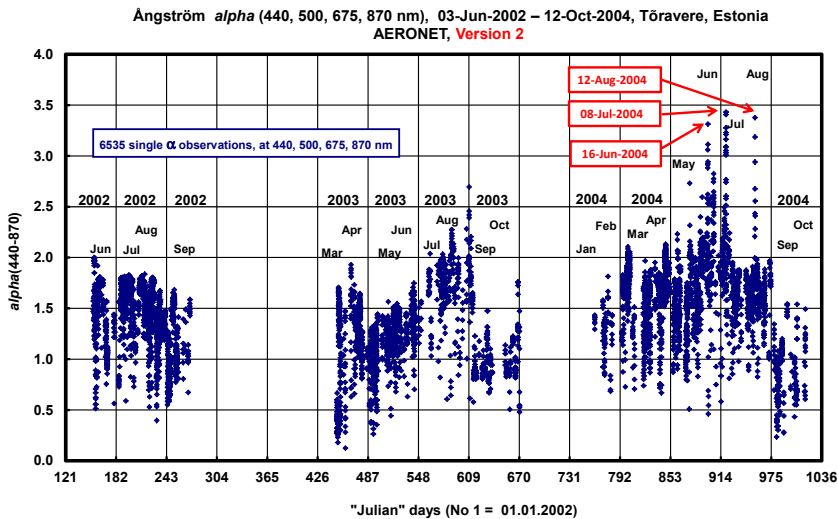
Fig. 2.2. Evolution of the Ångström wavelength exponent at Tõravere during 2002–2004, as presented by AERONET. The highest values, $\alpha > 3$, occurred on 16-Jun, 08-Jul, and 13-Aug-2004. These days are specially indicated.

As mentioned above, no negative α values have been met. The exceptional highest values, when $\alpha > 3$, occurred during three days, when the aerosol particles were washed out by rain and fog. Respectively, during these days the AOD500 was very low:

a) 16-Jun-2004, AOD500 = 0.036, α = 3.3;
b) 08-Jul-2004, AOD500 = 0.035, α = 3.4;
c) 12-Aug-2004, AOD500 = 0.032, α = 3.4.

The lowest Ångström exponent, α = 0.124, occurred on 04-Apr-2003 and apparently corresponds to domination of particles from the coarse mode. From a climatological point of view, April in Estonia is a transitional month when there is neither snow nor lush fresh vegetation on the ground. A lot of coarse particles

15

are produced by breakup and suspension of bulk materials by the wind, *e.g.* sea salt and soil dust. This is also a month when warmer air temperatures and a higher number of frost-free days promote beginning of plant growth and pollen grains production.

Thus, April in Estonia should be also characterized with several types of biological aerosol particles – bacteria, fungal spores and pollen grains which fall within coarse size range. According to Matthias-Maser & Jaenicke (2000) the bioaerosols in Germany reach to almost a quarter of the total aerosols in an urban/rural influenced region. However, the authors did not find strong characteristic annual variation, neither in number, in volume, nor in percentage concentration of bioaerosols. The presumption that in winter the concentration of bioaerosols would decrease was not confirmed. The production mechanisms of bioaerosols in winter (re-flotation, decaying processes) are more pronounced than expected. But the authors concluded that rural influence leads to an increase of large and giant bioaerosol particles (pollen, spores), and urban influence increases microbial aerosol (bacteria).

Returning to Estonia and thinking about future aerosol investigations, more measurements of different aerosol types in the different regions (*e.g.* Tartu, Tõravere, Tahkuse, Järvselja) are necessary to get a realistic estimation of seasonal abundance and diversity of bioparticles and their contribution to physical properties of the total aerosol.

Note that the low Ångström exponent values are not necessarily linked to high turbidity, *i.e.* to high AOD500 or β = AOD1000. The last ones act as scaling not shaping factors.

2.2. Broadband parameters of atmospheric column transparency

Routine measurements in classical actinometry are mainly broadband observations. Continuously, up to now, one of the most important observed broadband quantities is direct solar beam at normal incidence, or simply, direct irradiance. Archived data of this quantity allow retrieval of time series of five different parameters of column transparency and turbidity:

(a) broadband (integral) transmittance or transmission coefficient, τ_m;
(b) broadband (integral) relative attenuation coefficient, $1 - \tau_m$;
(c) broadband (integral) optical depth of the atmosphere, δ_m;
(d) the atmospheric integral transparency coefficient (AITC), p_m;
(e) the Linke turbidity factor, $T_{L, m}$.

The well-known Bouguer-Lambert law links these parameters (Ohvril *et al.*, 2009):

$$S_m = S_0 \tau_m = S_0 e^{-m\delta_m} = S_0\, p_m^m = S_0 e^{-m\,\delta_{CDA,m}\,T_{L,m}} . \qquad (2.5)$$

Here: S_m – the measured broadband solar irradiance at optical mass m,

S_0 – the extraterrestrial broadband solar irradiance, its average value, the "solar constant" is 1.367 kWm^{-2},

$\delta_{CDA,\,m}$ – the optical depth of an ideal, *i.e.* clean and dry atmosphere (CDA).

Note again that optical depths, δ_m and $\delta_{CDA,\,m}$, correspond to a unit optical path, $m = 1$, but in the direction of the actual position of the sun, whose elevation is characterized with actual optical mass m. For that, the term "optical density" would better reflect their content than "optical depth".

The five broadband parameters, (a) τ_m; (b) $1 - \tau_m$; (c) δ_m; (d) p_m; (e) $T_{L,\,m}$, represent transparency or turbidity, averaged over the entire solar spectrum. These parameters depend, according to the Forbes effect, on solar elevation, even in the case of a stationary and azimuthally homogeneous atmosphere.

To eliminate the Forbes effect, the generally accepted practice is to reduce broadband characteristics of transparency or turbidity from the actual optical air mass m to a standard air mass, mainly to $m = 2$ (solar elevation $h \approx 30°$). Historically, several other values of m were used: $m = 1, 1.5, 2,$ and 3. However, for control measurements, the case $m = 1$ (the sun at the zenith) is not available at most radiometric stations, while $m = 3$ correspond to a solar elevation that is too low (19.3°), when often the sun may be screened by clouds, trees, or other obstructions. Of the remaining values, $m = 1.5$ and $m = 2$ the last one is preferred as it is an integer.

It seems that quite successful methods have been developed to attempt reducing the observational data via the AITC p_m. For this reason, the AITC p_2 is the central parameter in actinometric studies. Two different methods to calculate the AITC p_2 have been used. In the case of the Estonian databases, the coefficient p_m was first calculated. Transition from p_m to p_2 was then performed as a second step (Myurk and Okhvril, 1990; Ohvril *et al.*, 1999):

$$p_2 = p_m \left(\frac{2}{m}\right)^{\frac{\log p_m + 0.009}{\log m - 1.848}} . \qquad (2.6)$$

In the case of Moscow and Ukrainian databases, coefficient p_2 was, until the 1990s, calculated directly from measured direct irradiance from the actinometric network of the former USSR using special transformation tables, and later, by a formula developed by Evnevich and Savikovskij (1989):

$$p_2 = \left(\frac{I_m\, d^2}{1.367} \right)^{\frac{\sin h + 0.205}{1.41}}, \qquad (2.7)$$

where d is the actual Earth-Sun distance in astronomical units. Intercomparison of transformation formulas (2.6) and (2.7) showed comparable accuracy for the calculation of p_2 (Ohvril and Okulov, 1996; Ohvril *et al.*, 1999, Okulov *et al.*, 2001).

The AITC p_2 also allows easy calculation of the Linke turbidity factor, $T_{L,\,2}$ (Ohvril *et al.*, 1999):

$$T_{L,\,2} = -23 \log p_2 . \qquad (2.8)$$

The last formula (2.8) contains the assumption that the AITC for an ideal atmosphere, $p_{CDA,\,2} = 0.9047 \approx 0.905$. To derive an expression for the atmospheric optical depth, δ_2, an evident equality from Eq. (2.5) can be used:

$$e^{-\delta_m} = p_m , \qquad (2.9)$$

for $m = 2$, the logarithm gives:

$$\delta_2 = -\ln p_2 , \qquad (2.10)$$

and substitution into Eq. (2.8):

$$T_{L,\,2} = -23 \times 0.4343 \ln p_2 = -9.989 \ln p_2 \approx -10 \ln p_2 = 10\,\delta_2, \quad (2.11)$$

or

$$\delta_2 = 0.1\, T_{L,\,2} . \qquad (2.12)$$

Summarizing, the five parameters of atmospheric transparency and turbidity for the most important special case, $m = 2$, have simple mathematical relationships between each other. For analysis of time series of atmospheric transparency or turbidity, it is usually sufficient to use one of them, preferably the AITC p_2, because it allows an easy transition to other solar elevations, *i.e.* change of m.

2.3. General structure of broadband AOD models

There are three main input parameters for AODλ models.

The first one describes column attenuation of the broadband (panchromatic) direct solar beam: *e.g.* broadband transmittance (τ_m), Bouguer coefficient of column transparency (p_m), column broadband optical depth (δ_m), Linke turbidity factor ($T_{L,\,m}$) – they all are equal, linked by the Bouguer-Lambert exponential

law (Eq. 2.5). But p_2 is somewhat special because its available transitions from $m = 2$ to any other m. For this reason, the p_2 is the input parameter of several models in this study.

The second required input parameter to simple models is column humidity (water vapor) content. Its unit, "mass per unit area", is in practice usually given as the thickness of the layer of liquid water: 1 mm corresponds to 1 kg m^{-2} and 1 cm to 1 g cm^{-2}.

The third parameter, the Ångström wavelength exponent, α, is rather optional. As explained above, it is closely linked to the size distribution of aerosol particles, provided that the size distribution, in part, follows a power law (Liou, 2002). However, the column aerosol particles are in permanent change, expressing deviations from the power law. Thus the wavelength exponent is really an unstable parameter, which has different values for different parts of the solar spectrum. As it is poorly correlated with AODλ, its use in atmospheric optical models is questionable.

2.4. A three-layer structure of the column broadband transmittance

Spectral content of direct solar beam reaching the Earth surface is not equal during a day. Broadband characteristics, therefore, depend on solar elevation even in the case of stationary and azimuthally homogeneous atmosphere, causing the Forbes effect – virtual diurnal variation of atmospheric broadband optical characteristics (Ohvril *et al.*, 1999, 2009).

For this effect, even though spectral optical depth, and related spectral optical parameters (spectral transmittance, spectral Bouguer coefficient etc), are independent of optical mass m, their broadband counterparts are not. Although there are no good solutions for strict transformation of column broadband optical parameters from one solar elevation to another, multiannual pyrheliometric time series, recorded in various stations, mainly on the territory of the Former USSR, have stimulated creation of corresponding semi-empirical methods. Historically, a destination optical mass, $m = 1$, was initially chosen (Kalitin, 1938). However, for reference measurements the case, when the sun is at the zenith, is not available at most radiometric stations. The next integer number, $m = 2$ (solar elevation angle about 30°) was further preferred as a standard one in interpretation of pyrheliometric observations. Concerning aerosol optics, the same reference air mass is also recommended (Gueymard and Kambezidis, 1997). As shown above, a set of simple formulas (Eqs. 2.5–2.12) links different broadband optical parameters.

In this study, further limitation for the structure of extinction of broadband direct solar beam by three processes or substances is made:

(a) an ideal or clean and dry atmosphere (CDA), which includes Rayleigh scattering, absorption by ozone (O_3) and nitrogen dioxide (NO_2);

(b) integrated column water vapor or precipitable water, W;

(c) atmospheric aerosol particles.

Denoting their transmittances by $\tau_{CDA, m}$, $\tau_{W, m}$ and $\tau_{aer, m}$, respectively, it is of considerable computational convenience to express the incident broadband beam irradiance at normal surface, "beam irradiance", S_m, as a direct product of individual beam transmittances which is equal to a presumption of three successive extinction layers (Gueymard, 1998; Molineaux *et al.*, 1998):

$$S_m = S_0 \tau_{CDA,m}\, \tau_{W,m} \tau_{aer,m}\,, \tag{2.13}$$

where S_0 is the extraterrestrial broadband irradiance at the actual Sun-Earth distance, its average value, the "solar constant" is 1.367 kWm^{-2} (Lenoble, 1993).

On the other hand, use of broadband total transmittance, τ_m, and the Bouguer coefficient of transparency, p_m (Kondratyev, 1969):

$$p_m = \left(\frac{S_m}{S_0}\right)^{\frac{1}{m}} \tag{2.14}$$

enables to express S_m as

$$S_m = S_0 \tau_m = S_0 p_m^m\,, \tag{2.15}$$

which gives for broadband aerosol transmittance

$$\tau_{aer,m} = \frac{p_m^m}{\tau_{CDA,m}\tau_{W,m}}\,. \tag{2.16}$$

By similarity with Bouguer formula which, strictly speaking, is valid only for monochromatic beam, the following equation defines broadband aerosol optical depth, BAODm, which we denote in formulas by $\delta_{aer, m}$ (Gueymard, 1998):

$$\tau_{aer,m} = \exp\left(-m\delta_{aer,m}\right)_{.} \tag{2.17}$$

Combining this definition (2.17) with (2.16) one can obtain for the BAODm:

$$\delta_{aer,m} = -\frac{1}{m}\ln\tau_{aer,m} = -\frac{1}{m}\ln\frac{p_m^m}{\tau_{CDA,m}\tau_{W,m}}, \qquad (2.18)$$

$$\delta_{aer,m} = -\ln p_m + \frac{1}{m}\ln\tau_{CDA,m} + \frac{1}{m}\ln\tau_{W,m}. \qquad (2.19)$$

The BAODm is equal to the Unsworth-Monteith turbidity coefficient (Unsworth-Monteith, 1972; Gueymard, 1998). This parameter can be used to estimate aerosol contribution in attenuation of broadband direct beam, in addition to a clean-wet atmosphere, consisting of CDA and water vapor only (Kambezidis *et al.*, 1998).

Continuing further with $m = 2$, it has for the BAOD2:

$$BAOD2 = \delta_{aer,2} = -\frac{1}{2}\ln\tau_2 + \frac{1}{2}\ln\tau_{CDA,2} + \frac{1}{2}\ln\tau_{W,2} =$$

$$= -\ln p_2 + \ln p_{CDA,2} + \frac{1}{2}\ln\tau_{W,2}. \qquad (2.20)$$

Calculation of the BAOD2 is now reduced to availability of three broadband quantities:

(a) τ_2 or p_2 as results of broadband direct beam observations of S_m and following recalculations of τ_m to τ_2 or p_2, in order to go from optional air mass m to a fixed one, $m = 2$;

(b) $\tau_{CDA,\,2}$ or $p_{CDA,\,2}$ which should be calculated from models of ideal atmosphere, CDA;

(c) $\tau_{W,\,2}$ which first needs estimation of column precipitable water at zenith direction, W, and, as a second step, calculation of transmittance of column water vapor for entire slope column, $m = 2$.

Concerning broadband coefficients of transparency, $\tau_{CDA,\,2}$, of a CDA, they depend, besides of molecular (Rayleigh) scattering, on absorption by trace gases, mainly by O_3 and NO_2. For that, column amounts of trace gases should be first estimated.

3. THE DEVELOPMENT AND SHORTCOMINGS OF EARLY MODELS

This chapter reviews concepts which formed the basis of the AODλ estimation using broadband models: the history of their development, model components, testing and validation. In the very beginning, the necessity in a new AODλ estimation model raised when Qiu's model (2001), which uses an equivalent wavelength, λ_E, appears to be non-applicable for Estonian conditions because of an atypical behavior of the λ_E. During the further study, four separate models were developed, two of them were chosen for comprehensive final testing. All our models, except the last one were derived from a classic Moscow University AOD550 model.

3.1. The first AOD500 model

The first AOD500 model was expressed by the next formula (Kannel *et al.*, 2007):

$$\mathbf{AOD500 = 1.1^{\alpha} \big\{ \ (-0.7199\,\alpha - 0.6246)W^{(-0.0173\alpha - 0.0039)}\ln(p_2) +}$$

$$\mathbf{+ (-0.1414\,\alpha - 0.0925)W^{(-0.0243\alpha + 0.1646)} \ \big\}} \tag{3.1}$$

This result was derived from a Moscow University broadband AOD550 model (Tarasova and Yarkho, 1991a, 1991b). The Moscow model determinates AOD550 from ground-based measurements of solar direct irradiance (SDI) and column precipitable water, W, in cm. It assumes fulfillment of the Ångström formula (2.4) and allows changing the wavelength exponent, α. In total, the Moscow model consists of 13 analytical equations.

The Moscow model also assumes a fixed columnar O_3 content, 0.3 cm, while none of a NO_2 column is considered. Transition from the basic AOD550 to any other wavelengths, AODλ, is available using the Ångström formula (2.4). Moscow colleague, Yarkho-Gorbarenko used her model to analyze spatial and temporal variability of the AOD550 according to the broadband observations from 155 actinometric stations on the territory of the former USSR (Gorbarenko, 1997).

The Moscow model was chosen because of its relative simplicity and the changeability of the Ångström wavelength exponent, actually the last possibility is exceptional among the AODλ models. However, in order to create a more handy engineering method for quick AODλ determinations under Estonian summer conditions, three principal changes in the model were made.

First, replacement of broadband direct irradiance (S_m) to its counterpart, the AITC p_2, was made. The last corresponds to the Bouguer-Lambert coefficient of column transparency at optical mass $m = 2$ (solar elevation $\approx 30°$):

$$p_2 = \left(\frac{S_2}{S_0}\right)^{\frac{1}{2}}, \qquad (3.2)$$

where S_2 is the broadband direct irradiance at $m = 2$ and S_0 is direct irradiance at the top of the atmosphere (*i.e.* the solar "constant" corrected for the Sun-Earth distance). From a physical point of view, this replacement was made because p_2 is a more general parameter compared to S_m.

Second, fixing Ångström's α in Tarasova-Yarkho model, applying least-squares method between the limits of precipitable water of $1 < W < 60$ mm and using the Ångström formula the AOD550 output was transferred to $\lambda = 500$ nm (*i.e.* AOD500) allowing to present the Moscow model only by a single formula:

$$\mathbf{AOD}(\alpha,500) = (1.1^\alpha)\Big\{(-0.7578\alpha - 0.6575)W^{(-0.0173\alpha-0.0039)}\ln(p_2) +$$
$$+ (-0.1488\alpha - 0.0974)W^{(-0.0243\alpha+0.1646)}\Big\} \qquad (3.3)$$

Third, in order to achieve a better agreement with the AERONET observations at Tõravere during 2002–2004, the AOD500 output was reduced by 5%.

These three changes led to a single expression (3.1) that depends on three parameters: α, W (cm) and p_2.

For an atmosphere with a fixed wavelength exponent, *e.g.* $\alpha = 1.3$, which is often used (Liou 2002), the three-parameter expression (3.1) changes to a simple, two-parameter one:

$$\mathbf{AOD}(1.3;\ 500) = -1.766\,W^{-0.0264}\ln(p_2) - 0.313\,W^{0.133}, \quad (3.4)$$

or fixing $\alpha = 1.5$, which was used in a numerical experiment to "predict" the AOD500 observations at Tõravere, Estonia during summer months, June, July, August, 2002–2004:

$$\mathbf{AOD}(1.5;\ 500) = -1.967W^{-0.0298}\ln(p_2) - 0.351W^{0.128}. \quad (3.5)$$

According to the linear approximation in Fig. 3.1, $y = 1.023\ x$, the predicted values of the AOD500 overestimate the reference AERONET values by only 2.3%.
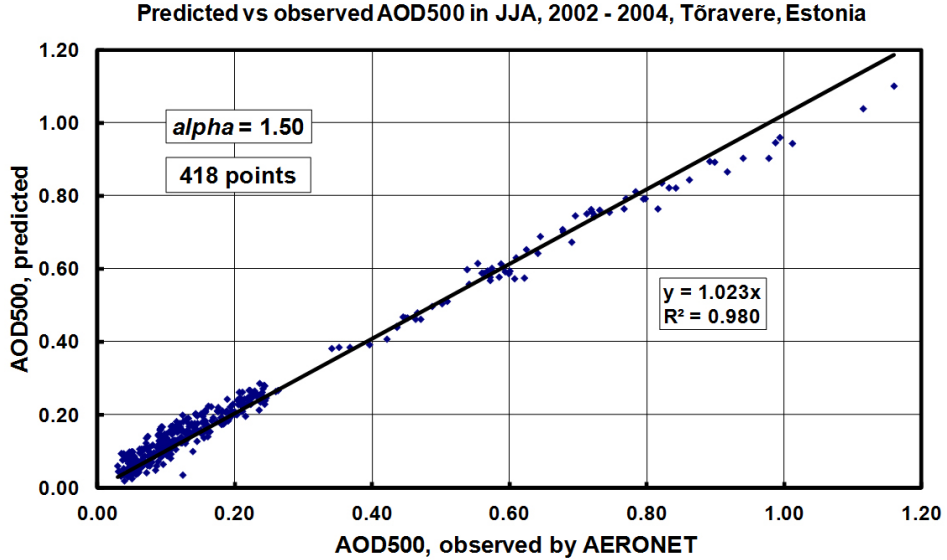
Predicted vs observed AOD500 in JJA, 2002 - 2004, Tõravere, Estonia

Fig. 3.1. Modeled versus measured AOD500 for summer (June, July, August, 2002–2004) at Tõravere, Estonia. Equation (3.5) and a fixed Ångström wavelength exponent, $\alpha = 1.50$, are used for calculation of all 418 points. Trendline, $y = 1.023\,x$, indicates that the model overestimates slightly, by 2.3% the AERONET AOD500 values.

Formulas like (3.4) and (3.5) can be used for transition from column broadband transparency p_2 and column precipitable water, W (in cm), to spectral AOD500 in conditions when the Ångström exponent can be expressed with a stable climatological value.

3.2. Revised version of the AOD500 model

The first model (Eq. 3.1) was derived using AERONET observations at Tõravere during 2002–2004 and it was tuned to get a good agreement in Estonian conditions (artificial lowering by 5%). Observations during the next two years revealed also a necessity to better consider circumsolar radiation.

The matter is that the actinometer AT-50 which measures the SDI, has a full field of view (FOV) ~10 degrees. However, the solar disk fits only at a spatial angle of 32 arc minutes (~0.5 degrees). Thus, in turbid days when aerosol optical depth is high, the circumsolar, "parasitic" irradiance around the solar disc is also remarkable. Due to such a wide spatial opening angle of the AT-50 instrument, it considers this circumsolar irradiance as a part of direct irradiance. If not corrected, this imperfection of the instrument creates a false comprehension about better column transparency and therefore lowers AODλ values. Consequently, in order to correct the imperfection, estimated AODλ values

should be increased, whereby the lower values (cleaner atmosphere) should be raised less than the bigger values (more turbid atmosphere). The problems associated with circumsolar radiation will be discussed in more details in Section 5.

A decision was made to develop a second, revised version of the model which would better eliminate influence of circumsolar irradiance. Actually, the revision process started from the state of the parameterization of Moscow Uni-versity model (Eq. 3.3).

The most important change in the revised version was addition of a correction factor

$$0.75\, p_2^{-0.4}, \tag{3.6}$$

also artificial constants in (3.1) were eliminated. The final form of the revised model is as follows (Kannel, 2007; Ohvril *et al.*, 2009):

$$AOD\,500 = 0.75\, p_2^{-0.4} \cdot 1.1^{\alpha} \left\{ (-0.7578\,\alpha - 0.6575)\, W^{(-0.0173\,\alpha - 0.0039)} \ln(p_2) + \right.$$
$$\left. + (-0.1488\,\alpha - 0.0974)\, W^{(-0.0243\,\alpha + 0.1646)} \right\} \tag{3.7}$$

Eq. (3.7) is also further known as model T1.

Fixing the Ångström wavelength exponent, the three-parameter expression (3.7) reduces to a two-parameter one. For example, fixing the exponent to a common value, $\alpha = 1.3$:

$$AOD(1.3;\ 500) = p_2^{-0.4} \left(-1.394\, W^{-0.0264} \ln(p_2) - 0.247\, W^{0.133} \right), \tag{3.8}$$

however, for Estonia an all-season exponent is slightly bigger, $\alpha = 1.45$:

$$AOD(1.45;\ 500) = p_2^{-0.4} \left(-1.512\, W^{-0.029} \ln(p_2) - 0.27\, W^{0.129} \right). \tag{3.9}$$

Left panels in Figure 3.2 show an example how the model with fixed α came useful for a visual inspection of AERONET-Tõravere AOD500 products for two years, 2003 and 2005. During 2003, there was an autumn period, 06.09.2003–30.10.2003, when in total 216 AOD500 values were extraordinary large, apparently corresponding to very turbid air, but not supported by low broadband irradiance (*i.e.* characterized with low p_2 values). Analogous situation occurred during 03.09.2005–18.09.2005 when the number of suspicious AERONET observations was 221. Evidently, these questionable observations could appear due to spider webs, insects or other restrictions at the entrance or inside of the AERONET Cimel photometer.
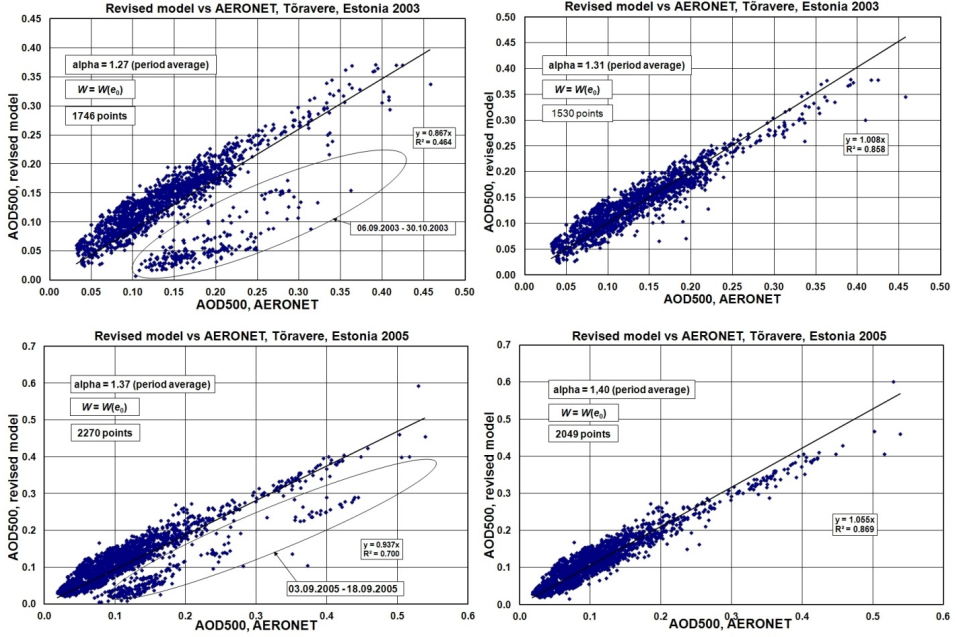
Fig. 3.2. AOD500 from model (Eq. 3.7) vs AERONET observations at Tõravere Estonia. Upper figures represent observations made in 2003, lower figures correspond to 2005. On the left panels, suspicious observations are pointed out by ovals. The suspicious observations are removed on the right panels.

3.3. BAOD versus AOD500

It is obvious that higher BAOD corresponds to higher AODλ. Molineaux *et al.* (1998), referring to Stothers (1996) and references in there, reported about an empirical finding that BAOD is simply equal to the AOD550 multiplied by a certain constant *C*:

$$\textbf{AOD550} = \textbf{\textit{C}} \cdot \textbf{BAOD.} \tag{3.10}$$

This constant, however, is dependent on the optical characteristics of aerosol particles (refractive index, single scattering albedo, phase function, etc) and apparently, on particle size distribution and solar elevation angle. All together, the constant *C* takes a value in a wide range, 1−1.7.

One of the intermediary results of the thesis was to use BAOD for a certain atmospheric mass, $m = 2$ (solar elevation, $h \approx 30°$), which, as already mentioned in Section 2.4, further is indicated by BAOD2. Instead of (3.7) the next formula was derived

$$\textbf{AOD}(\alpha, \textbf{500}) = \textbf{1.1}^{\alpha}\ \textbf{0.943}\ \textbf{\textit{e}}^{0.423\alpha}\ \textbf{\textit{W}}^{-0.02\alpha}\ \textbf{BAOD2,} \tag{3.11}$$

with three input parameters are: a) the Ångström exponent, α; b) precipitable water, W in cm; and c) broadband aeosol optical depth, BAOD2.

However, due to the further uncertainty in the Ångström wavelength exponent (details will be given in Section 6.2) the model (3.11) was abandoned. But, the interim result (3.11) gave an idea to proceed with BAOD2 finding a way for its calculation.

3.4. Further development of the AOD500 model

Let's proceed with Eq. (2.20) for broadband aerosol optical depth at $m = 2$:

$$\text{BAOD2} = -\ln p_2 + \ln p_{\text{CDA},2} + \frac{1}{2}\ln \tau_{W,2}, \qquad (3.12)$$

where p_2 represents the column broadband (panchromatic) transparency coefficient, $p_{\text{CDA},2}$ – broadband transparency coefficient only for an CDA, *i.e.* for an ideal atmosphere, and $\tau_{W,2}$ – broadband transmittance only for precipitable water vapor.

A CDA represents a fictitious (ideal) atmosphere that comprises only the effects of Rayleigh scattering and absorption by the atmospheric gases other than water vapor (Molineaux *et al.*, 1998). According to Gueymard (1998), it is enough to consider only two minor or trace gases, namely O_3 and NO_2 as absorbers of incoming solar radiation. In order to get an imagination about variability of column transparency of ideal atmospheres, with different O_3 and NO_2 contents, numerous runs of Gueymard's (1998) parameterization have been performed. Table 3.1 represents three specific results of them.

Row 1 corresponds to very low trace gases column concentrations: 150 DU (0.15 atm cm) for O_3 and only 0.07 matm cm or 88 pptv for total NO_2 column amount. Here pptv (parts per trillion by volume) $\equiv 10^{-12}$ and "total NO_2" means "tropospheric + stratospheric NO_2".

Row 2 considers typical values for Estonia and the Baltic Sea region: ozone content, 350 DU (0.35 atm cm); total NO_2 column amount 0.16 matm cm ($\equiv$ 0.16 DU) or 200 pptv.

Row 3 represents high column amounts: ozone content, 600 DU (0.6 atm cm), actually never observed over Estonia; total NO_2 column amount 1.2 matm cm ($\equiv$ 1.2 DU) or 1501 pptv corresponds to very polluted industrial/urban areas

Listed above extreme and typical ozone and NO_2 column amounts were acquired from the next publications: Okulov, 2003; Ionov, 2010; Okulov and Ohvril, 2010; Veismann and Eerme, 2011.

Table 3.1. Results of Gueymard's (1998) parameterization runs to obtain broadband column transparencies ($p_{CDA,2}$ and logarithm of it) and transmittances ($\tau_{CDA,2}$) of ideal atmospheres with different O_3 and NO_2 contents

No	O_3 atm cm	NO_2 tropos atm cm	NO_2 stratos atm cm	NO_2 trop+strat atm cm	NO_2 trop+ strat pptv	$p_{CDA,2}$	$\ln p_{CDA,2}$	$\tau_{CDA,2}$
1	0.15	0.000 03	0.000 04	0.000 07	88	0.9081	-0.0964	0.8246
2	0.35	0.000 04	0.000 120	0.000 160	200	0.9042	-0.1007	0.8176
3	0.60	0.001 00	0.000 200	0.001 200	1501	0.8998	-0.1056	0.8096

The last three columns in Table 3.1 show a relatively small sensibility of transparency. Different column concentrations of the two main trace gases didn't change transmittance of CDA remarkably. Considering now that relative error of observed (by an actinometer) broadband direct beam is ±4% which leads to ±2% errors in coefficients p_2, one can assume that variabilities in the ozone cap and in the NO_2 column amount are a negligible source of errors and consider broadband optical parameters of different ideal atmospheres as constants, *e.g.*

$$\ln p_{CDA,2} = -\delta_{CDA,2} \approx -0.1, \tag{3.13}$$

from here it follows an approximate Bouguer broadband coefficient for ideal atmospheres:

$$p_{CDA,2} = \exp(-\delta_{CDA,2}) = e^{-0.1} = 0.90484 \approx 0.905, \tag{3.14}$$

and broadband transmittance (transmission, transmissivity) for ideal atmospheres:

$$\tau_{CDA,2} = \exp(-2\delta_{CDA,2}) = e^{-0.2} = 0.8187 \approx 0.819. \tag{3.15}$$

It is of interest to note that the group of Pierre Ineichen, the University of Geneva (Molineaux *et al.*, 1994) proposed, as a function of *m*, a general formula for optical depths of ideal atmospheres

$$\delta_{CDA,m} = 0.124 - 0.0285 \ln m, \tag{3.16}$$

from here, for $m = 2$, it follows $\delta_{CDA,2} = 0.104$, which matches with estimation (3.13). Some years later Molineaux *et al.* (1998) proposed another formula:

$$\delta_{\mathbf{CDA},\,m} = -0.101 + 0.235\,m^{-0.16}, \tag{3.17}$$

for $m = 2$ one obtains $\delta_{CDA,\,2} = 0.109$ which, compared to Table 3.1, corresponds to a polluted industrial/urban area.

In order to complete discussion about δ_{CDA} an historical note should be given. Molineaux *et al.* (1995) pointed out spectral data tables by Feussner and Dubois from the beginning of the 1930s where both, molecular scattering and absorption by the stratospheric ozone were taken into account. These tables enabled numerical integration and calculation of broadband optical depths, δ_{CDA}, which were fitted by the following simple equation (Kasten, 1980):

$$\delta_{\mathbf{CDA},\,m} = \frac{1}{9.4 + 0.9m}, \tag{3.18}$$

which for $m = 2$ gives, $\delta_{CDA,\,2} = 0.0893$. However, in this widely used relation, absorption by NO_2 was not taken into account, perhaps this is a reason of a lower δ_{CDA} value compared to this thesis and Pierre Ineichen's group estimations.

Considering further, according to (3.13), that $\delta_{CDA,\,2} = 0.1$, Eq. (3.12) rewrites in a simpler form

$$\mathbf{BAOD2} = -\ln p_2 - 0.1 + \frac{1}{2}\ln \tau_{W,\,2}, \tag{3.19}$$

the last result considerably simplifies the requirements on input parameters of AODλ broadband modeling.

3.4.1. Broadband optical parameters of column water vapor

The third variable on the right-hand side of Eqs. (2.20) and (3.19) is broadband transmittance of water vapor, $\tau_{W,\,2}$.

In order to calculate ability of solar radiation to pass the atmospheric water vapor, an amount of total column water vapor, W, should be first estimated. The number of measurement techniques for W observations has increased considerably from the 1990s and now includes ground-based and space-borne optical soundings, microwave radiometry, as well as propagation delay estimation using ground-based data from the GPS network. In most countries, however, the classic balloon-borne radiosounding remains the main routine method for W monitoring (Jakobson *et al.*, 2009), but the network of radiosonde stations is sparse and sondes are launched only 1–2 times per day. Therefore, especially for solar radiation and aerosol studies, correlation between W and surface meteorological parameters (mainly surface temperature and pressure of water

vapor) is used. A short historical review for W approximate calculations of W is listed by Okulov *et al.* (2002). Concerning the Baltic region, Jakobson *et al.* (2005) expressed seasonal means of W as linear functions of the geographical latitude degree.

Suppose that the amount of W is already known. For an investigation of how the W affects broadband transmittance through a hypothetical atmosphere consisting of water vapor only, we have to use some kind of radiative transfer model for it. However, there are two major problems. The first is the complexity of the extraterrestrial solar spectrum. The second is peculiarity of the water molecule, leading to an extremely complicated vibration-rotation absorption spectrum (Maurellis and Tennyson, 2003).

Nevertheless, during the last decades, progress has been made in models calculating the water vapor attenuation of the broadband solar beam, leading to larger values of absorption than some decades before. This statement follows, for example, from comparing of parameterizations proposed by Zvereva (1968) against the newer ones by Gueymard (1995, 1998) and Molineaux *et al.* (1998).

Due to historical reasons, a parameterization developed by Gueymard (1995, 1998) has been used in the University of Tartu from the very beginning of this millennium. Calculations are based on Gueymard's known SMARTS2 model. He used a solar spectrum of 1881 wavelengths, at 1-nm intervals within the most important part of spectrum (280–1700 nm). Although the method consists of 20 formulas, it was demonstrated by Ohvril *et al.* (2005), that in a particular case, for atmospheric optical mass $m = 2$, the transmittance of water vapor can be expressed by a single formula:

$$\tau_{W,2} = 1 - 0.137 \, W^{0.32}, \tag{3.20}$$

where W (cm) is precipitable water in the zenith direction.

Unfortunately, a very thorough paper by Molineaux *et al.* (1998) on pyrheliometric panchromatic and photometric monochromatic aerosol optical depths was discovered by our group later. Molineaux *et al.* (1998) proposed a general formula for optical depth of column water vapor:

$$\delta_{W,m} = 0.112 \, m^{-0.55} W^{0.34}, \tag{3.21}$$

which in a particular case, $m = 2$, gives

$$\delta_{W,2} = 0.0765 \, W^{0.34}. \tag{3.22}$$

Transition from optical depth to transmittance of water vapor:

$$\tau_{W,2} = \exp(-2\delta_{W,2}) = \exp(-0.153 \, W^{0.34}). \tag{3.23}$$

Table 3.2 shows that difference in transmittances of column water vapor, $\tau_{W,\,2}$, calculated according either by (3.23) or (3.20) is less than 0.61%.

Table 3.2. Intercomparison of transmittances of column water vapor, $\tau_{W,\,2}$, calculated according to (3.23) and (3.20), respectively

I	II	III	IV
Zenithal precipitable water, W_1 (cm)	$\tau_{W,\,2} =$ $\exp[-0.153 * W^{0.34}]$ (Eq. 3.23)	$\tau_{W,\,2} =$ $1 - 0.137 W^{0.32}$ (Eq. 3.20)	Difference Between II and III
0.1	1.0000	1.0000	0.00%
0.2	0.9325	0.9344	-0.21%
0.3	0.9153	0.9181	-0.31%
0.5	0.8861	0.8903	-0.46%
1.0	0.8581	0.8630	-0.56%
1.5	0.8389	0.8440	-0.60%
2.0	0.8239	0.8290	-0.61%
2.5	0.8115	0.8163	-0.60%
3.0	0.8007	0.8053	-0.57%
4.0	0.7826	0.7865	-0.50%
5.0	0.7676	0.7707	-0.40%
6.0	0.7548	0.7569	-0.29%
7.0	0.7434	0.7446	-0.16%
10.0	0.7155	0.7138	0.25%

Plots of transmittances $\tau_{W,\,2}$ – calculated according to Zvereva (1968), Gueymard (1998), Ohvril *et al.* (2005) and Molineaux *et al.* (1998) – are given in Figure 3.3.
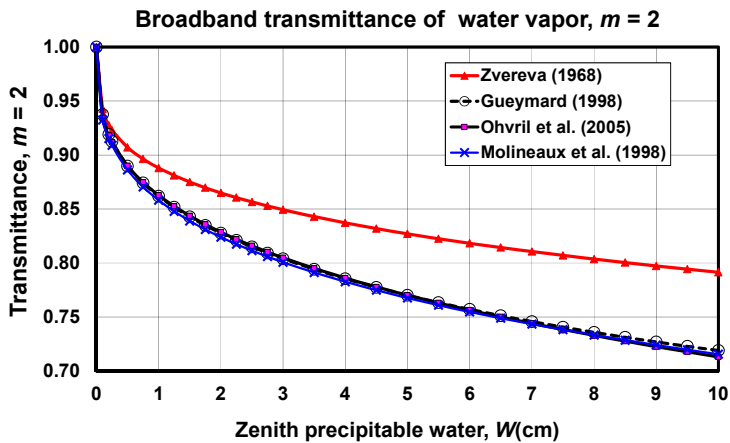

Fig. 3.3. Broadband transmittances of water vapor for optical mass $m = 2$ (solar elevation $\approx 30°$) as functions of precipitable water in the zenith direction, W (cm).

Two results are evident:

a) the two approximations (3.20) and (3.23), respectively, provide an excellent agreement with Gueymard's complicated parameterization – it is difficult to distinguish the three lower curves from each other in Figure 3.3;

b) Zvereva's parameterization, as an older one, gives considerably weaker attenuation of direct solar beam irradiance than the three models after her.

For the sake of comparison, broadband optical depths of water vapor for $m = 2$,

$$\delta_{W,2} = -\frac{1}{2}\ln\tau_{W,2}, \tag{3.24}$$

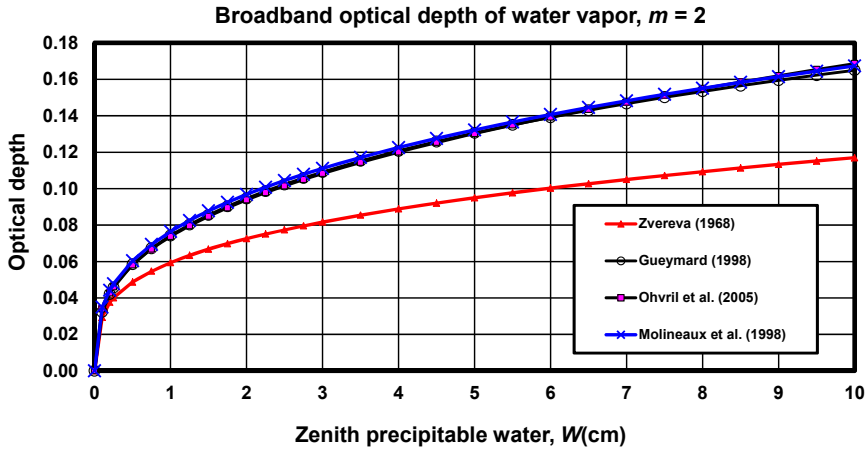corresponding to all four considered parameterizations, are shown in Figure 3.4.

Fig. 3.4. Broadband optical depths of water vapor for optical mass $m = 2$ (solar elevation $\approx 30°$) as functions of precipitable water in the zenith direction, W.

As expected, the three newer parameterizations ideally match between each other but the Zvereva's older model considerably underestimates optical depth of column water vapor.

The three coincidental curves in Figures 3.3 and 3.4, respectively, allow a quick visual estimation of broadband transmittance and broadband optical depth of water vapor (at $m = 2$) for any amount of zenith precipitable water W.

For example, a planetary mean column humidity, $W = 2.5$ cm (Peixoto, 1992) corresponds to transmittance 0.82 and optical depth 0.10. A typical summer precipitable water in the Baltic area, 2.0 cm, gives a transmittance of 0.83, and an optical depth of 0.094. During winter, at lower column humidity, transmittance and optical depth are more sensible to W changes, but the average diurnal PtP (Peak-to-Peak) changes in W are usually low, *e.g.* in the Baltic region, PtP = 0.64 mm for the summer and only 0.2 mm for the winter. Of

course, the W can show fast variations, reaching up to 5 mm/hour during several hours, but exclusively during changes in the synoptic situation and substitution of airmasses above the location of observation (Jakobson *et al.*, 2009). We should not worry about these transitional weather cases, because, as a rule, cloudiness restricts observations of direct solar beam during synoptic changes.

3.4.2. Aerosol optical depth relation with precipitable water

Substitution of (3.20) into (3.19) gives the final equation for the BAOD2:

$$\mathbf{BAOD2} = -\ln p_2 - 0.1 + \frac{1}{2}\ln\left[1 - 0.137W^{0.32}\right], \qquad (3.25)$$

where the zenith W is in cm. This important result will be used for transition from BAOD2 to AOD500 below.

Figure 3.5 gives a visual review about values obtained by BAOD2 as a function of two input variables, p_2 and W. Five fixed values of precipitable water have been used. The lowest one, $W = 0.1$ cm, corresponds to a cold winter atmosphere, $W = 1.0$ cm is typical in Estonia in April and October (Oku-lov, 2003; Okulov and Ohvril, 2010). As mentioned, $W = 2.5$ cm, is a planetary mean. During hot and sultry summer days in Estonia, a value $W = 4.0$ cm has been reached, and finally, $W = 6.0$ cm corresponds to a tropical atmosphere. The figure allows a rough evaluation of the change in BAOD2 due to a change in W, for a given coefficient of transparency, p_2. Considering small PtP changes in diurnal evolution of W, the BAOD2 has a low diurnal variability due to W.
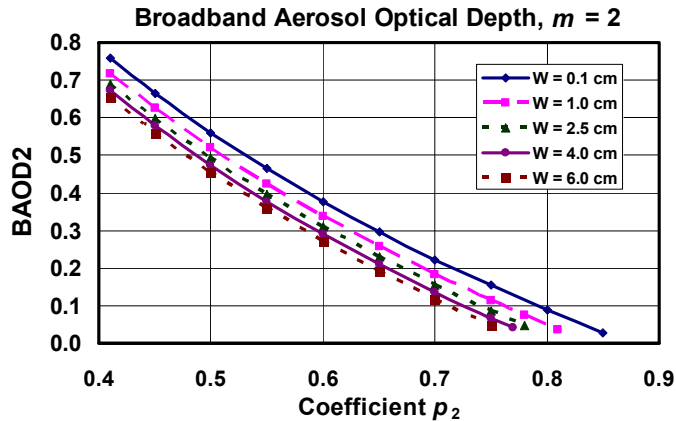

Fig. 3.5. Broadband aerosol optical depth as plotted against broadband column transparency coefficient. Calculations are implemented for $m = 2$ and a set of values of zenith precipitable water, from $W = 0.1$ to 6.0 cm.

A practical note should be made in regard to practical calculations of BAOD2. Obviously, a condition

$$\text{BAOD} \geq 0, \qquad (3.26)$$

should be followed. However, sometimes calculations according to (3.25) give negative results. Usually it happens due to overestimation of W using approximate methods. Thus, during inspection of radiation and column humidity databases, a control should be made to remove incompatible pairs of p_2 and W. To derive an appropriate condition, p_2 as a product of transmittances is represented:

$$p_2 = \left[\tau_{\mathrm{CDA},2} \tau_{W,2} \tau_{\mathrm{aer},2} \right]^{0.5}, \qquad (3.27)$$

where transmittance of an ideal atmosphere $\tau_{\mathrm{CDA},2} = 0.8187$. Denoting by $p_{2,\,\mathrm{max}}$ the maximal coefficient of column transparency, which corresponds to absence of aerosol attenuation, expressed by $\tau_{\mathrm{aer},\,2} = 1$, the previous equation can be written

$$p_{2,\,\mathrm{max}} = \left[0.8187 \times \tau_{W,2} \right]^{0.5}. \qquad (3.28)$$

Inserting here transmittance of water vapor yields to desired condition,

$$p_2 \leq p_{2,\,\mathrm{max}} = \left[\tau_{\mathrm{CDA},2} \tau_{W,2} \right]^{0.5} \approx \left[0.8187 - 0.112 W^{0.32} \right]^{0.5}, \qquad (3.29)$$

which is visualized in Fig. 3.6. Insertion of aerosol particles into a wet and clean atmosphere would diminish values of column transparency, p_2.
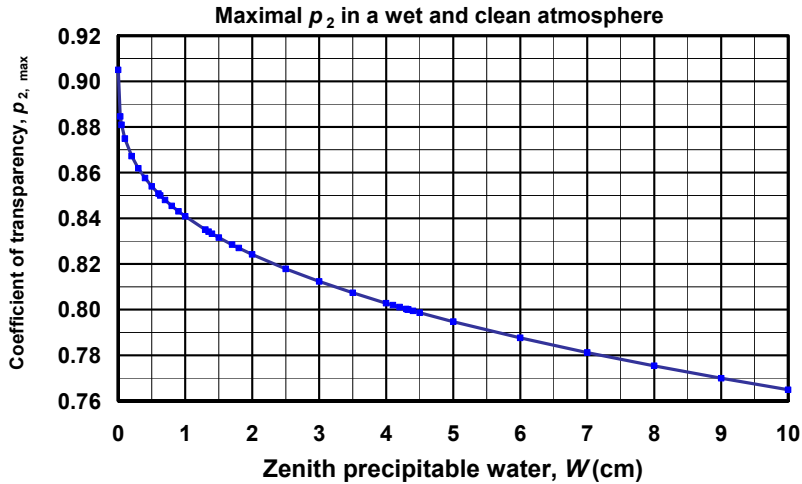

Fig. 3.6. Maximal possible broadband Bouguer coefficients of transparency, $p_{2,\,\mathrm{max}}$, for a wet and clean atmosphere (without aerosol particles).

For a typical precipitable water summer value in Estonia, $W = 2$ cm, a maximal coefficient of column transparency is: $p_{2, \, max} = 0.82$, for the highest Estonian summer value, $W = 4$ cm, calculation gives $p_{2, \, max} = 0.80$. Insertion of aerosol particles into a wet and clean atmosphere would reduce values of column transparency, p_2.

3.4.3. Comparing spectral and broadband optical depths

Routine measurements of broadband solar direct irradiance were started in Estonia already in 1931. In addition to a wide set of broadband observations performed during several decades, regular measurements of spectral solar direct irradiance were started at Tõravere in June 2002. An autonomous AERONET sunphotometer, Cimel CE 318-1, generously provided by B. Holben's team from the NASA Goddard Space Flight Center, is used. Simultaneous registration of both, spectral and broadband irradiances, gives a possibility to compare spectral and broadband parameters of transparency or turbidity, and to develop approximate methods for evaluation of AODλ using only broadband parameters and integrated column water vapor.

Deriving a next version of the "broadband" model (further also known as model T2), 19 592 complex observations from all seasons during 2002–2009 have been used. Precipitable water (in mm) was calculated according to an approximation:

$$W(e_0) = 1.48 \, e_0 + 0.40, \qquad (3.30)$$

where e_0 (mb) is the 12 UTC ground water vapor pressure. This parameterization was developed according to clear sky radio-soundings in Tallinn (Okulov *et al.,* 2002). Note, that unlike total column humidity W, its surface counterpart, ground water vapor pressure, e_0 has a remarkable diurnal cycle. For that, in approximations like (3.30), the e_0 should correspond to a fixed time, *e.g.* to 12 GMT. This condition, obviously, leaves the estimated column humidity unchangeable during a day.

Figure 3.7 compares total column humidity as a function of surface water vapor pressure, $W(e_0)$, with W(AERONET) which are considered as reference values. As an average, prediction overestimates the reference only by 3%, but the coefficient of determination, $R^2 = 0.83$ only, indicates some scatter of $W(e_0)$ around the W(AERONET).

In cases of relatively dry winter air ($W < 0.5$ cm) prediction of W by (3.30) has a root mean square deviation (RMSD) equal to 0.135 cm (Table 3.3, the 1st column). Compared to the mean value of this particular range, $W = 0.25$ mm, the deviation is 54%.
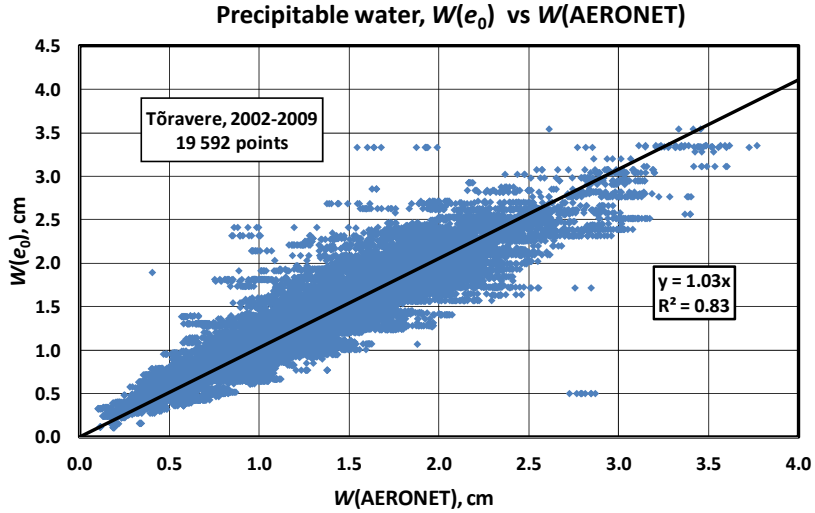
Fig. 3.7. Precipitable water $W(e_0)$, estimated using ground water vapor pressure is plotted against reference precipitable water, W(AERONET), calculated from solar photometry (Tõravere, all seasons of 2002–2009, 19 592 points).

Table 3.3. Root mean square deviations (RMSD) of W prediction for different W ranges

W(AERONET) range, cm	0–0.5	0.5–1.0	1.0–1.5	1.5–2.0	2.0–2.5	2.5–3.0	3.0–4.0
Observations, % of 19 592	9.6%	25.6%	27.0%	22.6%	11.6%	2.7%	0.9%
RMSD, cm	0.135	0.239	0.287	0.293	0.271	0.300	0.368
Relative RMSD, %	54%	32%	23%	17%	12%	11%	11%

For higher W amounts the relative RMSD is lower, reaching a final level of RMSD $\approx$ 11–12% for W(AERONET) > 2 cm. Note that uncertainty in W(AERONET) is typically less than 12% (Holben *et al.*, 1998).

In Figure 3.8 two sets of broadband optical depth, BAOD2, calculated by (3.25) have been compared. For both sets, the same input of observed column transparency, p_2, is used but with two different values for precipitable water, W(AERONET) and $W(e_0)$, respectively. Both BAOD2s are strongly correlated, $R^2 = 0.993$, having an excellent linear relationship, $y = 0.997\,x$. This result confirms that BAOD2 is not sensitive to estimations of precipitable water (at least for Tõravere).
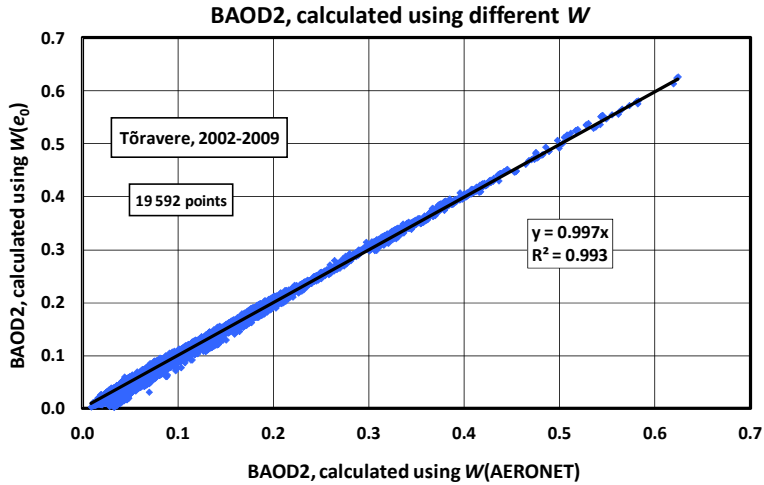
Fig. 3.8. Broadband aerosol optical depth (BAOD2, $m = 2$) calculated using column humidity $W(e_0)$, estimated by surface water vapor pressure, is plotted against the BAOD2, estimated by W(AERONET); Tõravere, 2002−2009, 19 592 points.

The relationship between the spectral AOD and its broadband counterpart, BAOD2 is presented in Figure 3.9. Here a large set (the same 19 592 joint observations from 2002−2009) of AOD500, observed by the AERONET sun-photometer (Level 2, Version 2) at Tõravere are plotted against the BAOD2, calculated by (3.25).
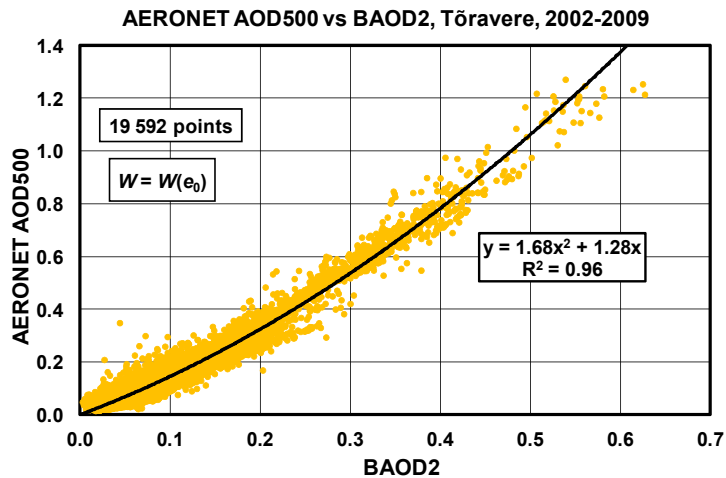

Fig. 3.9. AOD500 as observed by AERONET at Tõravere, Estonia, plotted against the broadband aerosol optical depth, BAOD2, for optical mass $m = 2$, years 2002−2009, 19 592 single observations.

Remind that the results plotted in Figure 3.9 were calculated for a given location, Tõravere, without any presumptions about the properties of aerosol particles in the column (the Ångström exponent, size distribution, absorption coefficient, phase function, etc). The two optical depth parameters, AOD500 and BAOD2, are strongly correlated ($R^2 = 0.96$) through the following second degree polynomial:

$$AOD500 = 1.7 \, (BAOD2)^2 + 1.3 \, (BAOD2), \qquad (3.31)$$

where BAOD2 is calculated by (3.25) using observed coefficients of column broadband transparency, p_2, and column humidity, $W(e_0)$, estimated by a simple model (3.30). As expected, replacement of $W(e_0)$ by $W(AERONET)$ caused only negligible changes in Figure 3.9 (respective Figure with this particular test is not presented).

In Figure 3.10, values of AOD500, predicted by (3.31) using BAOD2 as a function of p_2 and $W(e_0)$, are compared to the reference AOD500, as observed by AERONET at Tõravere.
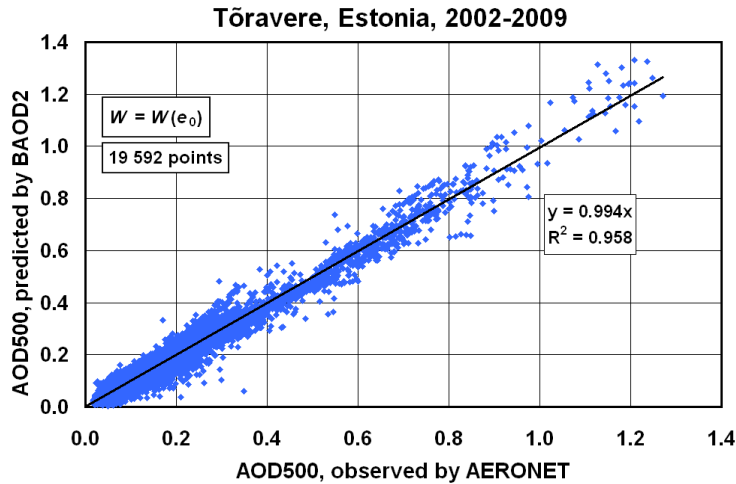
Fig. 3.10. AOD500 as predicted by broadband aerosol optical depth, BAOD2 at $m = 2$, plotted against AOD500 as derived from the AERONET Tõravere observations from 2002–2009 (19 592 points).

In Figure 3.10, 81.8% of points belong to a range of a rather clean air, AOD500(AERONET) < 0.2, where the RMSD between predicted and reference values is 0.022. The last number apparently represents uncertainty of this quite rough broadband approach to predict AOD500 for a quite typical turbidity range at a particular geographical location – Tõravere. For comparison, the instrumental uncertainty in AOD500(AERONET) is 0.01 (Holben *et al.,* 1998). The

RMSD of prediction increases with increasing AOD500 until RMSD = 0.106 in very turbid cases, when AOD500 = 1.0–1.3 (Table 3.4).

Table 3.4. Root Mean Square Deviation of AOD500 prediction at different turbidity ranges at Tõravere, comparison with AERONET

AOD500 range	0.0–0.2	0.2–0.4	0.4–0.6	0.6–0.8	0.8–1.0	1.0–1.3
Observations, % of 19 592	81.8%	13.8%	2.3%	1.5%	0.4%	0.2%
RMSD	0.022	0.035	0.042	0.047	0.081	0.106
Relative RMSD, %	22%	12%	9%	7%	9%	9%

Relative RMSD, in regard to the middle value of the first range, AOD500 = 0.1, is 22% and less than 12% for higher turbidities. This accuracy is not bad reminding again that creating this broadband approach, no presumptions were made about season, meteorological situation, microphysical parameters of aerosol particles etc. For the entire observed range of optical depth, covering the AOD500 = 0–1.3, there is an excellent linear relationship ($y = 0.994\ x$) and close correlation ($R^2 = 0.958$) between predicted and the reference AERONET values (Kannel *et al.*, 2012).

4. USED DATASETS FOR DEVELOPING AND TESTING AOD MODELS

In this chapter, broadband and spectral databases used for developing and testing AOD models are described. In addition, a new cloud screening algorithm is revealed.

4.1. Broadband and spectral databases of direct solar beam

Both, broadband and spectral, solar direct irradiance observations have been made in Tartu-Tõravere meteorological station, Estonia, Lat N = 58.255 deg, Lon E = 26.46 deg.

Tõravere is a village located 20 km from Tartu (the second largest city in Estonia with population ~100 000). Environment of Tõravere could be classified as a rural one. However, the observation centre is located 5 km away from a small town Elva with population about 6000. The Tartu-Elva road, 0.5 km south from the station, has relatively intensive traffic only during peak-hours, thus the site cannot be considered as traffic influenced.

The data have been derived from two independent observational instruments situated at Tõravere station:
(a) actinometer AT-50, also known as the "Yanishevski" pyrheliometer,
(b) sun photometer Cimel CE 318-A, a well-known AERONET instrument.

The first is an old classic broadband instrument which is still in use in order to maintain homogeneity of multidecadal time series of broadband solar direct irradiance (SDI). The observations are performed by Estonian Environment Agency, formerly known as Estonian Meteorological and Hydrological Institute (EMHI). It should be noted that the initial SDI time series are not cloud-screened. The absence of an effective cloud screening algorithm obliged us to create a data processing module to extract the clear sky portions of the dataset (more details below, in Section 4.2).

The second device is a one, supported by a powerful software (including cloud-screening) for retrieval of several aerosol properties and characteristics, also amount of water vapor and concentrations of some trace gases (*e.g.* O_3, NO_2). The photometer is operated by a well-known NASA project AERONET (Aerosol Robotic Network).

While the actinometer has been worked at Tartu-Tõravere 66 years already (since 1950), the AERONET-project started there quite lately, in June, 2002. From then, the autonomous continuous observations have been performed and corresponding data are freely accessible via the AERONET official website, http://aeronet.gsfc.nasa.gov/.

In the disposal, there were two independent datasets together, for years 2002–2011:
(a) a broadband or actinometric database with raw SDI values;
(b) a spectral or AERONET database with extracted AOD500 and Ångström alpha values.

Merge of these two different datasets has been designed under a condition that the time difference between single observations made by two separate instruments doesn't exceed 5 minutes. The joint dataset enabled further comparison (matching) of predicted AOD500 values with observed real data from the AERONET. Also the merged dataset enabled to validate AOD500 results predicted by other models.

4.2. About cloud screening algorithms for ground based solar radiation data

Automatic global projects and programs for monitoring of aerosol column optical depth (*e.g.* AERONET, GAW, AATR, TerraModis, AquaModis, ESR, RIMA, etc) provide information on natural and anthropogenic aerosol load, which is important in many local and regional studies as well as in climate change debates.

Automated, non-human observations enable massive data acquisition. However, concerning optical, including solar radiation measurements, quality of initial (raw) datasets is low. For instance, the automatic broadband Solar Direct Irradiance at normal incidence (SDI) observation technology, used by Estonian Environmental Agency, stores data with regularity of a minute, starting already from 00 UTC, January 1, when the sun is deeply below the horizon. Each raw daily set contains 1440 observations, an annual set more than half a million, mainly outliers, not suitable for further data processing. Thereby, cloud screening (cleaning or filtering of raw data from cloudy portions) and quality assurance are extremely essential prior to proceed with processing and interpretation of solar irradiance data.

Of course, in cases of small data amounts, it is possible to perform manual-visual selection of moments corresponding to clear solar disc conditions and appropriate it for further analysis. Manual-visual examination secures high quality of sampling but is time-consuming and expensive, it cannot be applied massively.

A number of investigators have carried out different approaches for filtration of cloudy moments from time series of solar radiation data. As a rule, these approaches are instrument and measured physical parameter specific. Below there are brief review about four examples.

4.2.1. First example of cloud screening

As a first example, Long & Ackerman (2000) presented an automated method to identify periods of clear skies for a 160° FOV pyranometers measuring surface downwelling total and diffuse shortwave irradiances. Thus, having two parallel time series, one for total and the other for diffuse shortwave irradiance respectively, a third time series, for the ratio of diffuse to total irradiance can be calculated. The three time series were analyzed as functions of solar zenith angle. Supposing no diurnal changes in column water vapor and aerosol amounts, also changes between clear-sky days, four different tests were derived, as a first approximation, to eliminate data that occur under cloudy solar disc. While each individual test is not sufficient to determine whether the solar disc was clear or not, but any moment that successfully passes all tests, most probably corresponds to clear solar disc

4.2.2. Second example of cloud screening

Second example refers to AERONET team who operates a global network of automatic sun/sky CIMEL radiometers CE-318. The team has developed their own method of cloud detection (Holben *et al*., 1998; Smirnov *et al*., 2000). The sun direct spectral measurements are acquired in approximately 10 seconds across eight spectral bands, which are located between $340 < \lambda < 1020$ nm. A sequence of three such measurements is taken 30 seconds apart to yield a triplet observation per wavelength. Note that actually the final AERONET product of AODλ has a time interval about 15 min between such successive observations. Rapid triplet observations belong solely to technology of cloud detection – the temporal variation of cloud optical depths is typically greater than the variation of aerosols. Observations with stable triplets should be retained and those with high-frequency changes should be eliminated as cloud-contaminated cases. As an additional criterion the AERONET's automatic cloud screening algorithm uses a certain standard deviation which limits variations in single AODλs compared to the daily AODλ average course.

4.2.3. Third example of cloud screening

As a third example here are a description of principles of an automated cloud screening algorithm designed for Multi-Filter Rotating Shadowband Radiometer (MFRSR) data by Alexandrov *et al*. (2004). Although the MFRSR performs measurements of solar spectral irradiance at six wavelengths (415-940 nm), detection of clouds is based solely on wavelength $\lambda = 870$ nm, *i.e.* on the channel which is away from spectral regions with trace gases and water vapor absorption. Under these assumptions, in a favorite case of clear solar disc, when the line of sight between the sun and the instrument is free of clouds, the direct

normal spectral irradiance at 870 nm, $I(870)$, depends only on extinction (absorption and scattering) by aerosol particles and extinction due to Rayleigh scattering:

$$I(870) = I_0(870)\,e^{-[\delta_{aer}(870)+\delta_R(870)]m}, \qquad (4.1)$$

where $I_0(870)$ is the TOA irradiance, $\delta_{aer}(870)$ is aerosol optical depth, $\delta_R(870)$ is its Rayleigh scattering counterpart, which can be calculated independently, and m is the air mass.

However, the MFRSR performs measurements also in undesired cases when there is a cloud in front of sun. In that case, the Cloud Optical depth (COD, $\delta_{cld}(870)$), should be also considered

$$I(870) = I_0(870)\,e^{-[\delta_{aer}(870)+\delta_{cld}(870)+\delta_R(870)]m}. \qquad (4.2)$$

In order to facilitate the further cloud screening process, the episodes of thick clouds, $I(870) \approx 0$, should be removed from the timeseries and thin clouds should be kept.

Omitting the wavelength from formulas, for the sake of brevity, total spectral optical depth of three factors (aerosol+cloud+Rayleigh), $\delta_{total} = \delta_{total}(870)$:

$$\delta_{total} = \delta_{aer} + \delta_{cld} + \delta_R = -\frac{1}{m}\ln\frac{I}{I_0}. \qquad (4.3)$$

Alexandrov $et\ al.$ (2004) defined an aggregate total spectral optical depth, $\delta = \delta(870)$, which include two factors, aerosols and a thin cloud. This is estimated with

$$\delta = \delta_{total} - \delta_R = \delta_{aer} + \delta_{cld} = -\frac{1}{m}\ln\frac{I}{I_0} - \delta_R. \qquad (4.4)$$

It should be noted that usually optical depth of aerosol particles is less than optical depth of clouds. However, COD of thin clouds (cirrus) appears to have similar values with AOD, thus they cannot be separated by their values. But δ_{aer} tends to be more stable from observation-to-observation compared to considerably more turbulent δ_{cld}. In other words, the structure and size of fluctuations of AOD and COD are different. The last fact allows identifying observations where the undesired COD is present.

For that Alexandrov $et\ al.$ (2004) introduced an additional, inhomogeneity parameter, ε, which characterizes the degree of horizontal inhomogeneity of optical depth the atmosphere:

$$\varepsilon = 1 - \frac{\exp(\overline{\ln \delta})}{\overline{\overline{\delta}}} \, , \qquad (4.5)$$

here the overbar indicates a moving average, over 15 data points. Considering that intervals between the MFRSR observations of the same wavelength is 20 seconds, the moving average is over a 300 seconds = 5 min window. A favorable homogeneous situation, δ = const during 15 successive data points gives $\varepsilon = 0$ and corresponds to clear solar disc. For extremely inhomogeneous dataset ε is close to 1. This parameter is invariant with respect to multiplication of δ by a constant factor. This means that ε characterizes fluctuations in cloud field regardless of the magnitude of optical depth. However, difficulties may arise with some types of thin extended clouds like Cirrostratus whose optical depth resembles AOD multiplied by a constant factor, while ε is invariant under such transformation.

Thus, to firmly separate clear sky from thin clouds, there is a need to modify the original optical depth while retaining the structure and size of their fluctuations. This was done by subtracting moving average of optical depth (over 15 datapoints = 5 min window; δ with overbar) from the optical depth time series δ and adding back a constant value, $\delta_{const} = 0.2$, which is more typical as an AOD value than COD value. The renormalized optical depth is now

$$\delta' = \delta - \overline{\delta} + \delta_{const} \, , \qquad (4.6)$$

and the modified inhomogeneity parameter, ε', respectively:

$$\varepsilon' = 1 - \frac{\exp(\overline{\ln \delta'})}{\overline{\overline{\delta'}}} \, . \qquad (4.7)$$

The statistical distribution of values of the new inhomogeneity parameter ε' over a month (September 2000) shows two distinctive maxima that correspond to the aerosol and cloud modes, respectively. Aerosols have a lower ε' than clouds. The threshold (transition) value between the two modes, $\varepsilon' = 2\times10^{-4}$, below that the observations are considered clear and above that they are considered cloudy. It is noted that this approach can misidentify a very short clear sky interval between clouds as being cloudy, but the probability of this situation is small and these short intervals are not so important for actinometry.

4.2.4. Fourth example of cloud screening

The fourth example describes an iterative cloud screening method presented by Chen *et al.* (2014) for the UV-MFRSR (the ultraviolet version of MFRSR). The UV-MFRSR receives the direct normal, diffuse horizontal, and total horizontal

solar radiation at seven UV channels (300, 305, 311, 317, 325, 332 and 368 nm). The method was derived in frames of the UV-B Monitoring and Research Program funded by the U.S. Department of Agriculture.

In this method the total optical depth (TOD) from measurements of direct normal irradiance by the 368-nm channel is first calculated. Here "total" means the value of cloud plus aerosol optical depth. Rayleigh scattering and gaseous absorption are already subtracted. Cloudy points have higher total optical depth values than clear points. Therefore, clear points have lower TOD values while the cloudy points have bigger values. The algorithm calculates the TOD difference between a target point (*i.e.* point under consideration at the moment) and pairs of all indeterminate points. Further, the algorithm considers the target as a cloudy point if the TOD difference exceeds a certain threshold value. All points are of indeterminate status at the beginning of cloud screening. Each point is examined with all other indeterminate points. If new cloudy points are found, then a new iteration of examination is triggered. The cloud screening finishes, when no new cloudy points are found in the last iteration. The surviving indeterminate points are considered clear solar disc points.

In addition to four examples above Chen *et al.* (2013, 2014) reviewed ground-based cloud screening methods published over the last two decades and made a classification of different algorithms. They list four common types of cloud screening (for mainly of narrowband data):

a) cloud screening is performed on non-calibrated voltage data;
b) cloud screening is performed on calibrated irradiance data (total and diffuse);
c) cloud screening is performed on derived AODλ data;
d) cloud screening uses collocated auxiliary equipment/data (sunshine duration sensors and standard human observations on cloudiness fall into this category).

Unfortunately, cloud screening of direct solar broadband irradiance time series is not presented in this list. For that, keeping in mind a general ideology of current dissertation to elaborate as simple as possible but reliable calculation schemes, a decision was made to create a new, easy programmable module for cloud screening of recorded time series of broadband solar direct irradiance.

4.3. Identification of clear solar discs from broadband direct beam measurements

In this dissertation, a new simple cloud screening algorithm is proposed for calibrated solar direct irradiance at normal incidence (SDI) data.

4.3.1. The outline of a new simple algorithm

For a single observational day it is designed as follows.

First, all SDI "non-sunny" values below a threshold value, 200 W/m^2, are removed. Note that upon the WMO analysis of measurement data from many measuring stations with Campbell-Stokes sunshine recorders, and comparison with collocated pyranometers, it turned out that the threshold value for "sunny" was ranging between 70 W/m^2 and 280 W/m^2 of SDI. However, this is an enormous range, of 400%, and obviously such an uncertain criterion is not appropriate to use as an overall standard. For that, in 1981, a certain value of 120 W/m^2 for SDI, was defined by the WMO as the threshold for "sunny" (Rösemann, 2011).

Here, the cut-off level is at 200 W/m^2, which is higher compared to the WMO threshold of 120 W/m^2. For Estonia, lower occasions than 200 W/m^2 belong to very low solar elevation ($h<5°$) when increasing of cloudiness near the horizon restricts optical measurements. Summarizing, a decision was made that the clear solar disc SDI values lower than 200 W/m^2 are probably unreliable and these observations should be eliminated.

Second, based the algorithm screening tests (Section 4.3.2), it was also considered that before the local noon, until 12 o' clock in True Solar Time (TST), the values of the SDI, starting from $i = 1$, should have an increasing trend, in general. This condition is expressed by a criterion that the next SDI reading, a value labeled by $i+1$ in the sequence, constitutes at least a certain L part of the previous reading, i:

$$\text{SDI}(i + 1) \geq L \times \text{SDI}(i), \qquad (4.8)$$

where different level constants, $97\% < L < 100\%$, were set in experimental runs of the screening algorithm. Apparently, due to increase in solar elevation angle during transition from i to $i + 1$, the all L values, $L = 100\%$ included, enable a slow decrease in column transparency before the local noon. If the target SDI($i+1$) value does not satisfy condition (4.8), then the observation is definitely cloudy. The surviving values are considered belonging to clear solar disc moments.

However, after the local noon, considering that a SDI course, starting from $j = 1$, should be in general decreasing, a condition:

$$\text{SDI}(j + 1) \leq L \times \text{SDI}(j), \qquad (4.9)$$

does not work. The matter is that a cloudy situation for any post-noon moment, labeled by $j + 1$, actually completes the post-noon sequence of measurements. For that, denoting the total post-noon number of SDI measurements by N, screening should start from the end of time series, from the moment $j = N$, and applied for $j = N - 1$, $j = N - 2$, $j = N - 3$, etc, until the noon is again reached for $j = 1$. For post-noon measurements the screening condition is

$$\text{SDI}(j - 1) \geq L \times \text{SDI}(j), \tag{4.10}$$

where the target now is the the $\text{SDI}(j - 1)$ value.

The algorithm performs better when the first SDI values of sequences ($i = 1$ and $j = N$, respectively) belong to clear solar disc. Fortunately, in the case of Cu-clouds it is easily achieved. In the presence of thin Ci-clouds additional criteria should be introduced for $i = 1$ and $j = N$, *e.g.* a particular threshold values for given solar elevations and given season. If in the same location column aerosol measurements are available (*e.g.* AERONET) then Ci-clouds could be detected by particles size distribution (cloud particles are bigger compared to conventional aerosol particles). In frames of this dissertation this kind of algorithm update and additional "manual" inspection were not applied.

4.3.2. Algorithm implementation, test runs

Results of cloud screening test runs for Tõravere SDI measurements during the entire year of 2011, using five different severity constants, L, are given in Table 4.1.

Table 4.1. Statistics of cloud screening test runs for the entire year of 2011, Tõravere, Estonia

The level constant, L	Number of retained measurements
97%	73 688
98%	70 579
99%	63 445
99.5%	54 715
100%	42 361

Note that the total number of single SDI records (observations) during 2011 was, $365 \times 24 \times 60 = 525600$. Using the mildest, $L = 97\%$ screening level, it retains 14% of all observations and use of the most severe one, $L = 100\%$ level, retains 8%.

A review about performance of this simple algorithm can be obtained in Table 4.2 and in Fig. 4.1 where results of cloud screening are presented for two particular days at Tõravere: for an almost clear day, May 8th, 2011, and for a day with broken cloudiness, May 20th, 2011.

Table 4.2. Statistics of cloud screening test runs for two particular days at Tõravere, Estonia

The level constant, *L*	Number of retained measurements	
	08 May 2011 (an almost clear day)	20 May 2011 (a cloudy day)
97%	859	329
98%	856	259
99%	852	193
99.5%	820	154
100%	577	114
Number of AERONET observations	61	15

Merely by visual inspection one can conclude that the most severe screening constant, L = 100%, secures the most accurate selection of clear solar disc moments. Therefore, conditions (4.8) and (4.10) can be rewritten as:

$$\text{SDI}(i + 1) \geq \text{SDI}(i), \text{ for } i = 1, 2, 3, \ldots, \text{ before the local noon,} \quad (4.11)$$

$$\text{SDI}(j - 1) \geq \text{SDI}(j), \text{ for } j = N, N - 1, N - 2, \ldots, \text{ after the local noon.} \quad (4.12)$$

Based on current testcases, the screening level values between $0.98 \leq L \leq 1.0$ are used throughout of the dissertation. Presented cloud screening module for broadband direct-beam measurements is easy programmable and allows to get rid of worthless observations which litter and burden databases. In this dissertation it was implemented in a Unix-type computing environment using simple bash/dash scripts.
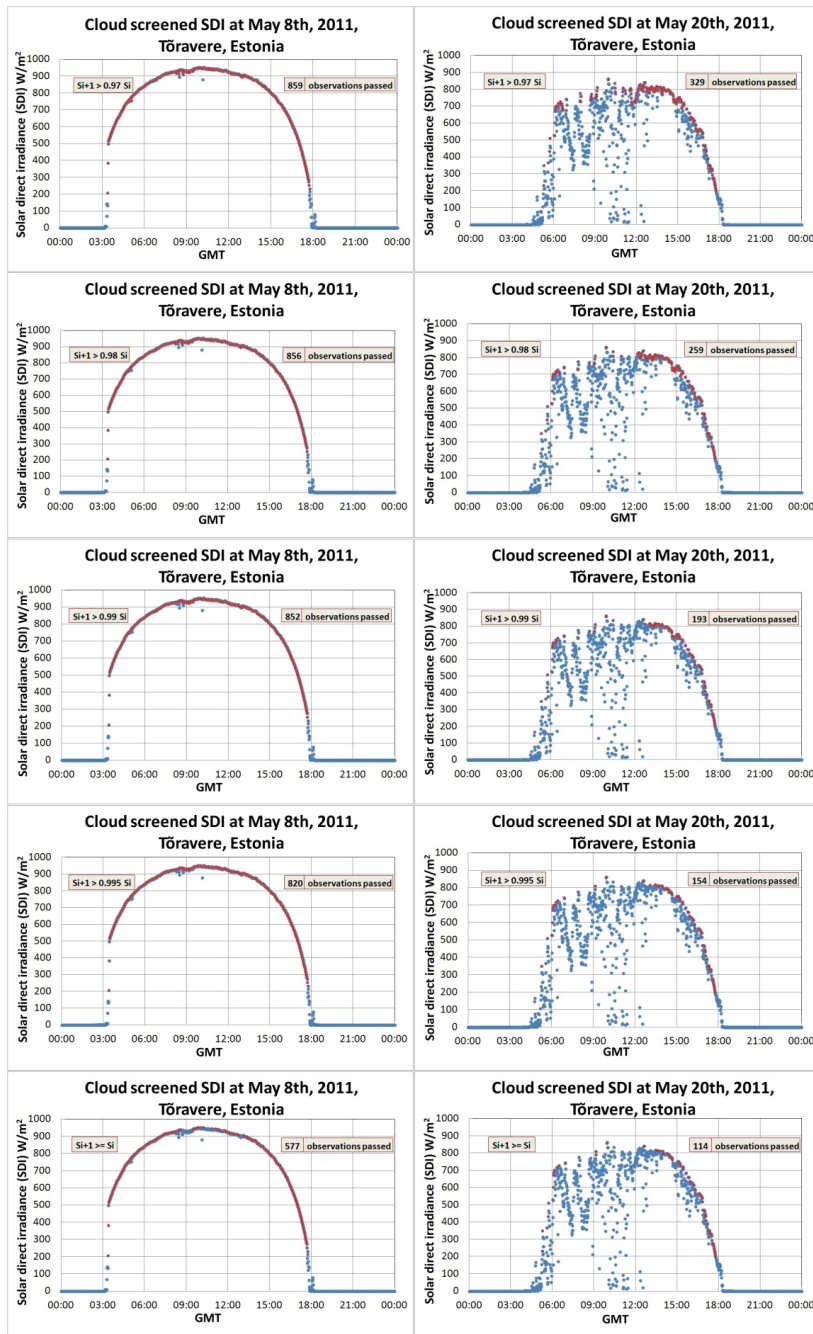
Fig. 4.1. Application of a simple cloud screening algorithm for solar direct irradiance measurements at Tõravere, Estonia. The left blocks represent an almost clear day, May 8th, 2011 and the right blocks a day with broken cloudiness, May 20th, 2011. For the both top graphs the severity constant is, $L = 97\%$, for bottom graphs, $L = 100\%$. Estonia belongs to the Eastern European Time zone (EET), 2 hours ahead of the UTC/GMT.

5. TEST OF AODλ MODELS

In this chapter, several AODλ models created in different institutions (including the models expressed by Eqs. 3.7 and 3.31) will be compared against the reference AERONET AOD500 measurements at Tõravere, Estonia, during 2002–2011. Also the satellite AOD500 observations will be compared against some models (Kannel *et al.*, 2014). Based on several statistics, a "hexathlon competition" between models for AOD500 better estimation will be performed.

5.1. Tested models

For a quick review of the used broadband models, together with their inputs and outputs, are listed in Table 5.1.

5.1.1. Models M1 and M2

These two models were developed in the Meteorological Observatory of the Moscow State University (Tarasova and Yarkho, 1991a, 1991b). Model M1 consists of 13 formulas (not given in this work). This is somewhat general and unique model because it allows to vary coefficient α - the Ångström wavelength exponent. Model M2 is a simplified version of M1, where the Ångström exponent has a fixed value, α = 1. The last simplification allows calculation of AOD550 using only one formula

$$\text{AOD550} = \frac{\ln S_m - \left(0.189\, W^{-0.183} + \dfrac{0.880\, W^{-0.009} - 1}{\sin h} \right)}{0.813\, W^{-0.002} - 1 + \dfrac{0.435\, W^{-0.0321} - 1}{\sin h}}. \quad (5.1)$$

Here S_m is broadband direct solar irradiance recalculated to average Sun-Earth distance, h is the solar elevation angle and W zenith precipitable water, in cm. The M2 was widely used for monitoring of aerosol turbidity on the Russian territory (Abakumova and Gorbarenko, 2008).

   According to report by authors (Tarasova, Yarkho, 1991a, 1991b) they had no opportunities to check their calculation procedures using in parallel spectral AOD550 measurements. For that their models were verified indirectly using, in parallel to the S_m observations, simultaneous observations of direct photosynthetically active radiation (PhAR, 0.38–0.71 μm). The verification took place in a scientific field base at Zvenigorod (near Moscow) in May of 1989, when 86 parallel measurements were made. However, the weather conditions in May of

1989 did not allow to make conclusions about suitability of the models to consider circumsolar radiation and calculate the AOD550 values under conditions of heavy smoke aerosol load which, because of huge forest and peat fires occurred during dry and hot summers around Moscow (like in 1972, 2002, 2010).

For the Moscow colleagues an opportunity for a comprehensive check of their models opened as early as in 2001. The next, extremely dry summer of 2002 favored again huge fires around Moscow and the city was filled with smoke (the CIMEL photometer is located nearby the main building of the university, on the territory of the University Botanic Garden). Prediction of AOD500 under conditions with large amount of smoke aerosols (at summer 2002) revealed a fact that the M2, under conditions of very turbid air, underestimates AOD550 compared to AERONET simultaneous observations (Chubarova, 2005).

As already briefly described above (Section 3.2), the main reason for underestimation of AODλ at high turbidities by the broadband models is because the models consider only a "true" narrow solar direct beam, exactly from the solar disc with its mean angular diameter of about 32 arc minutes. Actually the opening angles of older broadband instruments, but still in use for homogeneity of multidecadal time series, have considerably wider apertures reaching up to 10 degrees. For example, the Kipp&Zonen Linke-Feussner actinometer has an aperture of 10.2° (Gueymard, 1998; Garg and Prakash, 2006). The AT-50 actinometers, continuously in use in actinometric networks on the territory of the former USSR, have the full field of view, FOV = 10°.

Although the FOV of most current pyrheliometers is smaller (*e.g.* for the Eppley Laboratory Inc. normal incidence pyrheliometers (NIP), the FOV = 5.7°), the measured direct beam is anyway increased by undesirable diffuse irradiance intercepted by a broadband instrument (Gueymard, 1998; Carlund *et al.*, 2003).

The magnitude of this increase is greater at low solar elevation and heavy aerosol loading, and also in cases of large aerosol particles such as maritime aerosol, biological aerosol, desert or ground dust etc. In cases of small particles (*e.g.* almost pure molecular scattering in a clear atmosphere after a rain) circumsolar radiation is weaker. According to calculations made by Gueymard (1998) for FOV = 10.2°, the circumsolar magnification factor can reach 35% regarding the true direct irradiance. Increased artificial parasitic values of observed broadband direct beam, S_m, lead to underestimation of modeled AODλ. The artificial increase in readings of modern spectral photometric observations is decreased less due to smaller aperture (*e.g.* for the CIMEL-318 radiometer, the FOV = 1.2°).

5.1.2. Model M2a

Analysis of data from a smoky summer of 2002 when AERONET observations in Moscow were already available, led to a conclusion that a better match between predicted and observed values at AOD500* > 0.4, can be achieved by

substitution of initially predicted AOD500* with its increased counterpart, AOD500 (Chubarova, 2005):

$$\text{AOD500} = 1.301 \cdot (\text{AOD500*})^{1.095}. \qquad (5.2)$$

The correction, from AOD500* = 0.4 towards bigger values, increases initially predicted AOD500* but also leads to an artificial discard of corrected aerosol optical depths in a range of 0.4 < AOD500 < 0.477, an "empty zone" - rather a secondary visual defect than a functional failing. Application of model M2 together with correction for AOD500* > 0.4 is further denoted by M2a.

The third catastrophically dry and hot summer with flaming and smoldering wildfires around Moscow occurred in 2010. In contrast to two previous smoky periods, in 1972 and 2002, the summer of 2010 was characterized by higher aerosol optical depths reaching even a value of AOD500 = 4.6. In a review on radiation monitoring of all three smoky summers Chubarova *et al.* (2011a, 2011b) recommended implementation of correction by Eq. (5.2) from AOD500* = 0.5 onward which means an absence of corrected AOD500 even in a bigger range, 0.5-0.609.

5.1.3. Model M2b

However, in massive data processing, generation of a permanent empty zone for corrected AOD500 values by Eq. (5.2) is not desirable. On the other hand, for low AOD500* values, correction by Eq. (5.2) is not significant. Moreover, below a certain value, AOD500* ≤ 0.062, the implementation of Eq. (5.2), instead of the AOD500* initial value, enlargement leads to its reduction. For example, inserting AOD500* = 0.025 into Eq. (5.2) one obtains AOD500 = 0.023. In such cases the correction factor (*CF*):

$$CF = \frac{\text{AOD500}}{\text{AOD500*}} \qquad (5.3)$$

obtains values, *CF* < 1.0. Use of Eq. (5.2) only for AOD500* ≥ 0.063 (*CF* ≥ 1) avoids appearance of an empty zone for corrected AOD500 and secures a smooth correction. The use of Eqs. (5.1) and (5.2) together with a condition, for AOD500* ≥ 0.063 only, is further denoted by M2b.

5.1.4. Model M2c

Recently Gorbarenko and Rublev (2013) reported about using a solar elevation dependent correction of AOD550*. Assuming continental aerosols with a fixed Ångström exponent, α = 1, they derived a correction algorithm:

$$AOD550 = (AOD550^*) \left[0.9 + \frac{(AOD550^*)^{\frac{0.7}{0.75\sin h + 0.125}}}{5} \right], \qquad (5.4)$$

which they further applied for AOD550* > 0.5. Because AOD500* = 1.1×AOD550*, the next algorithm for 500 nm can be obtained:

$$AOD500 = (AOD500^*) \left[0.9 + 0.2 \left(\frac{AOD500^*}{1.1} \right)^{\frac{0.7}{0.75\sin h + 0.125}} \right]. \qquad (5.5)$$

However, the last formulas (Eqs. 5.4, 5.5) do not work correctly in cases of cleaner air, like the use of correction by Eq. (5.2). Instead of increasing the AOD550* or AOD500* values, they reduce it. For example, in a case of AOD500* = 0.36 and sin h = 0.5, Eq. (5.5) gives a reduced value, AOD500 = 0.34, which is not desired and that kind of correction should be avoided.

Hence, there is a lower limit of using equations (5.4) and (5.5) below what corrections do not work. This limit can be found inserting a condition (5.6) into (5.4) and (5.5):

$$AOD550 = AOD550^*, \qquad (5.6)$$

which gives the minimal turbidities, minAOD550* and minAOD500* respectively. Below these values, the corrections do not have a sense. The results depend on solar elevation:

$$minAOD550^* = 0.5^{\frac{0.75\sin h + 0.125}{0.7}} \qquad (5.7)$$

$$minAOD500^* = 1.1 \times 0.5^{\frac{0.75\sin h + 0.125}{0.7}}. \qquad (5.8)$$

For example:
    (a) sin h = 0.3, h = 17.46°, minAOD500* = 0.78,
    (b) sin h = 0.5, h = 30.00°, minAOD500* = 0.67,
    (c) sin h = 0.7, h = 44.43°, minAOD500* = 0.58,
These values are definitely higher than minAOD500* = 0.063 obtained for correction with formula (5.2) for M2b. The use of equations (5.1) and (5.5) together with condition (5.8) is denoted as model M2c.

Figure 5.1 compares results of earlier correction using Eq. (5.2) against the later one, Eq. (5.5), in regard to their common input counterpart, AOD500*. Calculations were performed for AOD500* ≥ 0, including values even below the minAOD500*. Differences between earlier and older correction appear at extremely large turbidities and low sun.

For AOD500* = 4 the correction by Eq. (5.2), published in 2005, gives AOD500 = 5.9, but the new one by Eq. (5.5), from 2013, gives AOD500 = 6.8, 8.5, 14.2 for sin h = 0.7, 0.5, 0.3, respectively.
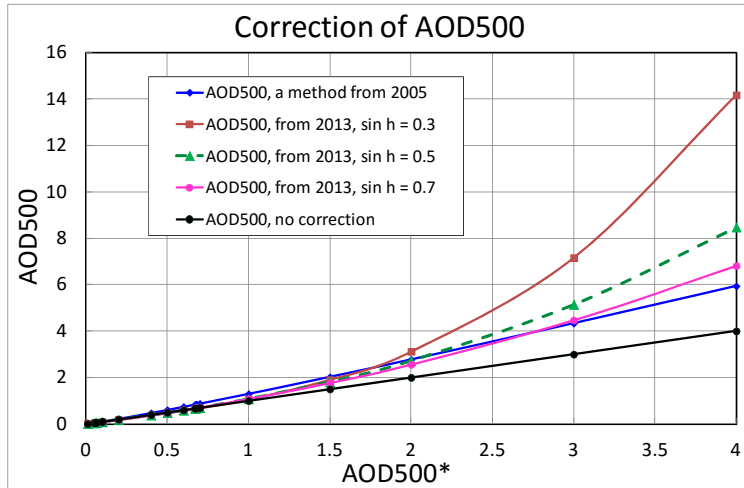

Fig. 5.1. Corrected aerosol optical depth at 500 nm (AOD500), by the method of Chubarova (2005; model M2a) and by the method of Gorbarenko and Rublev (2013; for three different solar elevations, h; model M2c) vs uncorrected AOD500*. The lowest curve, 1-to-1 line, is given for comparison.

5.1.5. Model G1

Apparently the most advanced broadband model was derived by Christian Gueymard (1998), further denoted as G1. The model, in original for prediction of AOD1000, contains about 30 formulas and allows varying several minor column gaseous components like O_3 and tropospheric and stratospheric NO_2.

However, based on our evaluations and supported by Gueymard's error analysis (2013), the variability of ozone amount can be considered a second order input because its small impact to solar broadband direct beam. Besides, nitrogen dioxide would only be of concern over polluted areas. Therefore, in the extensive runs of Gueymard's model during the study, the given fixed input values, typical for the Baltic Sea region: O_3 = 0.35 atm cm, NO_2(stratospheric) = 0.00012 atm cm, NO_2(tropospheric) = 0.00004 atm cm, p = 1013.25 hPa were used (Kannel et al., 2012).

Concerning the Ångström wavelength exponent, in accordance with Gueymard, it is in general not possible to know a priori whether the observed aerosol particles belong to the continental, maritime, or any other specific type. Therefore, a fixed conventional value of $\alpha = 1.3$, representative of particles of rural-continental origin, was proposed by Gueymard.

What concerns about wavelengths, while the preliminary output for models M1 and M2 is originally AOD550, for G1 it is the Ångström turbidity coefficient, $\beta = \text{AOD1000}$. Transitions to AOD500 are easy applying the Ångström exponential formula in a general form:

$$\mathbf{AOD(\lambda_2) = AOD(\lambda_1)\left(\frac{\lambda_2}{\lambda_1}\right)^{-\alpha}}. \tag{5.9}$$

5.1.6. Models T1 and T2

Two broadband models, T1 and T2, were developed at the University of Tartu. Model T1 is actually a modification of the M1 (Kannel *et al.*, 2007), with some changes to consider the effects of circumsolar radiation, denoted as the "revised model" above (Section 3.2 in this dissertation; Ohvril *et al.*, 2009). The model T1 is expressed by a single formula (Eq. 3.7) and has three input quantities: (a) Ångström exponent, α; (b) coefficient of column broadband transparency, p_2, transformed to atmospheric mass, $m = 2$; (c) precipitable water, W (Kannel *et al.*, 2007; Kannel, 2007; Ohvril *et al.*, 2009).

Model T2 was derived using barely a statistical approach (Section 3.4). In creating the method, a large database, including almost 20 000 complex, spectral and broadband direct solar beam observations at Tõravere, Estonia, during all seasons of an 8-year period, 2002–2009, was used (Section 4.1). Apparently, the model is local and, strictly speaking, could be used only in conditions similar to Tõravere (Kannel *et al.*, 2012). Monthly climatology of column optical parameters for Tõravere will be given below in Section 6.1. Model T2 relies only on two input parameters: (a) the Bouguer column broadband transparency coefficient, p_2; (b) amount of precipitable water, W. These parameters allow to calculate, for $m = 2$, a specific quantity, the column broadband aerosol optical depth (BAOD2). According to Kannel *et al.* (2012), the two optical depth parameters, AOD500 and BAOD2, are strongly correlated, $R^2 = 0.96$, through a second-degree polynomial (Eq. 3.31). This finding allows an easy calculation of AOD500. Table 5.1 lists all, in total eight, considered broadband AODλ models with their input and output quantities.

Table 5.1. List of considered broadband $AOD\lambda$ models. Possible inputs are: h – solar elevation; S_m – broadband direct solar irradiance; p_2 – broadband (integral) Bouguer coefficient of column transparency for optical air mass $m = 2$; W – precipitable water; α – Ångström wavelength exponent; O_3 – column ozone content; NO_2 – column nitrogen dioxide content

No	Acronym; reference	Input	Number of formulas	Output	Correction of prediction
1	M1; Tarasova, Yarkho, 1991a, b	h, S_m, W, α $O_3 = 300$ DU	13	AOD550	Not used
2	M2; Abakumova, Gorbarenko, 2008	$h, S_m, W, \alpha = 1$ $O_3 = 300$ DU	1	AOD550	Not used
3	M2a; Chubarova, 2005	$h, S_m, W, \alpha = 1$ $O_3 = 300$ DU	2	AOD500	For AOD500 > 0.4
4	M2b; Chubarova, 2005	$h, S_m, W, \alpha = 1$ $O_3 = 300$ DU	2	AOD500	For AOD500 ≥ 0.063
5	M2c; Gorbarenko, Rublev, 2013	$h, S_m, W, \alpha = 1$ $O_3 = 300$ DU	2	AOD550	Depends on solar elevation
6	G1; Gueymard, 1998	$h, S_m, W, \alpha = 1.3,$ O_3, NO_2	> 30	AOD1000	Not used
7	T1; Kannel, 2007, Ohvril *et al.*, 2009	p_2, W, α $O_3 = 300$ DU	1	AOD500	Not used
8	T2; Kannel *et al.*, 2012	p_2, W	2	AOD500	Not used

5.2. Verification of AOD models against AERONET

Test runs of the 8 selected models contained $N = 26091$ single calculations of AOD500 by each model and a following comparison against the reference AOD500(AERONET) values. Two models, M1 and T1, allow to vary the input value of the Ångström exponent, α. For this reason, additional runs with variation of α were performed for models M1 and T1.

To obtain quantitative measures on the accuracy of the models, two linear regression parameters, slope and correlation R^2 (actually coefficient of determination), and the following three commonly used cumulative statistics (Iqbal, 1983; Gueymard, 1993, 2003) are used:

a) the mean bias deviation (MBD), expressing the average deviation (difference) of the predicted values, $y_i = $ AOD500(Model), from the reference value, $x_i = $ AOD500(AERONET):

$$\mathbf{MBD} = \frac{1}{N} \sum_{i=1}^{N} [y_i - x_i],$$
(5.10)

ideally, a zero value of MBD should be obtained;

b) the root mean square deviation (RMSD), a measure of the variation of predicted values around the reference values:

$$\mathbf{RMSD} = \frac{1}{N}\left[\sum_{i=1}^{N}(y_i - x_i)^2\right]^{1/2}, \qquad (5.11)$$

the RMSD is always positive, however, a zero value is ideal; note that a few large variations of the predicted amount of AOD500 from the observed AOD500(AERONET) can substantially increase RMSD;

c) the mean absolute relative deviation (MARD), also known as mean absolute percentage deviation (MAPD), expressing the average value of relative deviations:

$$\mathbf{MARD} = \frac{1}{N}\sum_{i=1}^{N}\left|\frac{y_i - x_i}{x_i}\right|. \qquad (5.12)$$

The amount of column water vapor (W) is an input parameter to all considered AODλ models. In this work, the W was estimated from surface conditions using its correlation with water vapor pressure, e_0 (3.30; Okulov $et\ al.$, 2002). On the level of monthly means, the used correlation performs pretty good (below, in Chapter 6.1), but for single observations the coefficient of determination, $R^2 = 0.83$ (Fig. 3.7), indicates a moderate scatter of $W(e_0)$ around W(AERONET) (Kannel $et\ al.$, 2012). Overestimation of W leads to underestimation of AODλ, even to physically unrealistic negative AODλ. For the sake of brevity, sensibility analysis of considered models in regard to possible W errors is not included in the present study. Only the number of predicted negative AOD500 values together with a number of corrections (to consider circumsolar radiation in cases of large turbidities) applied for each run of the model is given (Table 5.2).

Results of the 8 main runs, which can be identified with the yellow background in Table 5.2, are presented in Figure 5.2, where each panel also contains performance statistics of the run: slope, correlation (actually, R^2), numbers of corrected values and predicted negative AOD500 values.

Table 5.2. Inputs of the Ångström exponent (column 3) and performance statistics (columns 4 to 10) for AOD500 predictions by different models against AOD500 (AERONET) observations during 2002-2011. In each run, the total number of predictions is 26091. Numbers in bold indicate the best results in column. Negative predictions are physically unrealistic

| 1	2	3	4	5	6	7	8	9	10
Row	Model, Figure	Ångström alpha as input	Number of corrections	Slope	R^2	Negative predictions	MBD	RMSD	MARD
1	M1	1.2	not used	0.935	0.933	107	-0.002	0.032	0.203
2	M1, Fig. 5.2	1.3	not used	0.974	0.936	129	0.003	0.030	0.214
3	M1	1.4	not used	1.016	0.938	143	0.009	0.031	0.233
4	M1, Fig. 5.4	individual	not used	1.055	0.945	159	0.013	0.032	0.247
5	M2, Fig. 5.2	1.0	not used	0.912	0.923	45	-0.004	0.034	0.203
6	M2a, Fig. 5.2	1.0	822	**0.995**	0.947	45	**0.001**	0.029	0.201
7	M2b, Fig. 5.2	1.0	21733	1.060	0.947	45	0.011	0.033	0.230
8	M2c, Fig. 5.2	1.0	213	0.917	0.927	45	-0.004	0.033	0.203
9	G1, Fig. 5.2	1.3	not used	0.972	0.929	1	0.009	0.029	0.221
10	T1	1.2	not used	0.915	0.934	**0**	-0.003	0.032	0.197
11	T1, Fig. 5.2	1.3	not used	0.962	0.936	1	0.004	0.029	0.211
12	T1	1.4	not used	1.009	0.938	1	0.011	0.030	0.232
13	T1, Fig. 5.4	individual	not used	1.088	0.941	2	0.017	0.037	0.253
14	T2, Fig. 5.2	not used	not used	1.013	**0.957**	**0**	0.005	**0.026**	**0.188**
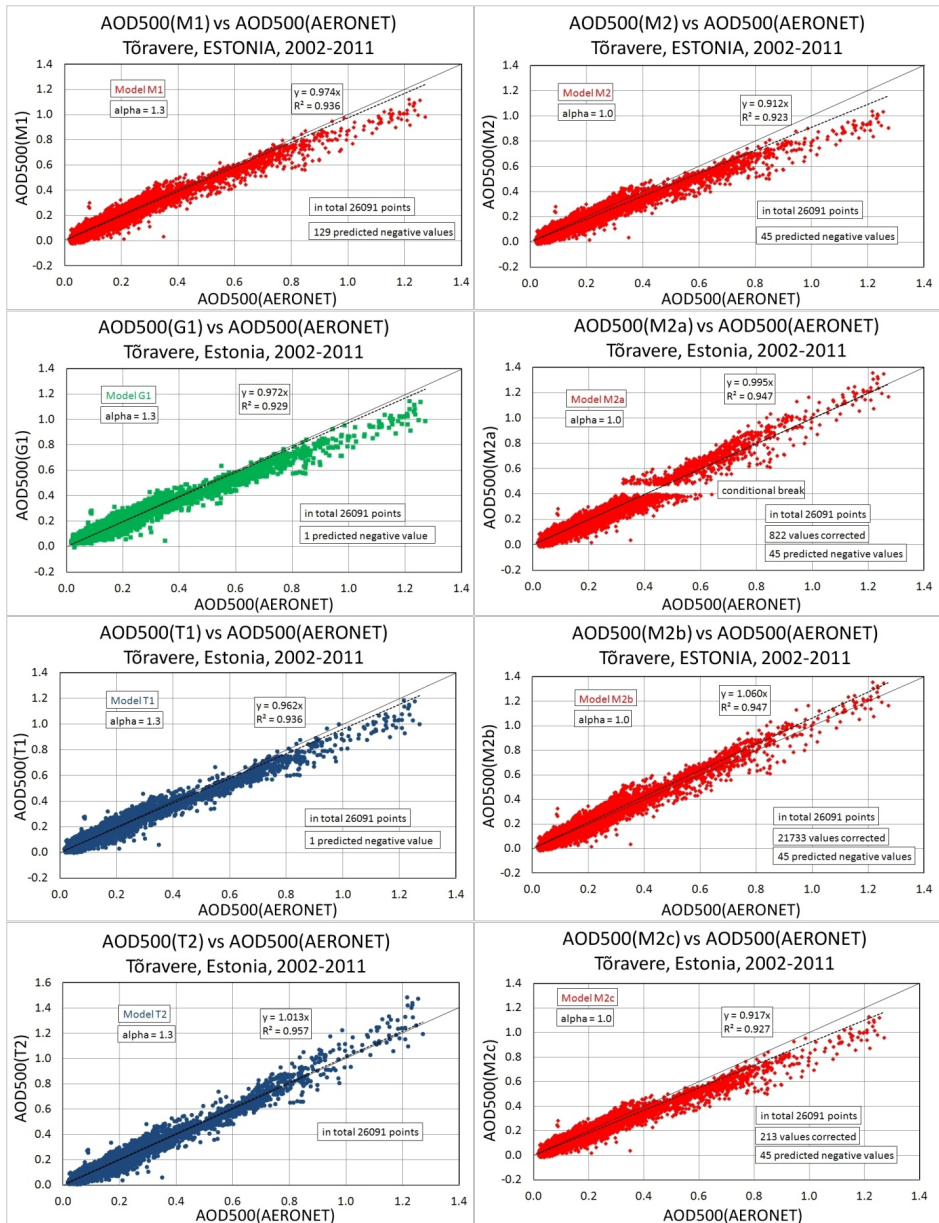
Fig. 5.2. Results of main runs of eight different models: predicted AOD500 against the AOD500(AERONET) reference observations. Each panel contains 26091 single predictions for 10 years 2002–2011. All months, except December, are included. The Ångström exponent is fixed, $\alpha = 1$ or $\alpha = 1.3$, respectively. The three models, M2a, M2b, M2c, use an individual correction scheme which improves predictions at greater turbidities. Dashed lines represent linear regression. Solid lines give 1-to-1 relationships.

Table 5.2, besides of eight main runs, also lists results of 6 additional, special runs: (a) two runs for both, M1 and T1 with different fixed wavelength exponent (with the gray background), α = 1.2 and α = 1.4, respectively; and (b) a run for both, M1 and T1 with a priori known, *i.e.* individual wavelength exponents (with the blue background). The last 2 special runs, with individual wavelength exponents, will be visualized below, in Figure 5.4 (Section 5.3).

From Table 5.2, which includes six different statistics, one can rank the accuracy of performance by different models in regard to different statistics (including various Ångström α, if applied). For ranking purposes, a "hexathlon" is organized where models listed in Table 5.2 are competitors. A single penalty point will be given for the best result in each single *event* (presented by successive columns 5, 6, 7, 8, 9, 10, respectively) of the "hexathlon"; two penalty points gets the second result, etc. Finally, the worst result in each "event" deserves 14 penalty points. Theoretical best overall score of a model can reach 6 penalty points, if the model would win in every single "event". Summarizing the overall performances, two models give slightly better results. The T2 model appears to score 15 penalty points, which was the best result, and the M2a, 16 points as the "first runner-up" (Figure 5.3). These two models can be recommended, because of their consistently high performance in all items, for evaluation of AOD500 in environmental conditions similar to Tõravere. The two models, M1 (row 4), and T1 (row 13) that consider a priori known Ångström exponents did not stand out. This unexpected result will be analyzed in Chapters 5.3, 6.2 and 6.3, respectively.
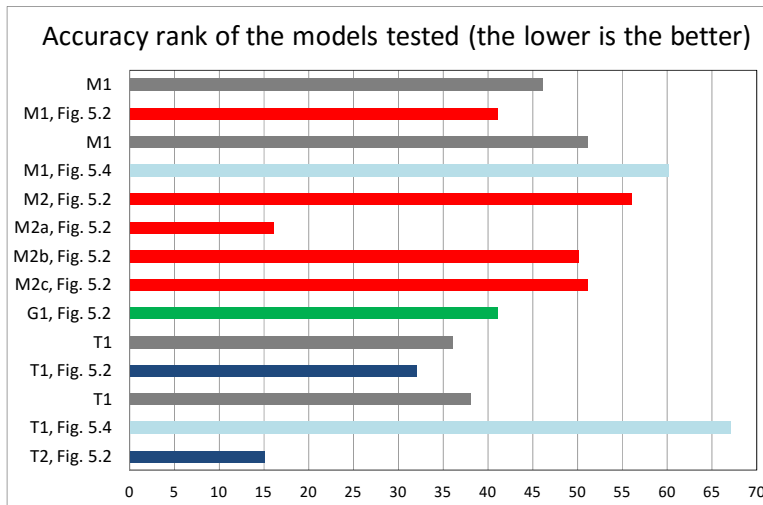

Fig. 5.3. "Hexathlon" of accuracy results of the tested AOD models. Six different statistics correspond to six "events" in Table 5.2. "Event" winner scores 1 penalty point, theoretical best result is 6 penalty points as a winner in all "events". Model T2 wins with 15, and M2a scores second position gaining 16 penalty points.

5.3. Fixed vs individual Ångström exponent

Usually broadband models for calculation of AODλ do not enable change of the Ångström wavelength exponent, α. Regarding that, the M1 model (created in the Moscow State University) and its derivate, T1 (created in the University of Tartu), represent an exception. Nevertheless, it is meaningful that authors of the M1 themselves actually have not used this opportunity, they first started to use M2 and then M2a, where in both, the exponent is fixed, α = 1. In the Gueymard's model G1 the exponent is also fixed, α = 1.3. However, the M1 and G1 assume validity of the Ångström exponential formula (Eq. 2.4). On the other hand, this means that the aerosol radius-number, or size-number distribution, $n(r)$, (usually represented in $cm^{-3}\mu m^{-1}$ if *in situ* volume concentration is measured, or in $cm^{-2}\mu m^{-1}$ in the case of column observations) is partly given by the Junge power law (Deepak, Box, 1979; Liou, 2002):

$$n(r) = C(r)\,r^{-(\alpha+3)},\qquad(5.13)$$

where C is a scaling factor proportional to particles volume or column concentration and r is a particle radius. "Partly given" means that only the downgoing part of a size distribution (onward from the maximum) can be approximated with the power law.

The merged, 26 091 observation database for years 2002–2011 (described in Section 4.1) is special, because each single observation contains also an Ångström AERONET-evaluated exponent, α(440-500-675–870), calculated as a best fit for the indicated four wavelengths. In this way the database enabled to consider a priori known Ångström exponents for prediction of every single AOD500 values.

However, special runs of models M1 and T1 with a priori known α (rows 4 and 13, Table 5.2) gave no expected improvement of the predictions comparing with main runs with constant α values (Figure 5.4).
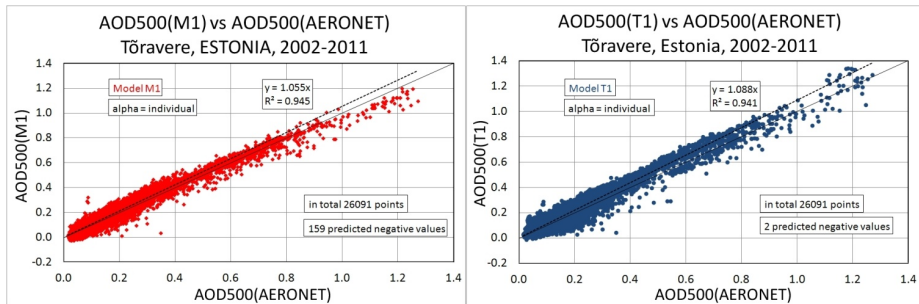

Fig. 5.4. Predicted AOD500 with M1 (left panel) and with T1 (right panel) against the AERONET observations. In each single prediction of total 26091, the Ångström exponent is considered a priori known. Dashed lines represent linear regression. Solid lines give 1-to-1 relationships. Performance statistics of both runs (rows 4 and 13, Table 5.2, respectively) is not so resulting compared to runs of the model M1 with appropriately fixed α, or runs of T2 without any use of α at all.

So, the a priori known Ångström exponents did not improve AOD500 predictions. But, should they? Consider the Ångström formula is obeyed, then the exponent enables only transition from a known $AOD\lambda_1$ to any other $AOD\lambda_2$, not to start with the magnitude of $AOD\lambda_1$ itself. In terms of the Ångström formula, prediction of $AOD\lambda_1$ can be done using a second parameter, the Ångström turbidity coefficient, β.

In Section 6.1 a background examination of seasonal variability of some column optical and humidity properties at Tõravere, 2002–2011, will be presented. However, there will be more to say about the Ångström exponent in Sections 6.2 and 6.3.

5.4. Verification against satellite measurements

Due to their extensive spatial coverage, satellite spectral AOD observations have been widely used to estimate the large-scale spatial and temporal variability of column and surface aerosol load (Li *et al*., 2015). Below, the focus has targeted on intercomparison of daily mean column AOD500 values above Tõravere from several origin, retrieved by satellite, AERONET and broadband model T2.

Both, Terra- and AquaMODIS satellite information systems allow downloading of daily mean AOD550 and Ångström exponent for 1×1 deg nadir pixels. Using the Ångström formula, the AOD550 values can be transformed to AOD500 ones. In this thesis, Tõravere has been considered in the center of the 1×1 deg geographical area (Fig. 5.5). During 2010, there were 94 days when data from all the three AOD instruments (two satellites and the Tõravere AERONET photometer) as well as observations from broadband actinometer were available. Results of AOD500 comparisons are plotted in four panels of Fig. 5.6, where the left panels represent tests of AquaMODIS and TerraMODIS against daily means of AERONET as a reference instrument. Although the uncertainty for slope is about 6% only, the consistency of data in both cases is low, $R^2 = 0.775$ and 0.702, respectively.
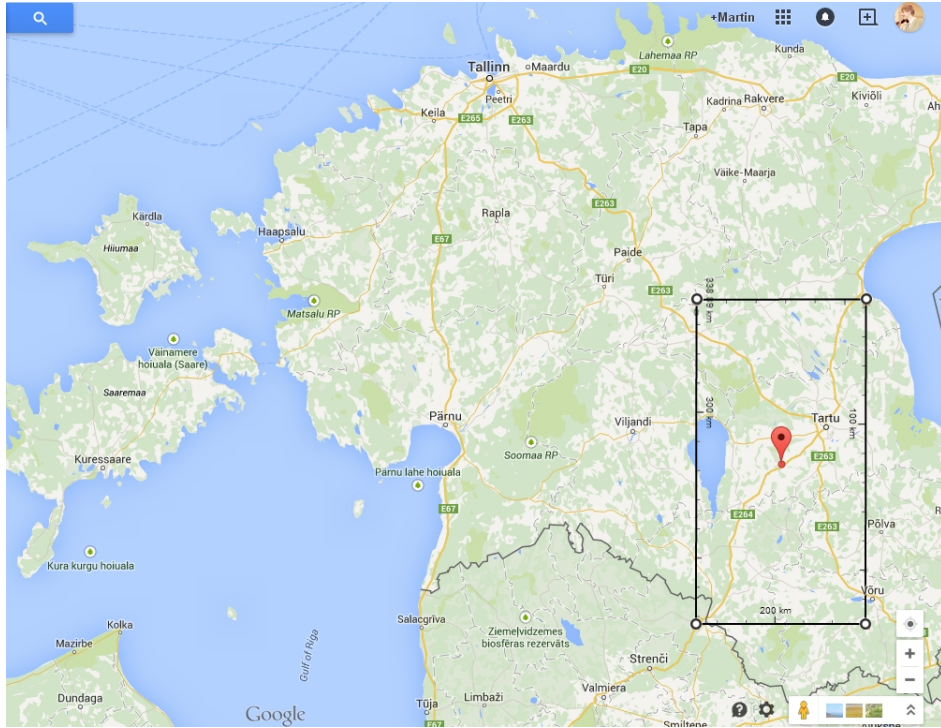
Fig. 5.5. Estonian map provided by Google Inc., where 1x1 deg pixel around Tõravere meteostation (the red balloon) is marked. The width of the rectangle is ~58 km, the height ~112 km.

In the right panels of Fig. 5.6, the AOD500 daily means from BAOD are tested against TerraMODIS and AquaMODIS satellites, respectively. As expected, the uncertainty for slope is bigger, about 10% and the consistency is slightly lower ($R^2 = 0.747$ and 0.682, respectively) than comparing satellite data against the AERONET data in the left panels.

But, what is special in all panels of Fig. 5.6, is a possibility to get negative AOD500 values by both satellites. Apparently, this kind of mistakes happens due to overestimation of column precipitable water, W. There aren't negative predictions neither by AERONET observations nor by the BAOD model calculations.
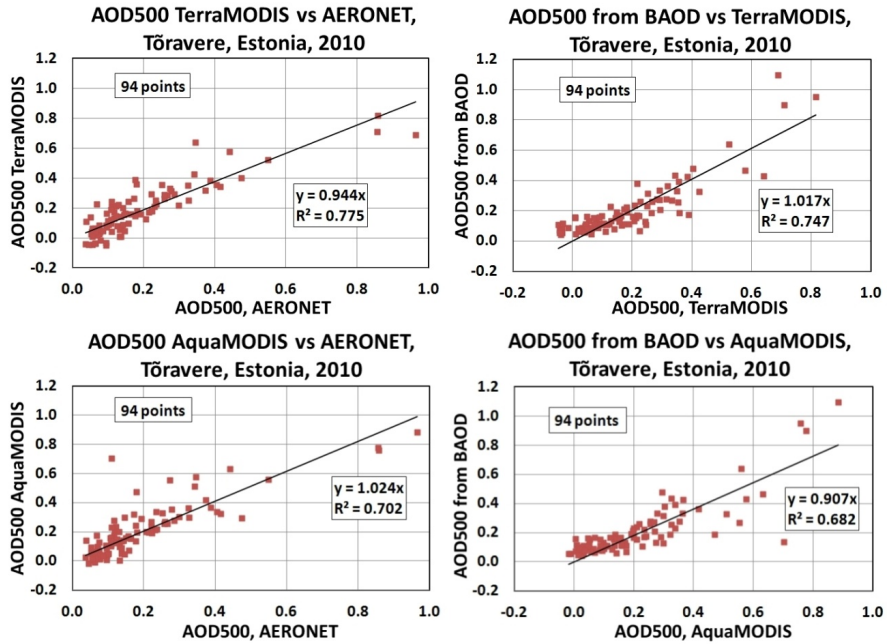
Fig. 5.6. The left panels: AOD500 daily means from the MODIS satellites plotted against the reference, AERONET Tõravere observations. The right panels: AOD500 daily means as predicted by broadband aerosol optical depth, BAOD2 (model T2), plotted against AOD500 observed by the MODIS satellites. Note that in several occasions the satellite observed AOD500 values are negative. In total, 94 daily means are used.

6. CLIMATOLOGY ANALYSIS

In this chapter several atmospheric column optical and humidity parameters as observed at Tõravere (such as transmittance, optical depth, precipitable water etc) are analyzed in terms of monthly means. Also the problems associated with Ångström exponent are discussed.

6.1. Variability of column optical and humidity parameters

Figure 6.1 (Kannel *et al.*, 2014) provides monthly means of the Ångström α and AOD500 and, in addition, seasonal variation of the fine mode fraction (FMF), which is one of the AERONET inversion products describing contribution of fine particles to AOD500. The AERONET inversion code finds the minimum of the size distribution within the radius interval from 0.439 to 0.992 μm. This minimum, approximately at 0.6 μm radius, is used as a separation point between fine and coarse mode particles. Using that separation, the inversion code calculates contribution of fine particles to formation of AOD500 (AERONET Inversion Products, 2010; O'Neill *et al.*, 2001). The AERONET term, "fine particles", actually includes three traditional subregions of aerosol size distribution: the nucleation, Aitken and accumulation mode, respectively.

As expected, the intra-annual evolution of the Ångström exponent is consistent with monthly changes in the FMF. The higher α values in summer (Jun-Jul-Aug) indicate domination of fine aerosol particles.

Somewhat surprising is a local minimum of AOD500 in June. Concerning the cold season, there are no good explanations to the higher AOD500 in January and November compared to February and October, this is a topic of further studies.

The monthly means of column transparency (p_2) for 2002–2011 (Fig. 6.2) are in opposite phase with AOD500, with an expected local maximum of transparency in June (Kannel *et al.*, 2014). Actually, higher column transparency in June was noticed already since 1994. This finding can be partly explained by a general cleaning of the European atmosphere as a part of the global brightening (Ohvril *et al.*, 2009; Okulov and Ohvril, 2010). During June, the Estonian landscape is already totally covered with fresh vegetation restricting creation (take off) and vertical distribution of soil dust particles. The number of forest and bog fires is also low in June.
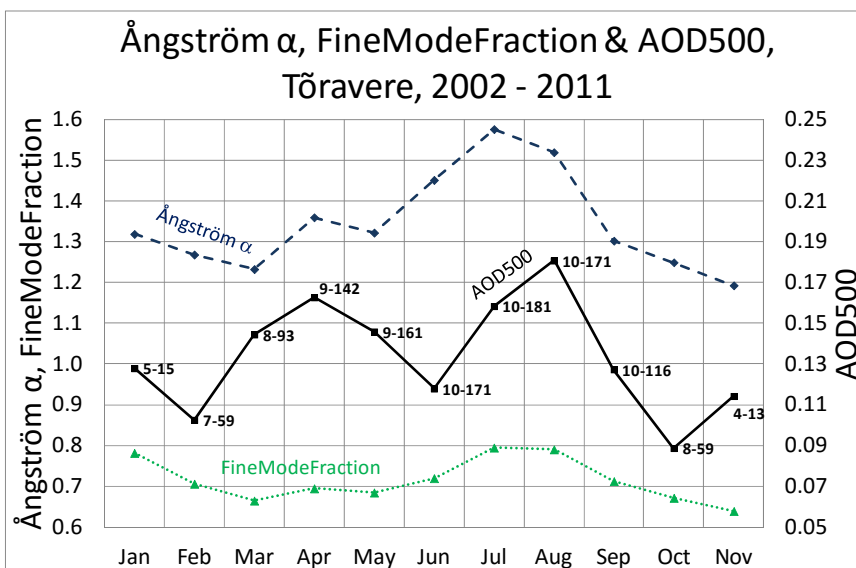
Fig. 6.1. Monthly means of the Ångström exponent, AOD500, and fine mode fraction at Tõravere, Estonia. Labels give total numbers of single months and days during 2002–2011 when the AERONET observations were performed: *e.g.* in January, the AERONET observations took place in 5 different years containing together 15 observational days.
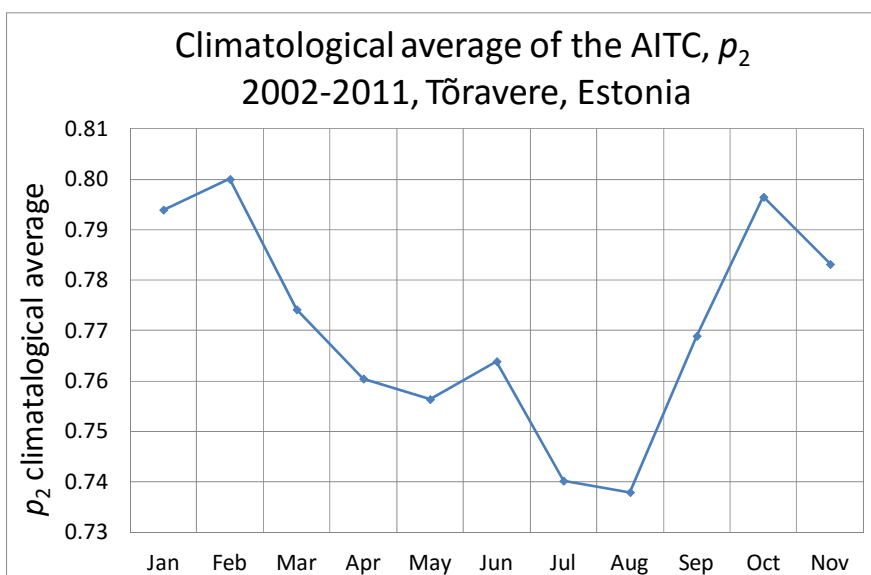

Fig. 6.2. Monthly means of the atmospheric integral transparency coefficient p_2 at Tõravere, Estonia, 2002-2011. In the merged database, there were no observations in December.

Besides broadband direct irradiance or column broadband transparency, the second main input parameter in AODλ broadband models is column precipitable water, W.

In the present study, column precipitable water was evaluated from surface humidity and temperature, (Eq. 3.30). This parameterization was developed from daytime clear sky radio-soundings in Tallinn (Okulov *et al.*, 2002). For Tõravere, a comparison of column humidity predictions, from $W(e_0)$, against W(AERONET), where the last was considered as a reference, was made (Fig. 3.7).

Use of almost 20 000 parallel observations, where humidity data from broadband instruments and the reference, W, estimation from AERONET, were available from 2002-2009, showed that the W prediction overestimates the reference as an average only by 3%. Regarding monthly means of W over all considered years (2002-2011), approximation (Eq. 3.30) gives values close to those obtained by the AERONET photometer (Fig. 6.3) (Kannel *et al*., 2014).
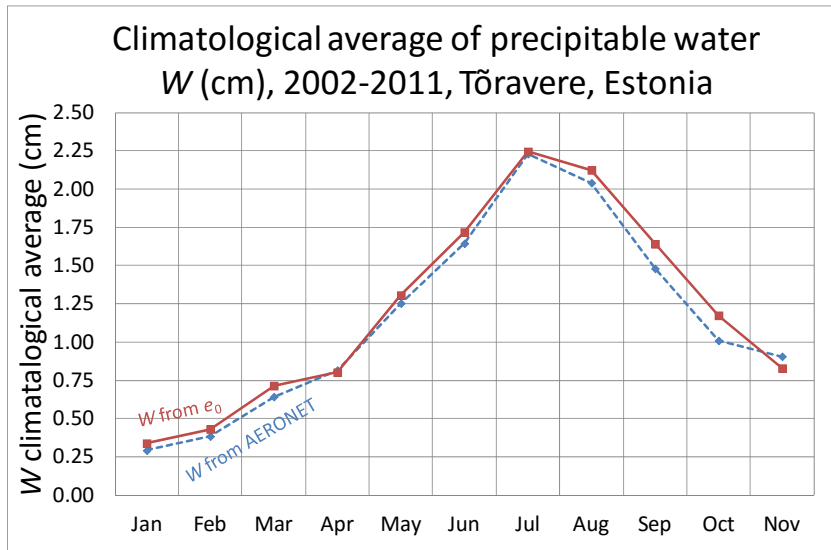

Fig. 6.3. Monthly mean precipitable water at Tõravere, Estonia, 2002-2011. Solid line corresponds to estimations through surface water vapor pressure, $W(e_0)$. Dashed line represents AERONET photometric observations, W(AERONET). In the merged database, there were no observations in December.

In order to reveal structure of the extinction of broadband direct solar beam in a slant atmospheric column m, we represent its total transmittance τ_m in three successive layers or substances: an ideal atmosphere, water vapor, aerosol particles (Section 2.4; Kannel *et al.*, 2012). Combining (2.13) and (2.15) gives:

$$\tau_m = \tau_{\text{CDA},m}\ \tau_{W,m}\tau_{\text{aer},m}\ .\tag{6.1}$$

Figure 6.4 (Kannel *et al*., 2014) shows monthly mean broadband transmittances for named three layers at Tõravere, calculated from our joint 10-year, 2002–2011, database. The plots were prepared using only meteorological data (direct solar irradiance and surface water vapor pressure), not spectral AERONOT observations. Noticeable is the summer maximum of aerosol broadband transmittance in June, apparently being the main reason of higher total column transmittance in this month. The lowest total transmittance occurs in July and August, caused by low transmittances of both, column water vapor and aerosols. The total transmittance is lower than any of its components and is therefore scaled to the more sensitive secondary vertical axis.

In the climatological average of all observed 10-year period, the total transmittance $\tau_m = 0.59$ and $p_2 = 0.77$. February is the month of the best overall transparency (and transmittance) with the values of $\tau_m = 0.64$ and $p_2 = 0.80$ respectively.
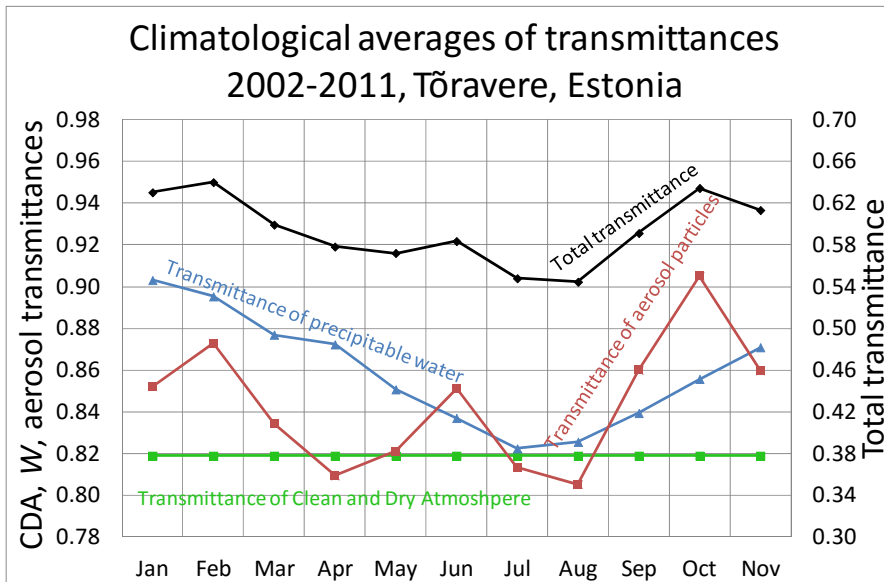

Fig. 6.4. Broadband transmittances, for a slant column, $m = 2$ (solar elevation $h \approx 30°$) of different atmospheric layers at Tõravere, Estonia, 2002-2011. Calculations are based solely on meteorological and broadband actinometric, not the AERONET spectral observations. Total transmittance is scaled to the secondary vertical axis. In the merged database, there were no observations in December.

Transmittance is one of classic actinometric parameters. It allows, as seen in Fig. 6.4, easy quantitative, proportional evaluation of contribution of each of three main atmospheric component layers to attenuation of broadband direct solar beam. However, studying relations between aerosol load (*e.g.* aerosol number concentration, volume or mass concentration, etc) and column aerosol optical properties, another quantity, optical depth δ is often used, as well as by the AERONET team (Holben *et al*., 1998) and by the Global Atmosphere Watch program (Aaltonen *et al*., 2006). It follows from definition of column optical depth, $\delta_{aer, m}$:

$$\tau_m = \exp(-m\delta_m),$$
(6.2)

that

$$\delta_m = -\frac{1}{m} \ln \tau_m,$$
(6.3)

and a multiplicative equation for column transmittances (6.1) transforms to an additive one for column optical depths,:

$$\delta_m = \delta_{CDA,m} + \delta_{W,m} + \delta_{aer,m}.$$
(6.4)

Figure 6.5 (Kannel *et al*., 2014) shows seasonal variation of total broadband optical depth (δ_m), and its division into three main atmospheric constituents. The figure can be used, as background information, for an easy interpretation of yearly evolution of column aerosol and water vapor load.

As one can observe from Fig. 6.5, column total broadband aerosol optical depth ($\delta_{aer,m}$) has a wave-shape seasonal evolution, which, in terms of interannual variability, agrees well with AOD500 (Fig. 6.1). But seasonal evolution of $\delta_{aer,m}$ is reversed to p_2 (Fig. 6.2) as well as to transmittance due to aerosol particles (Fig. 6.4). There are lower AOD500 values in February, June and October. There are no good explanations for a slightly cleaner air in February compared to January and March. Concerning June, the Estonian landscape is just totally covered with rampant vegetation restricting creation and vertical distribution of soil dust particles. The number of forest and bog fires is also low in Estonia in June.

April is a spring month when snow and ice have just thawed and the soil becomes dry and unprotected to wind erosion. Higher values of both, spectral and broadband aerosol optical depth, in April are apparently due to bigger (soil, dust) aerosol particles, because there is almost no increase in values of fine mode fraction, from February to May, FMF ≤ 0.7 (Fig. 6.1).

Supported by peaks in precipitable water, total broadband optical depth (δ_m) obtains its highest seasonal values, $\delta_m = 0.3$, in July and August. Also the role of fine mode fraction is highest in these months, FMF ≈ 0.8 (Fig. 6.1), an evidence of more small particles, apparently due to forest and bog fires on the Estonian territory and in the neighborhood.
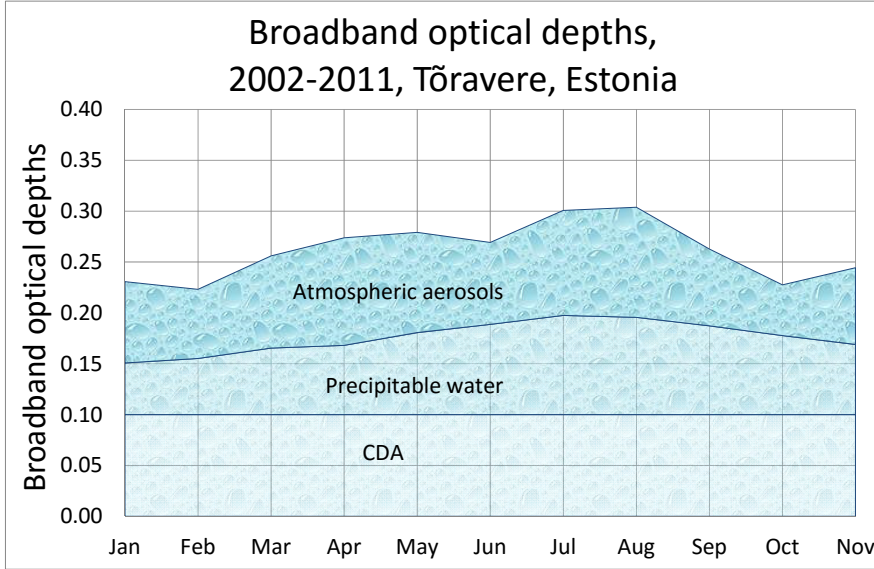

Fig. 6.5. Seasonal trends of broadband optical depths for main three atmospheric layers at Tõravere, Estonia, 2002-2011. Calculations correspond to a slant column, $m = 2$ (solar elevation $h ≈ 30°$). Monthly mean values are affiliated to beginnings of months. In the merged database, there were no observations in December.

In September and October rains wash out aerosol particles from the atmosphere, optical depth of total as well as of aerosols decreases.

6.2. Revisiting the Ångström formula

Returning now to the Ångström formula (2.4), it can be rewritten in the following form:

$$\mathbf{AOD}\lambda = \beta \times \left(\frac{\lambda}{\lambda_0}\right)^{-\alpha} = \beta \times \lambda_0^{\alpha} \times \lambda^{-\alpha} \quad . \tag{6.5}$$

However, for simplicity's sake, Schifrin's (1995) general concept will be abandoned and λ will be considered as with unit of μm and $\lambda_0 = 1$ μm. Hence, the Ångström classic presentation is returned:

$$\mathbf{AOD\lambda = \beta \times \lambda^{-\alpha}} \ . \tag{6.6}$$

Logarithm of this equation gives:

$$\mathbf{ln(AOD\lambda) = ln\beta - \alpha \ ln\lambda,} \tag{6.7}$$

Equation (6.7) represents linear dependence between the logarithm of aerosol optical depth, $y = \ln(AOD\lambda)$, and the logarithm of wavelength, $x = \ln\lambda$. In this linear dependence, $\ln\beta$ is the y-function's intercept and $-\alpha$ corresponds to the slope of the line in regard to the x-axis. The slope is expressed as

$$\mathbf{-\alpha = \frac{dy}{dx} = \frac{d\ln(AOD\lambda)}{d\ln\lambda} = \frac{\ln(AOD\lambda_2) - \ln(AOD\lambda_1)}{\ln\lambda_2 - \ln\lambda_1} = \frac{\ln\left(\frac{AOD\lambda_2}{AOD\lambda_1}\right)}{\ln\left(\frac{\lambda_2}{\lambda_1}\right)}} \ . \tag{6.8}$$

Popularity of the Ångström formula raised considerably after a famous work published in 1955 by Christian Junge (1912–1996). He showed that assuming aerosol particles to be spheres, the size distribution of large and giant particles can be expressed approximately by a simple law

$$\mathbf{\frac{dN(r)}{d(\log r)} = C \times r^{-\nu}} , \tag{6.9}$$

where r is the particle radius that formally can extend from almost zero to infinity, and N is the cumulative (integral) radius-number distribution function. Following Junge, the exponent in (6.9) is about 3, *i.e.* $\nu \approx 3$. Junge showed that two exponents, the Ångström wavelength exponent α and the power-law exponent ν depend on each other in a rather simple way:

$$\mathbf{\alpha = \nu - 2} , \tag{6.10}$$

e.g., $\nu = 3.3$ leads to $\alpha = 1.3$, *i.e.* to an average obtained by Ångström (1929, 1930). The power law size distribution is often referred to as "the Junge distribution" or as "the Junge/ Ångström approach".

However, linear equation (6.7) is an idealization and the dependence between $\ln(AOD\lambda)$ and $\ln\lambda$ is more complicated.

The next step on spectral behavior of AODλ was taken by Michael King and Dale Byrn (1976), who noted, that the monotonously decreasing aerosol size distribution (6.9) is never exactly followed nor have radii extending from zero to infinity. Both, non-Junge size distributions and radii extending finite radii limits, introduce some curvature on a ln(AODλ) vs 1nλ plot, but do not drastically alter the basic linear shape.

Since (Eq. 6.7) implies no curvature, King and Byrn (1976) added a second-order term that changes a linear fit with a parabolic fit:

$$\mathbf{ln(AOD\lambda) = a_0 + a_1 \ln \lambda + a_2 (\ln \lambda)^2.} \qquad (6.11)$$

Further development in interpretation of departures from linearity in slope of the logarithm of optical depth versus the logarithm of wavelength, is strongly related to the AERONET team. In an extended paper, Eck *et al.* (1999) used AERONET data from various climatic locations, studying wavelength dependence of aerosol optical depth for three common types of aerosol particles: (a) biomass burning; (b) urban-industrial; (c) desert dust.

The authors concluded that biomass burning and urban aerosols exhibit pronounced curvature in the ln(AODλ) versus ln λ relationship at high and moderate optical depths because of the dominance of accumulation mode size distribution (this induces a local minimum in size distribution which is not monotonously decreasing therefore). A second-order polynomial fitted to the measured AODλ values (λ = 340–1020 nm) gives excellent agreement with differences of the same order as the measurement uncertainty of AODλ (≈ 0.01–0.02).

As a complement to the Ångström exponent α, a measure of the curvature of the ln(AODλ) versus ln λ relationship, the authors (Eck *et al.* 1999) proposed the second derivative of ln(AODλ) versus ln λ or the derivative of α, *i.e.* α′, with respect to the logarithm of wavelength:

$$\mathbf{\alpha'(\lambda) = \frac{d\alpha}{d(\ln \lambda)}} \, . \qquad (6.12)$$

Apparently, for practical calculations of α′, when $d(\ln \lambda)$ is changed to $\Delta(\ln \lambda)$, a minimum of three wavelengths is required.

An answer to question "how the non-Junge types of aerosols can be modeled?", was given by O'Neill *et al.* (2001) and Schuster *et al.* (2006). The ideology of these works lies in a statement that the classical Ångström formula, related to monotonously decreasing (the Junge-type) size distribution, is not an exact description of nature. More detailed modular description of the particle size distribution is necessary. The authors proved that spectral behavior of the AODλ and its first and second spectral derivates (α and α′) can be largely

described in terms of a particles bimodal size distribution (mainly the accumulation and the coarse mode, respectively).

Concerning investigations of this dissertation, results of the four cited publications (King and Byrn, 1976; Eck *et al.,* 1999; O'Neill *et al.*, 2001; Schuster *et al.*, 2006) help us to interpret spectral behavior of AODλ, measured by AERONET at Tõravere and to explain a failed expectation to find links between the Ångström exponent α and the AODλ (below and in Section 6.3).

In Fig. 6.6, according to AERONET observations at Tõravere, three examples on wavelength dependence of the aerosol optical depths are given: (a) for high turbidity due to biomass burning when the accumulation mode is typically dominant); (b) for normal (intermediate) turbidity; and (c) for low turbidity *i.e.* very clear air, respectively.
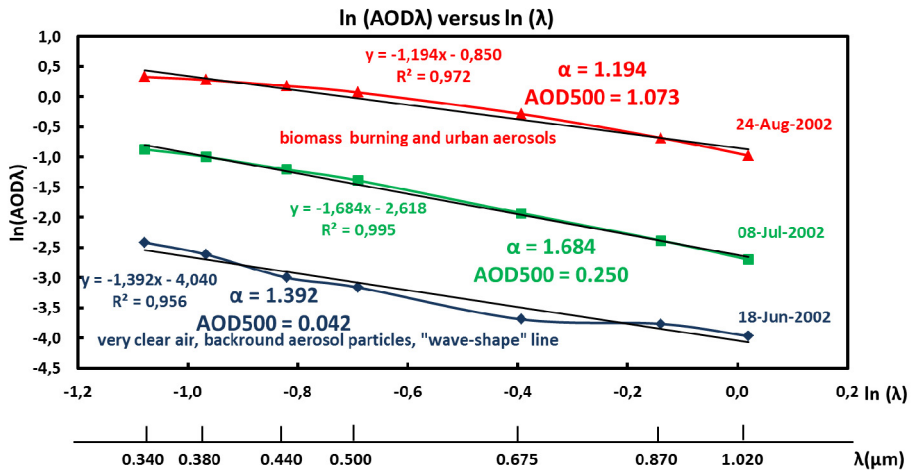

Fig. 6.6. Three plots of ln(AODλ) against lnλ at Tõravere: (a) 24-Aug-2002, a day with high turbidity, AOD500 = 1.07, with biomass burning aerosol particles inducing an obvious positive spectral curvature; (b) 08-Jul-2002, a day with normal turbidity, AOD500 = 0.25, the curvature is only weakly expressed; (c) 18-Jun-2002, a day with very clear air, AOD500 = 0.04, behavior of ln(AODλ) is irregular, resembling a "random-wave-shape" line.

The upper curve in Fig. 6.6, with its α = 1.194 and AOD500 = 1.07, corresponds to a day with high aerosol loading from biomass burning. According to HYSPLIT trajectory model, the air came to Tõravere at August, 24, 2002 from the northern Russia with north-east winds (Fig. 6.7, left panel). Satellite pictures by MODIS Rapid Response for the same time and place weren't informational because of heavy cloudiness. A better picture was taken probably a day before, on August 23rd, 2002 at 09:10 UTC, where fireplaces in south-eastern Estonia and more in the neighboring territories can be find (Fig. 6.7

right panel). There is a positive curvature in the presentation of ln(AODλ) versus lnλ indicating the dominance of accumulation mode size particles. A large value of the daily average FineModeFraction, FMF = 0.978, supports this idea.

Note that the AERONET inversion code finds the minimum of volume size distribution within the radii interval from 0.439 to 0.992 μm. This minimum is used as a separation point between fine and coarse mode particles. Using that separation, the code simulates optical thicknesses for both modes (O'Neill *et al.*, 2001; David M. Giles, personal communications; http://aeronet.gsfc.nasa.gov → AEROSOL INVERSIONS).
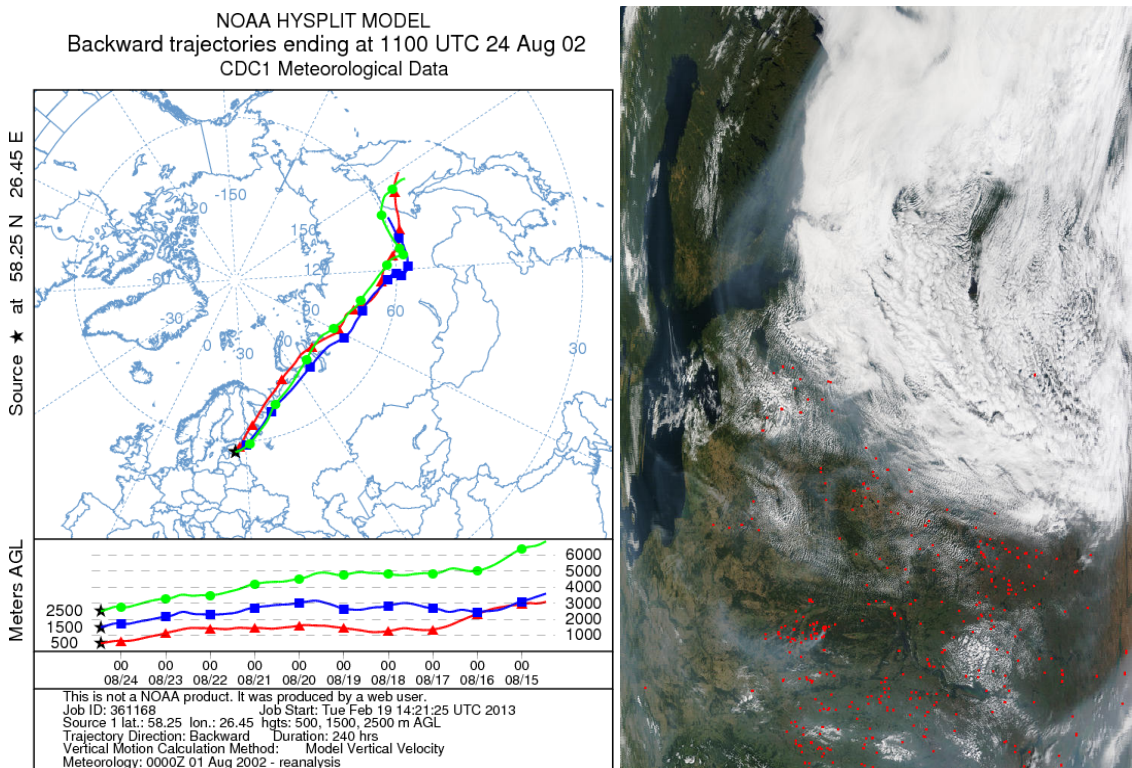

Fig. 6.7. HYSPLIT trajectory model at 24.08.2002 at 11:00 UTC on the left; Terra-MODIS satellite picture at 23.08.2002 at 9:10 UTC on the right (courtesy of K. Kattai).

For the middle curve in Fig. 6.6 (α = 1.68, AOD500 = 0.25) linear relationship, between ln(AODλ) and lnλ, fulfills better, especially in the red and near infra-red range 0.675-1.0 μm. Daily average FMF = 0.934.

In a case of very clean air, that is described with the lowest curve in Fig. 6.6 (α = 1.39, AOD500 = 0.04) the curve resembles a random wave; FMF = 0.584,

that indicates few smoke and relatively more coarse mode aerosol particles in the atmosphere than in an average.

6.3. A failed expectation with Ångström wavelength exponent

Unfortunately, annual cycles of reviewed column parameters (except the FMF) did not give expected relationships with annual cycle of the Ångström exponent (Fig. 6.1). Moreover, a plot of Ångström α against AOD500 revealed no correlation (Fig. 6.8). The α varies from 0.05 to 3.43 for cleaner air, when AOD500 < 0.2, encompassing the simple (nonclimatologic, ensemble) average of the exponent, $\alpha = 1.43$. Standard deviation (one sigma uncertainty) of the Ångström exponent for the whole database (ensemble) is, $\sigma = 0.35$. From this value, supposing normal distribution for α and coverage factor 3, the expanded 3σ-uncertainty becomes 1.05. Compared to the average ensemble value of this work database, $\alpha = 1.43$ which is close to the conventional value, $\alpha = 1.3$, irregularity of the Ångström exponent is really remarkable!
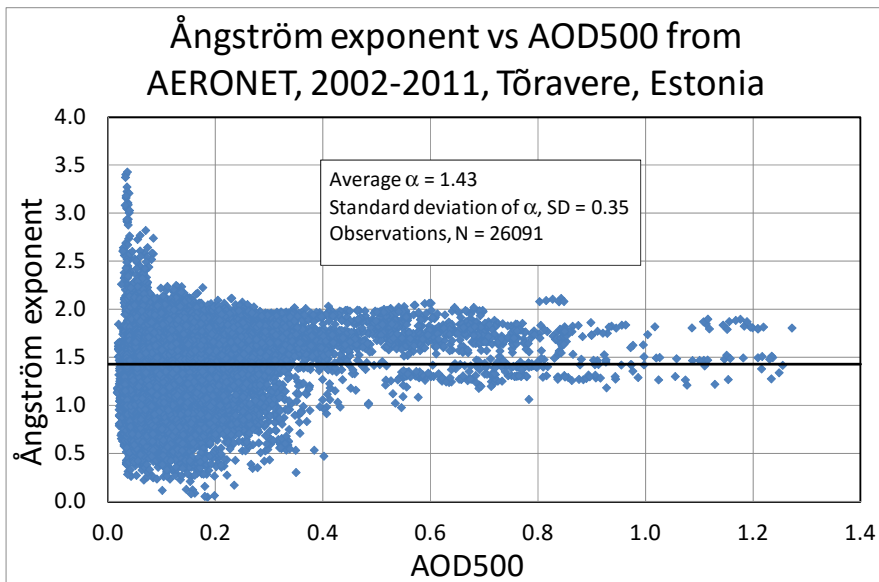

Fig. 6.8. Scattergram of the Ångström exponent against AOD500 at Tõravere, 2002–2011. No solid correlation between Ångström exponent and AOD500 can be detected.

For high turbidities, AOD500 > 0.85, the scatter of α is smaller, $1.2 < \alpha < 1.9$.

To conclude, Figure 6.8 is a visual argument about the lack of relationship between Ångström α and AOD500. Atmospheric aerosol particles, apparently, represent a composite of different origin and sizes which means that the relationship between $\ln(AOD\lambda)$ and $\ln\lambda$ is more complicate than a linear one. The Ångström exponent is not correlating with $AOD\lambda$ and thus, including it into broadband $AOD\lambda$ models does not improve the predictions.

It is worth noting that the Ångström exponent plots against AOD500 at Tõravere (Fig. 6.8) are remarkably consistent to analogous plots performed for the GSFC NASA AERONET USDA station (39 N, 77 W; O'Neill *et al.*, 2001), and therefore, confirm appropriateness of optical parameterization using bi-modal size distribution instead of the Junge/Ångström unimodal approach.

7. PLANS FOR FURTHER INVESTIGATION – CLOUD SCREENING ALGORITHMS AND INTEGRATION OF DATASETS

During the last decades, due to lack of money, scientific research in Estonia has become project based, sporadic. It has become difficult to maintain normal rhythm and continuity of investigations. Besides that, concerning environmental routine observations, in accordance with global trends, participation of human observers has diminished drastically or is missing at all. These factors also exasperate keeping quality and homogeneity of column optical databases, their updating and linking with other databases.

In Section 4.2 four cloud screening algorithms were reviewed. Also there were mentioned that the approaches are instrument and measured physical parameter specific. This statement means that cloud screening procedures need further development towards standardization. This is a challenging task.

Inasmuch as a human observer at Tõravere still makes regular observations of cloudiness, once per hour, consistency of the AERONET automated cloud screening method (for spectral AOD) as well as of a cloud-screening method proposed in Section 4.2 for broadband direct beam, can be evaluated in regard to visual-manual separation of clear moments. Although this topic stands out of this thesis, some ideas will be introduced and additional model runs will be performed in this chapter.

7.1. Two different cloud-screenings of Tõravere datasets, effects of sampling

One of the world longest time series of column transparency, during 1950–2015, is maintained and updated at Tõravere. Routine observations of broadband direct beam were performed by the Estonian Environment Agency (former Estonian Meteorological and Hydrological Institute). Calculations, through the whole time series, were accomplished by PhD Viivi Russak (Tartu Observatory). During the last 3 years her work was supported by project "Estonian radiation climate", funded by the European Regional Development Fund. By now this project is completed as well as her contract.

She used a diary of regular (once per hour) cloudiness observations at Tõravere and a 1 min record of broadband direct solar radiation at normal incidence. The fact that visual-manual selection of clear solar disc moments, together with further column transparency calculations, were implemented by the same person, secured homogeneity of time series of column transparency, p_2, for 1950–2015.

Separating from V. Russak's database monthly means of p_2 for years 2002–2012, Kaidi Kattai calculated, using this work's broadband model T2, monthly and annual means of AOD500 for these 11 years (Figs. 7.1 and 7.2) (K. Kattai, personal communication).
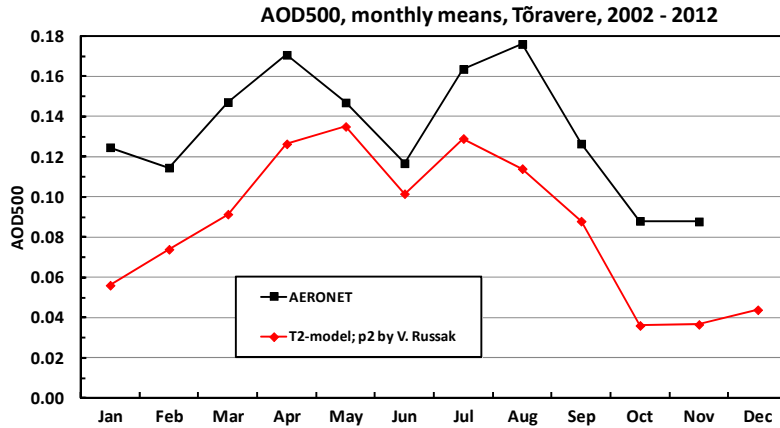
Fig. 7.1. Monthly means of AOD500 as observed by AERONET, and modeled by T2. There were no AERONET observations in December. Both techniques exhibit similar seasonal pattern but the AERONET AOD500 values systematically exceed those obtained by the broadband model T2. Courtesy by Russak & Kattai.

Both lines in Fig. 7.1 exhibit similar seasonality, with minimum in June. But the AERONET AOD500 product systematically exceeds monthly means of AOD500 got by model T2, which uses as an input the p_2 dataset created by V. Russak. The only explanation is that the Russak's dataset of column transparency corresponds to clearer moments compared to AERONET's dataset. For that, the AERONET annual AOD500 means also exceed those obtained by the broadband model T2 (Fig. 7.2).
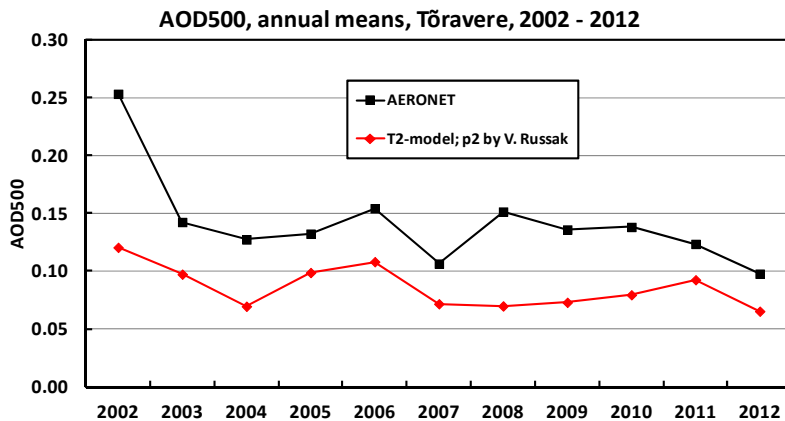

Fig. 7.2. Annual means of AOD500 as observed by AERONET (Jan-Nov) and modeled by T2 (Jan-Dec). The AERONET AOD500 product is systematically higher. Courtesy by Russak & Kattai.

Apparently, a lot of observation moments, which by the AERONET cloud screening process were accepted as "clear solar disc" ones, were removed by V. Russak as "cloudy solar disc". By now there are no answers to this discrepancy. A deeper analysis, how and why Russak's screening algorithm (sampling) is severer than AERONET's one, is a topic of further work. However, in frames of this thesis some evaluations were performed.

Some analysis of AERONET-Tõravere data obtained during 2002–2008, in total 18834 observations of spectral direct solar beam are proposed as follows. However, comparing these data with joint spectral-broadband dataset, 1280 AERONET observations (6.8%) did not find counterparts in joint dataset and were removed. The residual AERONET data set contained 17554 observations. Colleague V. Russak kindly agreed to share her expertise and to inspect these 17554 AERONET observations from 2002–2008 in order to remove measurements when there was a doubt of cloud-contaminated solar disc for her. Such a capacious additional AERONET data inspection, done by Russak, allowed us to create the next datasets for Tõravere, 2002–2008 below:

a) the AERONET dataset with 17554 AOD500 observations from 2002–2008, before the additional inspection by V. Russak; this dataset is further denoted as "all" observations; a simple (bulk, not weighted) average of it, AOD500 = 0.148;

b) after the additional inspection made by V. Russak, a stricter AERONET-Tõravere dataset was created, for 2002–2008; she accepted 8310 AERONET observations from the initial set of 17554 and removed 9244; the stricter AERONET dataset is further denoted as "clear" observations; here a simple average, AOD500 = 0.137;

c) a data set of removed 9244 observations, further denoted as "cloudy" observations, a simple average, AOD500 = 0.157; actually, as it will be shown below, the name doesn't mean that the removed observations certainly correspond to a cloud-contaminated solar disc.

Note that each row in any of three new dataset, for 2002–2008, contains joint AOD500, p_2 and W observations. This fact allowed rerunning the main verification tests for models M1, M2, M2a, M2b, M2c, G1, T1, T2 as it was done in Section 5.2.

In order to get a more quantitative evaluation, the AOD500 range is divided into eight bins: a) AOD500 < 0; b) 0.0 < AOD500 < 0.1; c) 0.1 < AOD500 < 0.2; d) 0.2 < AOD500 < 0.4; e) 0.4 < AOD500 < 0.6; f) 0.6 < AOD500 < 0.8; g) 0.8 < AOD500 < 1.0; h) AOD500 > 1.0.

The results are presented in three separate sub-tables in Table 7.1 and in Figure 7.3 and in eight panels of Figure 7.4.

Table 7.1. Turbidity distribution of AOD500 in three databases: (a) "all" observations, (b) "clear" observations" and, (c) "cloudy" observations, as observed by AERONET and predicted by eight broadband models. "Clear" and "cloudy" observations were separated by a manual/visual additional inspection, done by V. Russak

Number of AERONET **"all"** observations and model predictions in specific ranges**,** 2002-2008, Tõravere											
1	2	3	4	5	6	7	8	9	10	11	12
AOD500 range	AERONET			M1	M2	M2a	M2b	M2c	G1	T1	T2
AOD500 < 0	0	0.0%	0.0%	103	35	35	35	35	1	1	0
0.0 - 0.1	7994	45.5%	45.5%	7121	7491	7491	7011	7491	6047	6659	7204
0.1 - 0.2	6277	35.8%	81.3%	6939	7029	7029	6812	7029	8213	7739	7212
0.2 - 0.4	2424	13.8%	95.1%	2589	2301	2301	2747	2301	2540	2395	2304
0.4 - 0.6	457	2.6%	97.7%	508	506	225	476	506	495	488	446
0.6 - 0.8	293	1.7%	99.4%	242	157	346	346	151	211	221	267
0.8 - 1.0	73	0.4%	99.8%	40	32	89	89	32	35	34	79
AOD500 > 1.0	36	0.2%	100.0%	12	3	38	38	9	12	17	42
Sum:	17 554	100.0%	------	17 554	17 554	17 554	17 554	17 554	17 554	17 554	17 554

Number of AERONET **"clear"** observations and predictions in specific ranges, 2002-2008, Tõravere											
1	2	3	4	5	6	7	8	9	10	11	12
AOD500 range	AERONET			M1	M2	M2a	M2b	M2c	G1	T1	T2
AOD500 < 0	0	0.0%	0.0%	73	27	27	27	27	0	0	0
0.0 - 0.1	4301	51.8%	51.8%	3780	4010	4010	3760	4010	3217	3588	3919
0.1 - 0.2	2774	33.4%	85.1%	3149	3126	3126	3103	3126	3838	3522	3207
0.2 - 0.4	811	9.8%	94.9%	914	783	783	991	783	872	815	774
0.4 - 0.6	237	2.9%	97.7%	254	287	116	181	287	268	260	223
0.6 - 0.8	159	1.9%	99.7%	126	67	197	197	66	102	111	144
0.8 - 1.0	18	0.2%	99.9%	9	9	40	40	7	8	7	31
AOD500 > 1.0	10	0.1%	100.0%	5	1	11	11	4	5	7	12
Sum:	8 310	100.0%	------	8 310	8 310	8 310	8 310	8 310	8 310	8 310	8 310

Number of AERONET **"cloudy"** observations and predictions in specific ranges, 2002-2008, Tõravere											
1	2	3	4	5	6	7	8	9	10	11	12
AOD500 range	AERONET			M1	M2	M2a	M2b	M2c	G1	T1	T2
AOD500 < 0	0	0.0%	0.0%	30	8	8	8	8	1	1	0
0.0 - 0.1	3693	40.0%	40.0%	3341	3481	3481	3251	3481	2830	3071	3285
0.1 - 0.2	3503	37.9%	77.8%	3790	3903	3903	3709	3903	4375	4217	4005
0.2 - 0.4	1613	17.4%	95.3%	1675	1518	1518	1756	1518	1668	1580	1530
0.4 - 0.6	220	2.4%	97.7%	254	219	109	295	219	227	228	223
0.6 - 0.8	134	1.4%	99.1%	116	90	149	149	85	109	110	123
0.8 - 1.0	55	0.6%	99.7%	31	23	49	49	25	27	27	48
AOD500 > 1.0	26	0.3%	100.0%	7	2	27	27	5	7	10	30
Sum:	9 244	100.0%	------	9 244	9 244	9 244	9 244	9 244	9 244	9 244	9 244

The most interesting result which becomes obvious from Table 7.1 is that the "cloudy" dataset is actually not so cloudy! For 40% of its observations AOD500 < 0.1, and for 77.8% observations AOD500 < 0.2. Contribution of highest turbidity, AOD500 > 1.0, is only 0.3%, instead of expected 100%.

Domination of low AOD500 values for "cloudy" observations strengthens a doubt that performed severity of manual/visual selection was actually over-wrought. Figure 7.3, where the AOD500 percentage distributions for three particular datasets ("all", "clear", "cloudy") are presented, gives a visual confirmation in regard to this conclusion.
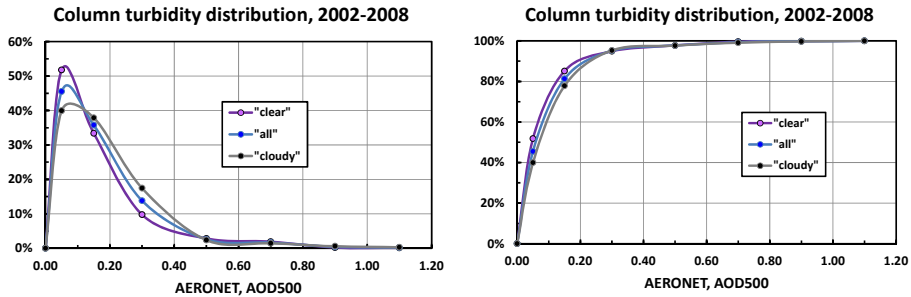

Fig. 7.3. Percentage column spectral turbidity distributions for all Tõravere AERONET observations during 2002–2008, for "clear" solar disc events (as accepted by manual/visual selection), and for "cloudy" events (as removed by manual/visual selection). Left panel – differential, right panel – cumulative distribution. Domination of low AOD500 values for "cloudy" observations and coincidence of all three curves, in right panel, from AOD500> 0.3, strengthens a doubt that performed severity of manual/visual selection was overwrought.

Next, using the input data from "clear" and "cloudy" datasets respectively, reruns of the models M1, M2, M2a, M2b, M2c, G1, T1 and T2 was performed. Results for both datasets, as presented in Fig. 7.4 and 7.5 respectively, are very similar to those ones obtained in Section 5.2 (Fig. 5.2). Results of these reruns also speak in favor that "cloudy" dataset actually represents clear solar disc.

In future, to complete inspection of the "cloudy" dataset, it is necessary to undertake two more steps and to examine, row by row, the "cloudy" dataset using additional information from:

a) diary of cloud observations at Tõravere by Environment Agency (former Estonian Meteorological and Hydrological Institute) in order to generalize which cloud types prevented to consider observations as clear solar disc ones; this item is time consuming and would be most appropriate to be performed by V. Russak, but she is retired by now;

b) AERONET microphysical, *e.g.* aerosol size distribution information (AERONET Inversion Products) in order to detect presence of cloud particles (water droplets, ice crystals).

Most likely both items for final examination of the "cloudy" dataset will be a topic of a diploma work even of a master thesis. I will be happy to share my expertise.
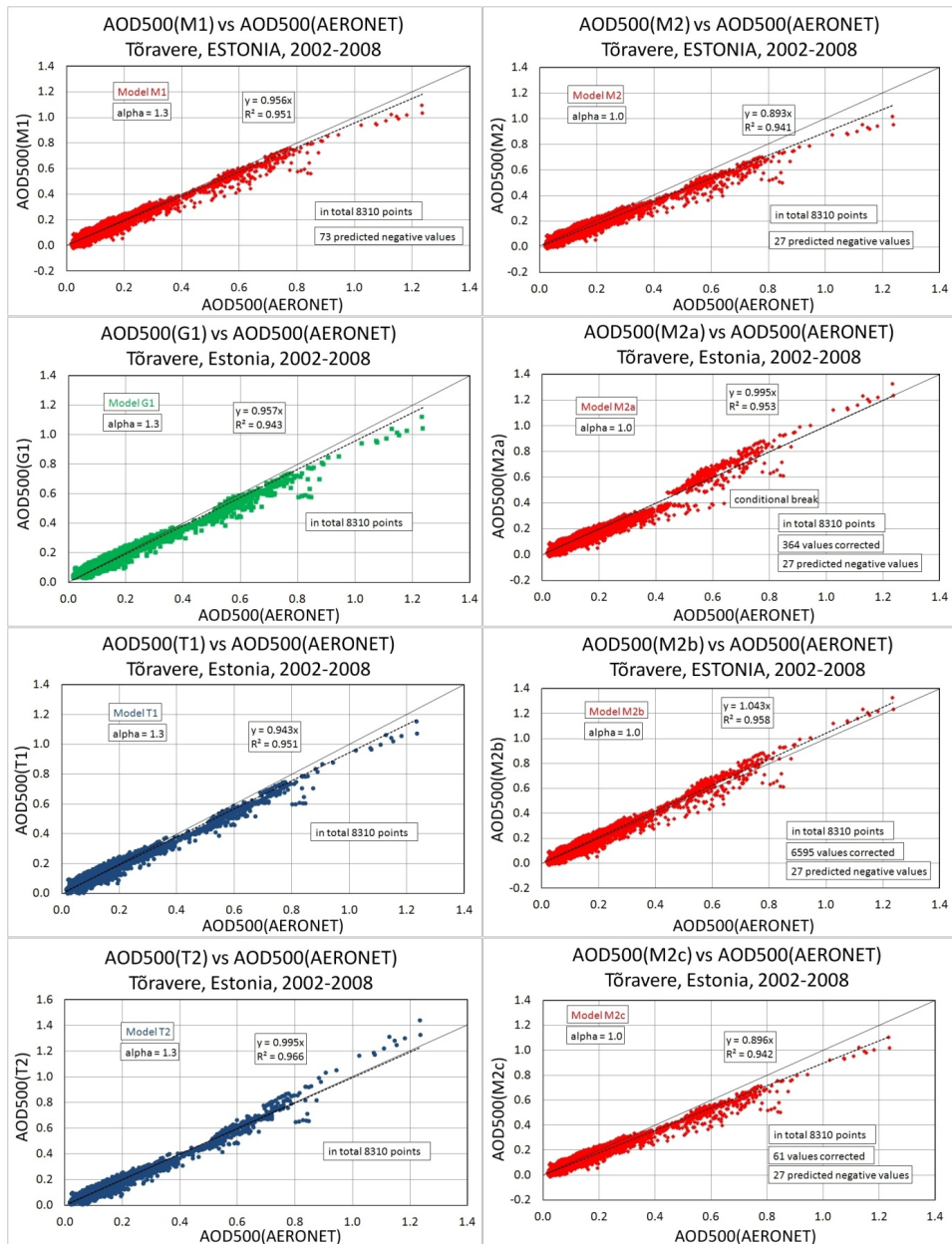
Fig. 7.4. Results of predictions of AOD500 by eight different models when the "clear" dataset was used as input. Dashed lines represent linear regression against the AERONET reference observations. Each panel contains 8310 single predictions for years 2002-2008. Solid lines give 1-to-1 relationships.
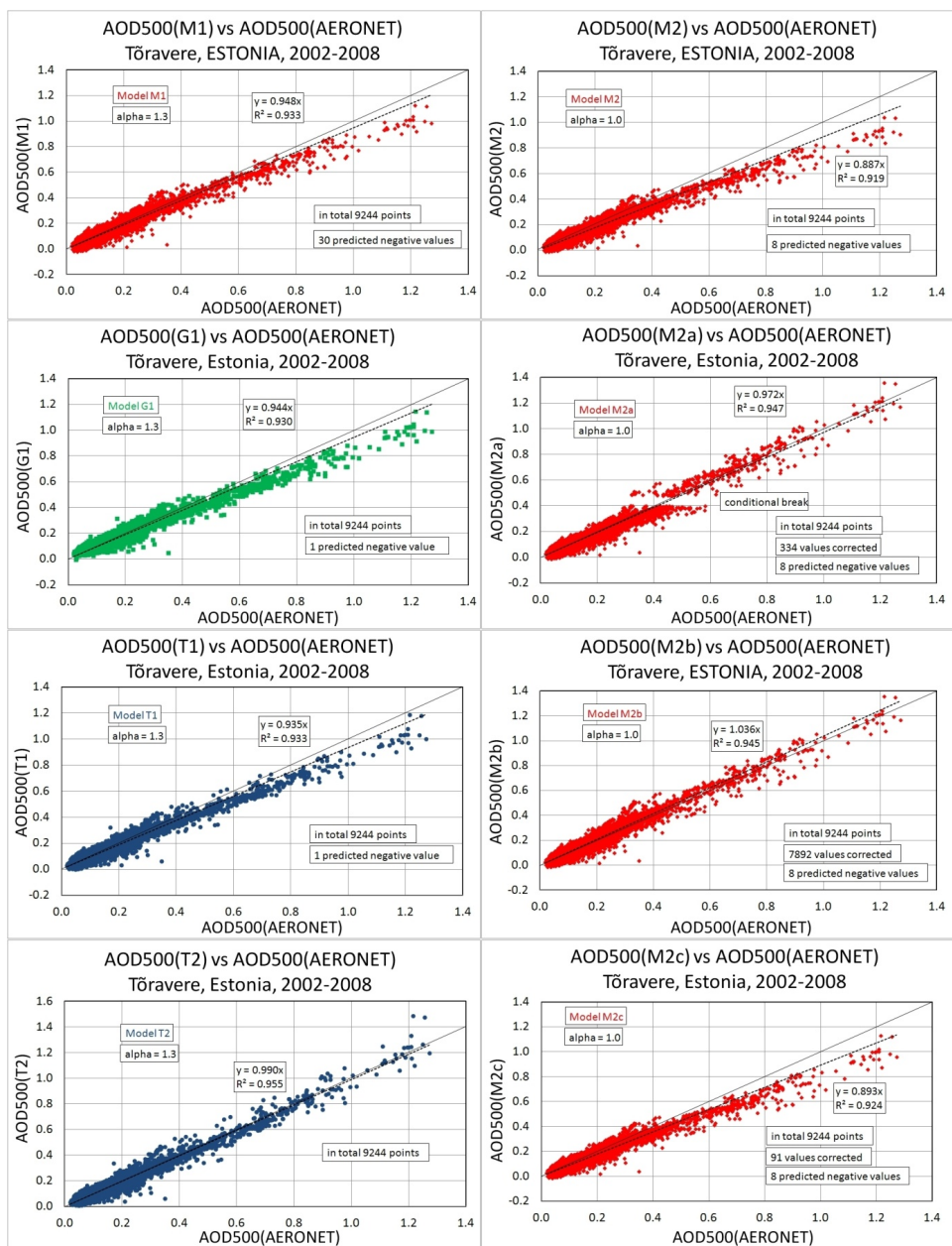
Fig. 7.5. Results of predictions of AOD500 by eight different models when the "cloudy" dataset was used as input. Dashed lines represent linear regression against the AERONET reference observations. Each panel contains 9244 single predictions for years 2002–2008. Solid lines give 1-to-1 relationships.

8. CONCLUSIONS

In this dissertation a spectral AOD500 modeling using broadband actinometric observations was discussed. Some AOD500 estimation models were developed, also the existing independent models were selected to test comprehensively their behavior and agreement in regard to AERONET AOD500 observational data at Tõravere, Estonia, during 2002–2011.

The main results of the dissertation are listed below.

Revised version of the AOD500 model, T1, Eq. (3.7) was proposed. It was a simple parameterization of the Moscow University (M1) model, however, with a substantial correction: a factor for consideration of circumsolar radiation was added. According to review of test runs (Fig. 5.2), the model T1 performed even better compared to some other broadband models.

For climatic conditions similar to Tõravere, a handier AOD500 evaluation model T2, expressed by Eq. (3.31) was developed using broadband aerosol optical depth (BAOD) as an input variable. The BAOD was calculated from broadband direct solar beam and amount of column humidity (precipitable water).

It was shown that use of ground water vapor pressure (e_0), as a proxy variable for calculation of precipitable water (W), is sufficient for AOD500 model estimation.

A simple cloudscreening algorithm was proposed (Section 4.2) for automated recordings of broadband normal direct beam. As a yearly average at Tõravere, this algorithm excludes more than 90% automatically registered "trash" observations of direct solar beam. The algorithm can be recommended for initial refinement of automated direct solar radiation data in radiation stations.

A merged database (Section 4.1) of spectral and broadband measurements was composed consisting of more than 26000 actino-meteorological and the reference AOD500 (AERONET) values, together also with the AERONET-calculated Ångström wavelength exponent, α(440-500-675–870), as well as AERONET-estimated precipitable water, W.

Named merged database allowed comprehensive testing of eight AOD500 prediction models. Among this set there were two models (M2a and T2), which performed better against AERONET observations during 2002–2011 (Figs. 5.2, 5.3). As a conclusion of intercomparison, these two models can be recommended for broadband estimations of AOD500. However, among of 26091 predictions, model M2a predicted 45 negative AOD500 values. The only models without negative predictions were models, T1 and T2.

Two of tested models (M1 and T1) were special because of their ability to consider the *a priori* known Ångström wavelength exponent α for each single prediction. However, use of the *a priori* known Ångström exponents (instead of a fixed one), did not improve the AOD500 predictions (Fig. 5.4) as it could be initially expected. The detailed analysis of Ångström wavelength exponent was discussed in Sections 6.2, 6.3, no correlation between the α and AODλ was found.

Seasonal evolution of Ångström exponent was consistent with changes in the Fine Mode Fraction (FMF) of atmospheric particles. The higher α values in summer (Jun-Jul-Aug) indicate domination of fine aerosol particles.

Concerning satellite AOD500 daily mean estimations, their consistency against the AERONET Tõravere measurements was rather low, $R^2 = 0.775$ for TerraMODIS, and $R^2 = 0.702$ for AquaMODIS, respectively. Even negative AOD500 values were proposed by satellites (Fig. 5.6).

A study of the annual courses of column optical parameters revealed an interesting fact about a spring-summer maximum of atmospheric column transparency in June. This finding was supported by low values of both, broadband aerosol optical depth and AOD500. Cleaner air in June can be explained: (a) by fresh vegetation, which restricts generation of dust, and (b) by low number of forest and bog fires in Estonia as well as in surrounding territories in this season.

This dissertation was a part of an environmental project "Estonian radiation climate", 2012–2015, funded by the European Regional Development Fund. Three institutions, University of Tartu, Tartu Observatory, Estonian Environment Agency, were participants of the project. However, with completion of the project, employment contracts with a group of experienced researchers (K. Eerme, O. Okulov, K. Rannat, V. Russak, U. Veismann) were also completed, project manager (H. Ohvril) continues as a part-time university teacher only.

Although actinometric surface measurements and observations at Tõravere are continuously carried on by Estonian Environment Agency, ability of their analysis and interpretation is from now considerably reduced. Without of analysis and interpretation of recorded time series, decline in quality actinometric measurements and observations is inevitable. This fact places Estonia in researches of physical climatology, atmospheric dynamics, column aerosol and humidity load, remote-sensing technology, global warming etc, at a distinct scientific disadvantage.

Because of sporadic and insufficient funding during the next years, analysis and interpretation of actinometric measurements and observations, performed at Tõravere, will be mainly implemented by students in frames of their diploma works and dissertations. But qualification of students is lower compared to experienced PhD-level scientists listed above. To make the drop in funding of radiation investigations less painful and to maintain continuation and homogeneity of actinometric time series at clear solar disc, the only possible solution is to elaborate smart computational schemes to clean the automated initial, raw recordings from unnecessary measurements/observations at cloud contaminated solar disc.

Standardization of sampling is not an easy task because the new automated cloud-screening schemes should have the same degree of severity with the previous, classic manual-visual schemes. In the end of the dissertation (Section 7) severity of the AERONET automated cloudscreening method was examined against the classic manual-visual cloudscreening performed at Tõravere by V. Russak from already the 1970s. Thanks to her contribution, the 1950–2015 Tartu-Tõravere time series of column transparency was created. Now, after her

retirement, there is still no clear answer about automated smooth lengthening of this unique sequence. But results of the intercomparison were interesting and challenging.

V. Russak inspected 17554 AERONET observations using manual-visual method from 2002–2008 (already screened by a scheme proposed in Section 4.3). She accepted 8310 observations (47.3%) considering them as "clear" solar disc ones and removed 9244 (52.7%) as "cloudy". Analyzing, by AOD500 values, distribution of observations in created two datasets("clear" and "cloudy"), it appeared that for "clear" dataset, 85.1% of observations belong to a turbidity region AOD500 < 0.2. For "cloudy" dataset, there were 77.8% of observations when AOD500 < 0.2. A large range, AOD500 < 0.4, involved 94.9% of the "clear" and 95.3% of the "cloudy" observations. Domination of low AOD500 values for "cloudy" observations means that the "cloudy" dataset is actually not so cloudy! Rerun of broadband models (AOD500 calculation from BAOD2 and W) confirmed a conclusion that the severity of the manual-visual cloudscreening carried out by V. Russak was actually overwrought.

In future, to complete inspection of the "cloudy" dataset, it is necessary to undertake the next steps and to examine, row by row, the "cloudy" dataset using additional information from diary of cloud observations at Tõravere which describe particles' microphysical parameters (AERONET Inversion Products) in order to detect presence of cloud aerosol particles.

In summary, the targeted objectives were accomplished:

a) several known AOD500 calculation broadband-models (M1, M2, M2a, M2c, G1) were analyzed and tested, enhancements for improvement were proposed (model M2b);

b) two original AOD500 calculation models (T1 and T2) were created, they both estimate well aerosol optical depth in Estonia;

c) a comprehensive merged database of spectral and broadband measurements as well as column humidity was created;

d) performance tests of AOD500 calculation models were completed and all models were ranked according to their ability to predict AOD500 values;

e) test runs of models revealed two autumn periods when the AOD500 values, recorded by the AERONET-Tõravere photometer, were abnormally large: 06.09.2003–30.10.2003, in total 216 suspicious recordings, 03.09.2005–18.09.2005, in total 221 suspicious recordings; evidently, these questionable observations appeared due to spider webs, insects or other restrictions at the entrance or even inside of the AERONET photometer (the tube of the photometer is open); detected suspicious periods were eliminated from the database;

f) a rather simple algorithm for cleaning of direct solar irradiance data from trash recordings was created and implemented, this algorithm is recommended for further use;

g) the AERONET-Tõravere data were also verified against satellite measurements; however, for estimation of AOD500, broadband models performed better.

BIBLIOGRAPHY

Aaltonen, V., Lihavainen, H., Kerminen, V.-M., Komppula, M., Hatakka, J., Eneroth, K., Kulmala, M., Viisanen, Y. 2006. Measurements of optical properties of atmospheric aerosols in Northern Finland. *Atmos. Chem. Phys.*, **6**, 1155−1164.

Alexandrov, M. D., Marshak, A., Cairns, B., Lacis, A. A., Carlson, B. E. 2004. Automated cloud screening algorithm for MFRSR data. Geophys. Res. Lett., 31, L04118, 5 pp, doi:10.1029 /2003GL019105.

Ångström, A. 1929. On the atmospheric transmission of sun radiation and on dust in the air. *Geografiska Annaler*, **11B**, 157–166.

Ångström, A. 1930. On the atmospheric transmission of sun radiation. II. *Geografiska annaler*, **12**, pp. 130–159.

Abakumova, G. M, Gorbarenko, E. V. 2008. *Atmospheric transparency in Moscow during the last 50 years and its variability on the Russian territory*. LKI Publishing, 188 pp (in Russian).

AERONET Inversion Products, 2010. *http://aeronet.gsfc.nasa.gov/new_web/ Documents/Inversion_products_V2.pdf*

Carlund, T., Landelius, T., Josefsson, W. 2003. Comparison and uncertainty of aerosol optical depth estimates derived from spectral and broadband measurements. *Journal of Applied Meteorology*, **42**, 1598−1610.

Chen, M., Davis, J., Tang, H., Ownby, C., Gao, W. 2013. The calibration methods for Multi-Filter Rotating Shadowband Radiometer: A review. *Front. Earth Sci.*, **7**, 257–270, doi: 10.1007/s11707-013-0368-9.

Chen, M., Davis, J., Gao, W. 2014. A new cloud screening algorithm for ground-based direct-beam solar radiation. *J. Atm. Oc. Techn*. American Meteorological Society. Dec. 2014, 2591-2605 doi: 10.1175/JTECH-D-14-00095.1.

Chubarova, N. E. 2005. Optical and radiative properties of smoke aerosol from AERONET data. *In: Handbook of Moscow environmental and climatic features, v. 1 "Applied climatic parameters, air pollution monitoring, dangerous weather phenomena, expected tendencies at XXI century"*, Geography department of MSU, 127-132 (in Russian).

Chubarova, N. E., Gorbarenko, E. V., Nezval, E. I., Shilovtseva, O. A. 2011a. Aerosol and Radiation Characteristics of the Atmosphere during Forest and Peat Fires in 1972, 2002 and 2010 in the Region of Moscow. Izvestiya RAN. *Fizika Atmosfery i Okeana*, **47** (6), 790–800 (in Russian).

Chubarova, N. E., Gorbarenko, E. V., Nezval, E. I., Shilovtseva, O. A. 2011b. Aerosol and Radiation Characteristics of the Atmosphere during Forest and Peat Fires in 1972, 2002 and 2010 in the Region of Moscow. Izvestiya, *Atmospheric and Oceanic Physics*, **47** (6), 729–738. Pleiades Publishing, Ltd (translation from Russian).

Deepak, A., Box, G.P. 1979. Analytic modeling of aerosol size distributions. *NASA Contractor Report 159170*, 162 pp.

Eck, T. F., Holben, B. N., Reid, J. S., Dubovik, O., Smirnov, A., O'Neill, N. T., Slutsker, I., Kinne, S. 1999. Wavelength dependence of the optical depth of biomass burning, urban, and desert dust aerosols. *Journal of Geophysical Research*, **104**, No. D24. 31,333−31,349

Evnevich, T. V., Savikovskij, I. A. 1989. Calculation of direct solar radiation and coefficient of atmospheric transparency. *Soviet Meteorology and Hydrology*, **5**, Allerton Press, New York, 92−95.

Garg, H.P., Prakash, J. 2006. *Solar Energy. Fundamentals and Applications*. Tata McGraw-Hill Publishing Company Limited, New Delhi, 435 p.

Gorbarenko, E. V. 1997. Spatial and temporal variability of the atmospheric aerosol thickness on the territory of former USSR. *In IRS' 96: Current Problems in Atmospheric Radiation*, W.L. Smith and K. Stamnes (Eds.). A. Deepak Publishing, Hampton, Virginia, USA, 774–777.

Gorbarenko, E. V., Rublev, A. N. 2013. Correction of aerosol optical thickness succession under strong atmospheric turbidity. In *Proceedings of International Symposium "Atmospheric Radiation and Dynamics" (ISARD-2013)*, 24–27 June 2013, StPtrb., StPtrb State University, p.105.

Gueymard, C. 1993. Critical analysis and performance assessment of clear sky solar irradiance models using theoretical and measured data. *Solar Energy,* **51** (2), 121–138.

Gueymard, C. 1995. SMARTS2, a simple model of the atmospheric radiative transfer of sunshine: algorithms and performance assessment. *Tech. Rep. FSEC-PF-270-95*, 78 p*.* [Available from Florida Sol. Energy Center, 1679 Clearlake Rd., Cocoa, FL 32922-5703].

Gueymard, C., Kambezidis, H. 1997. Illuminance turbidity parameters and atmospheric extiction in the visible spectrum. *Quarterly Journal of the Royal Meteorological Society*,, **123**, 679–697.

Gueymard, C. 1998. Turbidity determination from broadband irradiance measurements: a detailed multicoefficient approach. *Journal of Applied Meteorology*, **37**, 414-435.

Gueymard, C. 2003. Direct solar transmittance and irradiance predictions with broadband models. Part I: detailed theoretical performance assessment. *Solar Energy,* **74**, 355–379.

Gueymard, C. 2013. Aerosol turbidity derivation from broadband irradiance measurements: Methodological advances and uncertainty analysis. *Solar 2013 Conference*, Baltimore, MD, American Solar Energy Soc., 8 p.

Holben, B., Eck, T. F., Slutsker, I., Tanré, D., Buis, J. P., Setzer, A., Vermote, E., Reagan, J. A., Kaufman, Y. J., Nakajima, T., Lavenu, F., Jankowiak, I., Smirnov, A. 1998. AERONET – A federated instrument network and data archive for aerosol characterization. *Remote Sensing of Environment*, **66**, 1–16.

Ionov, D. V. 2010. Tropospheric NO_2 trend over St. Petersburg (Russia) as measured from space. *Russ. J. Earth. Sci.*, **11**, ES4004, 1–7.

Iqbal, M. 1983. *An Introduction to Solar Radiation*. Academic Press, 390 p.

Jakobson, E., Ohvril, H., Okulov O., Laulainen, N. 2005. Variability of radiosonde-observed precipitable water in the Baltic region. *Nordic Hydrology*, **36**, 423–433.

Jakobson, E., Ohvril, H., Elgered, G. 2009. Diurnal variability of precipitable water in the Baltic region, impact on transmittance of the direct solar radiation. *Boreal Environment Research,* **14**, 45–55.

Junge, Chr. 1955. The size distribution and aging of natural aerosols as determined from electrical and optical data on the atmosphere. *J. Meteor.*, **12**, 13–25.

Kalitin, N. N. 1938. *Actinometry*. Gidrometeorologicheskoe izdatelstvo. Leningrad-Moscow, 324 p. (in Russian).

Kambezidis, H. D., Katevatis, E. M., Petrakis, M., Lykoudis, S., Asimakopoulos, D. N. 1998. Estimation of the Linke and Unsworth-Monteith turbidity factors in the visible spectrum: application for Athens, Greece. *Solar Energy*, **62** (1), 39–50.

Kannel, M., Ohvril, H., Teral, H., Russak, V., Kallis, A. 2007. A simple broadband parameterisation of columnar aerosol optical thickness. *Proceedings of the Estonian Academy of Sciences. Bilogy, Ecology,* **56** (1), 57–68.

Kannel, M. 2007. *Modeling of spectral aerosol optical depth.* University of Tartu, Estonia, 37 p. (Master thesis, in Estonian).

Kannel, M., Ohvril, H., Okulov, O. 2012. A shortcut from broadband to spectral aerosol optical depth. *Proceedings of the Estonian Academy of Sciences*, **61** (4), 266–278, doi:10.3176/proc.2012.4.02 .

Kannel, M., Ohvril, H., Okulov, O., Kattai, K., Neiman, L. 2014. Spectral aerosol optical depth prediction by some broadband models. Validation with AERONET observations. *Proceedings of the Estonian Academy of Sciences*, **63** (4), 404–416, doi: 10.3176/proc.2014.4.06.

Kasten, F. 1980. A simple parameterization of two pyrheliometric formulae for determing the Linke turbidity factor. *Meteorol. Rdsch*. **33**, 124–127.

Kattai, K. 2014. *Investigation of atmospheric aerosol content with different methods*. University of Tartu, Estonia, 53p. (Master thesis, in Estonian).

King, M. D., Byrne, D. M. 1976. A method for inferring total ozone content from spectral variation of total optical depth obtained with a solar radiometer. *J. Atmos. Sci.*, **33**, 2242–2251.

Kondratyev, K. Y. 1969. *Radiation in the Atmosphere*, 912 pp., Academic, San Diego, Calif.

Lenoble, J. 1993. *Atmospheric radiative transfer*. A. Deepak, Hampton, Virginia USA, 532 p.

Li, J., Carlson, B. E., Lacis, A. A. 2015: How well do satellite AOD observations represent the spatial and temporal variability of PM2.5 concentration for the United States? *Atmos. Environ.*, **102**, 260-273, doi:10.1016/j.atmosenv.2014.12.010.

Liou, K. N. 2002. *An introduction to atmospheric radiation*. Academic Press, 583 p.

Long, C. N., Ackerman, T. P. 2000. Identification of clear skies from broadband pyranometer measurements and calculation of downwelling shortwave cloud effects. *J. Geophys. Res.*, **105**(D12): 15609–15626.

Matthias-Maser S., Jaenicke R. 2000. The size distribution of primary biological aerosol particles in the multiphase atmosphere. *Aerobiologia*, **16**, 207–210.

Maurellis A., Tennyson, J. 2003. The climatic effects of water vapor. *Physics World*, May: 29–33.

Molineaux, B., Ineichen, P., Delaunay, J. J. 1994. Development and performance assessment of a physical direct luminous efficacy model. In *North Sun '94: Solar Energy at High Latitudes*. Ed. Kerr McGregor. James & James, 395–400. Electronic version, 2013, by Earthscun.

Molineaux, B., Ineichen, P., Dealunay, J.J. 1995. Direct luminous efficacy and atmospheric turbidity – Improving model performance. *Solar energy*, **55** (2), 125–137.

Molineaux, B., Ineichen, P., O'Neill, N. 1998. Equivalence of pyrheliometric and monochromatic aerosol optical depths and a single key wavelengths. *Appl. Optics,* **37** (30), 7008–7018.

Myurk, Yu. Kh., Okhvril, Kh. A. 1990. Engineering procedure for adjusting coefficient of atmospheric transparency from one atmospheric mass to another. *Soviet Meteorology and Hydrology*, **1,** Alerton Press, New York, 89–95.

Nordisk Familjebok 20, 1934, *Klara Civiltryckeri A.-B.*: pp 1319–1321.

Ohvril, H., Okulov, O. 1996. Comparison of two methods for calculation of the atmospheric integral transparency coefficient, *Proceedings of the Estonian Academy of Sciences. Ecology*, **3** (4), 167−175.

Ohvril, H., Okulov, O., Teral, H., Teral, K. 1999. The atmospheric integral transparency coefficient and the Forbes effect. *Solar Energy*, **66** (4), 305−317.

Ohvril, H., Teral, H., Tee, M., Russak, V., Okulov, O., Jõeveer, A., Kallis, A., Abakumova, G., Terez, E., Guschchin, G., Terez, G., Olmo, F. J., Alados-Arboledas, L., Laulainen, N. 2005. Multi-annual variability of atmospheric transparency in Estonia. *SOLARIS 2005, 2nd Joint Conference.* International Forum of Experts in Solar Radiation, Hellenic Illumination Committee, Athens, 42–46.

Ohvril, H., Teral, H., Neiman, L., Kannel, M., Uustare, M., Tee, M., Russak, V., Okulov, O., Jõeveer, A., Kallis, A., Ohvril, T., Terez, E. I., Terez, G. A., Gushchin, G. K., Abakumova, G. M., Gorbarenko, E. V., Tsvetkov, A. V., Laulainen, N. 2009. Global dimming and brightening versus atmospheric column transparency, Europe, 1906−2007. *Journal of Geophysical Research*, **114**, 1−17, D00D12, doi:10.1029/ 2008JD010644.

Okulov, O., Ohvril, H., Teral, H., Tee, M., Russak, V., Abakumova, G. 2001. Multiannual Variability of Atmospheric Transparency in Estonia and Moscow. In *IRS 2000: Current Problems in Atmospheric Radiation,* W. L. Smith and Yu. M. Timofeyev (Eds.). A. Deepak Publishing, Hampton, Virginia, USA, 725–728.

Okulov, O., Ohvril, H., Kivi, R. 2002. Atmospheric precipitable water in Estonia, 1990−2001. *Boreal Environment Research*, **7** (3), 291−300.

Okulov, O. 2003. *Variability of atmospheric transparency and precipitable water in Estonia during last decades*. PhD dissertation. Tartu University Press, 79 p.

Okulov, O., Ohvril, H. 2010. *Column transparency and precipitable water in Estonia*. Variability during the last decades. Lambert Acad. Publish., Saarbrücken, Germany, 69 p.

O'Neill, N. T., Eck, T. F. Holben, B. N., Smirnov, A. Dubovik, O., Royer, A. 2001. Bimodal size distribution influences on the variation of Angström derivatives in spectral and optical depth space. *J. Geophys. Res.,* **106**, No. D9, 9787−9806.

Peixoto, J. P., Oort, A. H. 1992. *Physics of Climate*, American Institude of Physics, 520 p.

Qiu, J. 2001. Broadband extinction method to determine atmospheric aerosol optical properties. *Tellus* **53B**, 73–82.

Rösemann, R. 2011. *A guide to solar radiation measurement. From sensor to application. An overview of the state of the art*. Gengenbach messtechnik, 218 p.

Schuster, G. L., Dubovik, O., Holben, B. 2006. Angström exponent and bimodal aerosol size distribution. *J. Geophys. Res.,* **111**, D07207, 1−14, doi: 10.1029/ 2005JD006328.

Seinfeld, J. H., Pandis, S. N. 2006. *Atmospheric Chemistry and Physics: From Air Pollution to Climate Change*, 2nd edition, J. Wiley, New York. 1203 p.

Smirnov, A., Holben, B. N., Eck, T. F., Dubovik, O., Slutsker, I. 2000. Cloud-Screening and Quality Control Algorithms for the AERONET Database. *Remote Sensing of Environment*. **73** (3), 337–349

Shifrin, K. S. 1995. Simple relationships for the Ångström parameter of disperse systems. *Applied Optics*, **34** (21), 4480–4485.

Stothers, R. B. 1996. Major optical depth perturbations to the stratosphere from volcanic eruptions: pyrheliometric period, 1881−1960, *J. Geophys.Res.* **101,** 3901−3920.

Smirnov, A., Holben, B. N., Eck, T. F., Dubovik, O., Slutsker, I. 2000. Cloud screening and quality control algorithms for the AERONET database. Remote Sens Environ, 73(3): 337–349.

Tarasova, T. A., Yarkho, E. V. 1991a. Determination of atmospheric aerosol optical thickness from land-based measurements of integral direct solar radiation, *Meteorologiya y gidrologiya,* **12**, 66–70 (in Russian).

Tarasova, T. A., Yarkho, E. V. 1991b. Determination of atmospheric aerosol optical thickness from land-based measurements of integral direct solar radiation, *Soviet meteorology and hydrology,* **12**, Alerton Press, New York, 53–58 (translation from Russian).

Toledano, C., Cachorro, V. E., Sorribas, M., Berjón, A., Morena de la, B. A., Frutos de, A. M., Gouloub P. 2007. Aerosol optical depth and Ångström exponent climatology at El Arenosillo AERONET site (Huelva, Spain). *Quarterly Journal of the Royal Meteorological Society*, **133***, 795–807, doi:10.1002/qj.54.

Toll, V., Männik, A. 2014. Modelling derecho dynamics and the direct radiative effect of wildfire smoke upon it with NWP model HARMONIE. *In: Geophysical Research Abstracts: EGU General Assembly 2014*, Vienna, Austria.

Toll, V., Männik, A., Luhamaa, A., Rõõm, R. 2015. Hindcast experiments of the derecho in Estonia on 08 August, 2010: Modelling derecho with NWP model HARMONIE. *Atmospheric Research*, **158–159,** 179–191, doi:10.1016/j.atmosres. 2014.10.011

Unsworth, M. H., Monteith, J. L. 1972. Aerosol and solar radiation in Britain. *Quarterly Journal of the Royal Meteorological Society*, **98**, 778-797.

Veismann, U., Eerme, K., 2011. *Solar ultraviolet radiation and atmospheric ozone*. Ilmamaa, Tartu, 215 p. (in Estonian).

Zvereva, S. V. 1968. On the absorption of solar radiation by atmospheric water vapor. *In Actinometry and atmospheric optics. Reports of the sixth interdepartmental symposium on actinometry and atmospheric optics*, June 1966, Tartu, Valgus, 117–121 (in Russian).

ACKNOWLEDGEMENTS

SUMMARY IN ESTONIAN

Atmosfääriaerosooli optilise paksuse
laiaribaliste mudelite arendus

Nii Päikese laiaribalise ehk integraalse (kõiki lainepikkusi hõlmava) kui spektraalse otsekiirguse nõrgenemine atmosfääris on jaotatav kolmeks protsessiks: 1) hajumine ja neeldumine puhtas õhus ehk ideaalses atmosfääris, 2) neeldumine veeaurus, 3) neeldumine ja hajumine aerosooliosakeste (suitsus, tolmus, udus) tõttu. Vastavalt on atmosfääri optiline paksus esitatav kolme optilise paksuse summana. Selle summa kaks esimest liiget, ideaalse atmosfääri ja veeauru optilised paksused, on arvutatavad teades antud asukoha ideaalse atmosfääri koostist ja tegeliku atmosfääri niiskussisaldust antud vaatlushetkel. Summa kolmas liige, aerosooli kõiki lainepikkusi hõlmav optiline paksus, BAOD (Broadband Aerosol Optical Depth), on eelmistega võrreldes väga muutlik. Kui aga atmosfääri kogu optiline paksus on Päikese otsekiirgusest määratud, saab sellest kahe komponendi, ideaalse atmosfääri ja veeauru optiliste paksuste lahutamisega leida kolmanda ehk BAOD.

Õhusambas sisalduvate aerosooliosakeste iseloomustamiseks on spektraalne AODλ, eriti mõõdetuna mitmel lainepikkusel, oluliselt informatiivsem kui laiaribaline AOD, kuid spektraalmõõtmised on oluliselt keerukamad. Eestis alustati, USA NASA programmi AERONET (Aerosol Robotic NETwork) raames ja selle programmi poolt finantseerituna, Päikese otsekiirguse spektraalmõõtmisi 2002. aasta suvel Tõraveres. Sellest ajast alates täieneb pidevalt unikaalne spektraalsete AODλ väärtuste andmebaas Eesti kohal oleva atmosfääri kohta.

Käesolevas doktoritöös on hinnatud ideaalse atmosfääri koostist Eesti kohal, esitatud valemid integraalse otsekiirguse neeldumiseks veeaurus ja koostatud rohkem kui 20 000 vaatlusreast koosnev andmebaas spektraalse ja integraalse AOD ning õhusamba niiskussisalduse väärtustest Tõraveres aastatel 2002–2011.

Töös on tutvustatud autori kahte erinevat AOD500 hindamise mudelit ning nende tekkelugu. Nii esimene, mis põhineb Moskva Ülikooli kõige varajasemale, 1991. aasta mudelile, kui ka teine, antud väitekirjas koostatud orginaalne mudel, nn 'otsetee' integraalsetelt spektraalsetele AODλ väärtustele, võimaldavad edaspidi kolme liiki rakendusi: 1) spektraalse AODλ hinnanguid Tõraveres enne 2002. aastat, kui Päikese spektraalset otsekiirgust veel ei mõõdetud, 2) spektraalse AOD hinnanguid muudes meteojaamades ja ekspeditsiooniolukorras, kus piirdutakse vaid integraalse otsekiirguse mõõtmistega, näiteks Tiirikoja järvejaamas, 3) automaatselt registreeritud spektraalse AOD aegridade operatiivne kontroll, kui on tekkinud kahtlus Päikese otsekiirgust ekraneeriva takistuse (putukas, praht, suits lähipiirkonnas jne) sattumisest mõõteriista vaatevälja.

Lisaks toodud kahe mudeli kõrval on antud doktoritöös veel võrreldud 6 teiste autorite poolt arendatud AOD500 arvutamise integraalset ehk laiaribalist mudelit. Neist lihtsamad mudelid koosnevad vaid mõnest valemist ja vajavad

ainult kahte peamist sisendparameetrit, milleks on Päikese integraalse otsekiirguse kiiritustihedus koos Päikese kõrgusega või atmosfäärisamba läbipaistvuskoefitsient, ning atmosfääri veeaurusisaldus. Lihtsamates mudelites pole tehtud eeldusi aerosooliosakeste füüsikaliste omaduste kohta, kuid kaks mudelit (antud väitekirja tähistustes, M1 ja T1) lubavad kolmanda sisendparameetrina varieerida Ångströmi lainepikkuse eksponenti, α, mis on seotud osakeste suurusjaotusega.

Ainus analüüsitud keerukam mudel (G1) koosneb ca 30 valemist ja lubab spetsifitseerida atmosfääri gaasilist koostist detailsemalt, näiteks osooni ja lämmastikdioksiidi koguste kaudu.

AOD500 arvutused toetusid Tõraveres mõõdetud Päikese laiaribalisele otsekiirguse kiiritustihedusele, mille mõõteandmeid võib pidada kvaliteetseteks, sest Tartu-Tõravare meteojaam kuulub rahvusvahelisse kiirgusmõõtmiste võrgustikku BSRN ning Eestis on otsekiirguse mõõtmise kompetents juba 1930. aastatest. Teine sisendsuurus, õhusamba veeaurusisaldus, ei olnud otseselt (raadiosondeerimistega) mõõdetud, vaid leitud kaudselt, veeaururõhu kaudu, ometi kaudne hinnang sobis.

Kõigi mudelite poolt saadud AOD500 tulemusi võrreldi AOD500 tegelike väärtustega, mõõdetuna Tõraveres AERONET Cimel päikesefotomeetri poolt.

Mudelite võimekuse kvantitatiivseks analüüsiks koostati ulatuslik andmebaas, milles iga vaatlusrida ühendas nii meteojaamas mõõdetud suurused (Päikese integraalne otsekiirgus, veeaururõhk) kui AERONET fotomeetri samaaegselt mõõdetud suurused (AOD500 tegelik väärtus, Ångströmi lainepikkuse eksponent, $\alpha(440$-500-675–$870)$). Kokku sisaldas andmebaas 26091 integraalset-spektraalset vaatlust, mis leidsid aset kõikidel kalendrikuudel (välja arvatud detsember) kümne aasta jooksul, 2002–2011. Selline andmebaas võimaldas iga mudeli põhjalikku võrdlust AERONET tegelike AOD500 mõõtmistega.

Suhteliselt puhta õhu korral, kui AOD500 < 0.6, andsid kõik mudelid mõistlikke tulemusi. Saastatuma õhu korral, mil AOD500 > 0.6, kaldusid statistiliselt korrigeerimata mudelid aerosooli optilist paksust alahindama. Alahindamist põhjustab Päikese oreooli nn parasiitkiirgus, mis suurendab aktinomeetri poolt mõõdetud otsekiirgust ja loob mulje puhtamast õhust.

Testimistulemused tõstsid esile kaks mudelit, Tartus koostatud T2 ja Moskvas koostatud M2a. Tuleb siiski märkida, et Moskva mudeli M2a väljundis on kunstlik piirang, nimelt puuduvad arvutatud väärtused vahemikus 0.4 < AOD500 < 0.477.

Kõiki vaatlusaluseid mudeleid testiti lisaks kahe erineva sisendandmebaasiga. Neist esimene alternatiivne andmebaas hõlmas Tõraveres aastatel 2002-2008 teostatud mõõtmisi, mis olid inimese vaatluse poolt tunnistatud kvaliteetseks ja vajalikuks mõõtmiseks (nn selged hetked). Neid vaatlusi oli kokku 8310. Teine alternatiivne sisendandmebaas koosnes autori esialgsest automaatselt filtreeritud andmebaasist nn selgete hetkede väljaviskamise teel saadud andmetest. Hoolimata erinevatest sisendandmetest jäid mudelite AOD500 hindamistendentsid ning statistilised parameetrid sarnaseks.

Vaatlusalustest kaks mudelit, M1 ja T1, võimaldasid sisendsuurusena muuta ka Ångströmi lainepikkuse eksponenti, α. Tavapraktikas pole α väärtused *a priori* teada, koostatud andmebaasis selline võimalus aga sisaldus. Mõnevõrra ootamatult ei parandanud α kaasamine AOD500 arvutustulemusi. Leidmaks põhjusi selle ebaõnnestunud numbrilise eksperimendi kohta, analüüsisime atmosfäärisamba optiliste ja niiskusparameetrite sesoonset muutlikkust Tõraveres aastatel 2002–2011. Selgus, et Ångströmi α korreleerub vaid osakeste nn peenmoodi fraktsiooni (FMF) panusega AOD500-sse. Kuukeskmiste lõikes näitas FMF head korrelatsiooni Ångströmi eksponendiga ning peenosakeste domineerimist suvekuudel.

Kõrvalproduktina AOD500 mudelite võrdlemisele ilmnes, et atmosfääri läbipaistvusel on juunis kevad-suvine maksimum, põhjuseks ilmselt õhusamba väiksem aerosooliosakeste sisaldus. Esialgu oskame seda fakti põhjendada arvamusega, et juunis on Eestis välja kujunenud värske taimkate, mis takistab tolmu teket ja levikut. Samuti pole juunis veel levinud kohalikud raba- ja metsapõlengud. Kuid võimalik on ka atmosfääri tsirkulatsioonimustrite muutus ja lääne ning põhja poolt saabuvate õhuvoolude sagenemine juunis, seda hüpoteesi tuleks kontrollida.

Käesoleva väitekirja valmimisele aitasid kaasa kaks ETF granti ning hiljuti lõppenud Euroopa Regionaalarengu Fondi poolt toetatud projekt "Eesti kiirguskliima". Seoses nende uurimistoetuste lõppemisega on oluliselt kahanenud Eesti teadlaste aktinomeetriliste uuringute võimekus operatiivselt analüüsida KAUR poolt automaatselt mõõdetud aegridasid ning avastada kiirgusandurite võimalikud süstemaatilised kõrvalekalded (määrdunud või lumised instrumendikuplid, putukad instrumentide vaateväljas jne). Aktinomeetriliste uuringute jätkamine tulevikus hakkab ilmselt veelgi enam tuginema üliõpilaste lõputöödele ja väitekirjadele. Selget päikeseketast vajavates uuringutes tuleb koostada sobiva rangusega numbrilised filtrid puhastamaks aegridasid pilvede ja lennukijälgede mõjust.

PUBLICATIONS

CURRICULUM VITAE

Name: Martin Kannel
Date of birth: May 8th, 1983, Viljandi, Estonia
Contact: martin.kannel@ut.ee

Education:

2007–2016	University of Tartu, doctoral student in Physics
2005–2007	University of Tartu, MSc in Applied Physics (Environmental Physics)
2001–2005	University of Tartu, BA in Physics
1998–2001	Viljandi Maagümnaasium, high school

Employment:

2007–	Cybernetica AS, release engineer
2005–2008	Heino Eller Music School, administrator of IT-systems

International training:

2008, March	3 weeks in the University of Granada, Spain

ELULOOKIRJELDUS

Nimi: Martin Kannel
Sünniaeg: 8. mai 1983, Viljandi, Estonia
Kontakt: martin.kannel@ut.ee

Haridus
2007–2016   Tartu Ülikool, füüsika doktorant
2005–2007   Tartu Ülikool, magistrikraad rakendusfüüsikas
             (keskkonnafüüsika)
2001–2005   Tartu Ülikool, bakalaureusekraad füüsikas
1998–2001   Viljandi Maagümnaasium, keskharidus

Teenistuskäik:
2007–   Cybernetica AS, tarneinsener
2005–2008   Heino Elleri nimeline Tartu Muusikakool, IT-süsteemide
             administraator

Stažeerimine välismaal:
2008 märts, 3 nädalat Granada Ülikoolis (Hispaania)

DISSERTATIONES GEOPHYSICALES
UNIVERSITATIS TARTUENSIS

1. **Andres Kuusk.** The hot-spot effect in plant canopy reflectance. Tartu, 1991.
2. **Tiit Nilson.** Radiative transfer in non-homogeneous plant canopies. Tartu, 1991.
3. **Helgi Arst.** Atmosfääri ja mere kiirguskarakteristikud looduskeskkonna seisundi informaatoritena (vene keeles). Tartu, 1991.
4. **Juha Sarkkula.** Measuring and modelling water currents and quality as a part of decision making process for water pollution control. Tartu, 1992.
5. **Piia Post.** On the two radiatively effective cloud parameters. Tartu, 1993.
6. **Aadu Mirme.** Electric aerosol spectrometry. Tartu, 1994.
7. **Aare Luts.** Mathematical simulation of the evolutions of air ions. Tartu, 1995.
8. **Tiit Kutser.** Estimation of water quality in turbid inland and coastal waters by passive optical remote sensing. Tartu, 1997.
9. **Ülle Kikas.** Atmospheric aerosol in the Baltic region. Tartu, 1998.
10. **Tarmo Kõuts.** Processes of deep water renewal in the Baltic sea. Tartu, 1999.
11. **Anu Reinart.** Underwater light field characteristics in different types of Estonian and Finnish lakes. Tartu, 2000.
12. **Marko Kaasik.** Parameterisation of atmospheric boundary layer in the numerical model of air pollution transport. Tartu, 2000.
13. **Janek Laanearu.** Topographically constrained deep-water flows in channels. Tartu, 2001.
14. **Urmas Raudsepp.** Wind-driven circulation in the gulf of Riga. Tartu, 2001.
15. **Urmas Hõrrak.** Air ion mobility spectrum at a rural area. Tartu, 2001.
16. **Marko Vana.** Formation and evolution of atmospheric aerosol size spectrum by the occurrence of nucleation burst events in the atmospheric boundary layer; transport of the climatically active particulate air pollution. Tartu, 2002.
17. **Veljo Kimmel.** Analysis of methods of air quality assessment. Applications in Estonia. Tartu, 2002.
18. **Oleg Okulov.** Variability of atmospheric transparency and precipitable water in Estonia. Tartu, 2003.
19. **Aarne Männik.** Implementation and validation of the nonhydrostatic adiabatic core of the numerical weather prediction model hirlam. Tartu, 2003.
20. **Matti Mõttus.** Shortwave solar radiation field inside willow canopy. Tartu, 2004.
21. **Kalev Rannat.** Long weakly nonlinear waves in geophysical applications. Tartu, 2007.
22. **Rigel Kivi**. Observations of ozone, polar stratospheric cloud and water vapour profiles in the arctic. Tartu, 2007.

23. **Erko Jakobson.** Spatial and temporal variability of atmospheric column humidity. Tartu, 2009, 125 p.
24. **Sander Mirme.** Development of nanometer aerosol measurement technology. Tartu, 2011, 118 p.
25. **Hannes Keernik.** Estimating methods and variability of atmospheric humidity over the Baltic Region and the Arctic. Tartu, 2015, 105 p.